The Effects of Radial Migration on the Outskirts of Disc Galaxies

Adam J. Clarke

A thesis submitted in partial fulfilment
of the requirements for the degree of
Doctor of Philosophy

Jeremiah Horrocks Institute for Maths, Physics and Astronomy
University of Central Lancashire

May 2016

Declaration

The work presented in this thesis was carried out at the Jeremiah Horrocks Institute for Maths, Physics and Astronomy, University of Central Lancashire.

I declare that while registered as a candidate for the research degree, I have not been a registered candidate or enrolled student for another award of the University or other academic or professional institution.

I declare that no material contained in the thesis has been used in any other submission for an academic award. Data and models used in this thesis that are not my own are clearly cited in the text.

Signature of Candidate

17-05-2016

Date

Abstract

Since the discovery of radial migration a galaxy can no longer be considered to be a collection of annuli evolving in isolation. Previous works have considered the implications of migration on properties of disc galaxies, but most of these efforts concentrate on the Solar neighbourhood, where observational comparisons are at their best. Only a small number of studies have investigated the effect on the outer regions of galaxies. Using N-body+SPH simulations, I consider the effect of radial migration on the outskirts of disc galaxies. I demonstrate that when falling through a gas rich cluster environment, a galaxy can evolve from a type II profile to a type I profile with little increase in the radial velocity dispersions. Instead the cluster environment induces more spirals when compared to the same galaxy evolving in isolation, driving radial migration of stars into the outer disc and explaining the relative abundance of type I galaxies in cluster environments. I demonstrate that during the transformations of the profiles the galaxy evolves from a spiral to a lenticular galaxy and becomes redder. This significantly alters the position of the galaxy in the colour-mass plane, transitioning from the blue sequence to the green valley. Furthermore, these changes occur rapidly after the onset of ram pressure stripping. Finally I consider the effects of migration in disc galaxies with strong warps. I find that the warp remains isolated from the mixing effect of migration and thus forms a tight relation between age and metallicity. Stars forming in the warp settle into the disc, where they migrate across all radii, imprinting the warp AMR over the flattened, broadened disc AMR.

Contents

List of Figures

Acknowledgements

First I would like to thank my supervisor, Victor Debattista, for all the support, patience and discussions we have had over the past four years. You have shaped me into the scientist I have become and there have been plenty of times I have felt like giving up, but you always knew that I would find the answer with some hard work and perseverance. You taught me so much, that sometimes I felt like my brain was melting, but undoubtably without your support I would not have completed this thesis. Thank you.

To the students of the JHI, past and present and especially Dominic, Ben, Nicky, Mike, Gareth, Caroline and Sam, thank you for making these four years a blast. I have made friendships that will hopefully last for an age, and my wallet will be forever lighter thanks to Mike teaching me how to play Magic. I doubt anyone could get through a PhD without close support, both academically and emotionally, from friends.

I would like to send thanks to my collaborators. Firstly to Rok Roškar for giving me vast help in understanding migration, and finally convincing me to use python, which probably saved me months of work further on. David Cole for being ever patient and helpful explaining concepts while we shared an office. Thanks to everyone else I have crossed paths with over the past years, there are too many to list individually, but all of you have helped improve this work in some regard. I must also thank Giovanni Natale for considerable help in using DART-Ray and interpreting and understanding the colour transition work, especially in such a short

timescale.

A special thanks to Gordon Bromage, who very many years ago, at an open day, took the time to talk to an applicant about space and science, ensuring I chose UCLan and setting me on a long path that culminates with this piece of work.

I wish to also thank my panel, Alfonso Aragón-Salamanca and Dimitris Stamatellos for taking the time to read and examine this work and providing useful feedback for both this thesis and future publications. I'd also like to thank Anne Sansom and Mark Norris for helping me prepare for the viva.

And finally thank you to Urban, Davey, Greg, Gary, Kelvin and Mark. Without your incessant stupidity and distractions, I most certainly would not have gotten through this, so the next bottle of Dom is on me.

Cheers!

Dedication

To Elise, for without you I would not be the person I am today. You are the pillar that supports me when times get tough and for your unwavering belief that I could succeed and complete this work. Every day spent with you is a gift. To Mum, for putting so much effort into my early education, and for laying the groundwork for everything I have achieved since. And to Gdad and Satnan for your unconditional love. Thank you all, I could not have done this without your support.

"Getting an education was a bit like a communicable sexual disease. It made you unsuitable for a lot of jobs and then you had the urge to pass it on."

– Terry Pratchett, *Hogfather*

"You can never know everything, and part of what you do know will always be wrong. Perhaps even the most important part. A portion of wisdom lies in knowing this. A portion of courage lies in going on anyway."

– Robert Jordan, *Winter's Heart*

Chapter 1

Introduction

1.1 ΛCDM

Our current understanding of the universe is that the visible, baryonic matter observable as stars and gas only corresponds to $\sim 5\%$ of the total energy, with $\sim 26\%$ hidden in kinematically cold dark matter (CDM). The remaining $\sim 69\%$ (Planck Collaboration et al. 2015) of the energy budget comes in the form of dark energy which is needed to explain the accelerating expansion of the universe. This cosmology is known as ΛCDM. It has proven remarkably good at explaining large-scale structure (Davis et al. 1985), cosmic expansion (Garnavich et al. 1998; Perlmutter et al. 1999) and the polarisation of the cosmic microwave background (Kovac et al. 2002), and yet the nature of the dark matter particle is still unknown and undetected. Regardless, evidence from studies such as the Bullet Cluster (Markevitch et al. 2004) and the flatness of galaxy rotation curves (Babcock 1939; Rubin & Ford Jr. 1970; van den Bosch & Swaters 2001) at large radii make it the widely accepted cosmology at this time.

Since the Big Bang, 13.8 billion years ago, small deviations in the initially smooth matter distribution, arising from quantum perturbations which were later stretched out by inflation, have been amplified through gravity. Over-dense regions become

increasingly over-dense, whilst under-dense regions become more void-like, causing the matter to be distributed in a "cosmic web" of filamentary structure and voids. Gas is funnelled along this filamentary structure, cools and forms galaxies (e.g. Kereš et al. (2005) and references within).

1.2 Galaxies

There are four broad main classes of galaxies suggested by Hubble (1926) as shown in the Hubble sequence that can be seen in Figure 1.1.

Elliptical galaxies are spheroidal and have smooth isophotes. They are divided into subtypes ranging from E0 to E7, with the number given by the equation $n = 10 \times (a - b)/a$, where a and b are the semi-major and semi-minor axes respectively (Hubble 1926). Elliptical galaxies are pressure supported rather than rotationally supported and they are generally characterised by a lack of recent star formation (Faber & Gallagher 1976), although some star forming blue ellipticals have been observed (Huang & Gu 2009; Crocker et al. 2011). It is widely understood that ellipticals form from the merging of two or more disc galaxies (for a good review see de Zeeuw & Franx (1991) and references within).

Spiral galaxies have thin disc-shaped structures with features such as spiral arms (S type) and sometimes a central bar (SB type). These are further sub-divided depending on the tightness of the spiral arms, Sa/SBa being the most tightly wound and Sc/SBc being the least tightly wound. We discuss the formation of spiral arms and their consequences in Section 1.2.1. The two nearest large galaxies, our own Milky Way (MW) and Andromeda (M31), are both spiral galaxies, exhibit central bars and are roughly similar in size and mass. Spiral galaxies may also contain a central excess in the stellar distribution, referred to as a bulge. The sizes of bulges drop as you move along the Hubble sequence from elliptical galaxies to late type galaxies (Wyse et al. 1997). There are two categories of bulges. Classical

bulges look similar to early type galaxies, are dynamically hot and are thought to form via hierarchical merging (e.g. Renzini (1999)). Pseudobulges have disc-like kinematics and form through secular processes such as bars (e.g. for a good review on pseudobulge formation see Kormendy & Kennicutt Jr. (2004)).

A disc galaxy with no spiral arms is known as a lenticular galaxy (S0), which may also have a bar, then termed SB0. We discuss these galaxies in greater detail in Section 1.2.2.

Finally a galaxy that does not fit into any of the above categories is referred to as an irregular galaxy. Irregular galaxies are seen in our local universe (Large and Small Magellanic Clouds) but are not listed in many galaxy catalogues, since they are often very faint systems (for a good review see Gallagher III & Hunter (1984)).

Rather confusingly elliptical and lenticular galaxies were historically referred to as "early-type" galaxies, whilst spirals were known as "late-type" galaxies, because it was (incorrectly) thought that galaxies evolve from elliptical to spiral, along the Hubble sequence. Whilst it is now thought that spirals evolve into lenticular and elliptical galaxies via environmental processes or mergers, this nomenclature is still widely used.

The Galaxy Zoo project found that around two thirds of massive galaxies are spiral, one third are elliptical and a few percent are mergers (Lintott et al. 2011; Willett et al. 2013). Similarly the ATLAS^{3D} survey found in a sample of $\sim$ 900 galaxies, two thirds late-type galaxies and one third early-types (Cappellari et al. 2011). It has also been shown that the properties of galaxies may depend on their environment, and this is evident in the morphology-density relation (Dressler 1980). In low-density environments spiral galaxies are the most dominant and in high-density environments, such as clusters, elliptical and lenticular galaxies are more numerous.

1.2.1 The formation of spirals

Understanding the formation of spiral arms is one of the more challenging questions in galactic dynamics and still remains a topic of active research. Observationally the majority of spiral arms tend to be trailing, where the spiral arm points away from the direction of galactic rotation with only a handful which are leading (Buta et al. 2003; Byrd et al. 2008). Figure 1.2 shows a trailing spiral on the left and a leading spiral on the right, with the sense of rotation being clockwise.

There are three broad classifications of spiral arms as discussed by Elmegreen (1990); flocculent spirals with many short arms, multi-armed spirals and grand-design spirals. Around 60% of spiral galaxies show grand design spiral structure either in the inner regions or across the whole disc (Elmegreen & Elmegreen 1982; Grosbøl et al. 2004) and some galaxies have been seen to show grand design spirals in the infrared (old) population whilst also showing flocculent spirals in the optical (gas and young stars) (Block & Wainscoat 1991; Thornley 1996; Thornley & Mundy 1997). Whilst incredibly rare, some galaxies (such as NGC 4725 and NGC 4622) only exhibit a single spiral arm (Byrd et al. 1989; de Vaucouleurs et al. 1991). Any successful spiral formation theory must be able to provide reasonable explanations for these observations.

It has been understood for over a century that if the material composing spiral arms is permanent, the differential rotation will cause them to wind up, aptly known as the "winding problem" (Wilczynski 1896). Due to the ubiquity of spirals observed in nature, they must either be long lived or recurrent. To overcome the winding problem, Lin & Shu (1964, 1966) proposed that grand-design spirals are produced by quasi-stationary, wave-like density perturbations. Deforming circular orbits into elliptical ones by subjecting the disc to an $m = 2$ perturbation and superimposing many of these orbits, naturally causes a crowding which leads to the observed spiral structure shown in Figure 1.3. Because the spiral is a density wave, the material

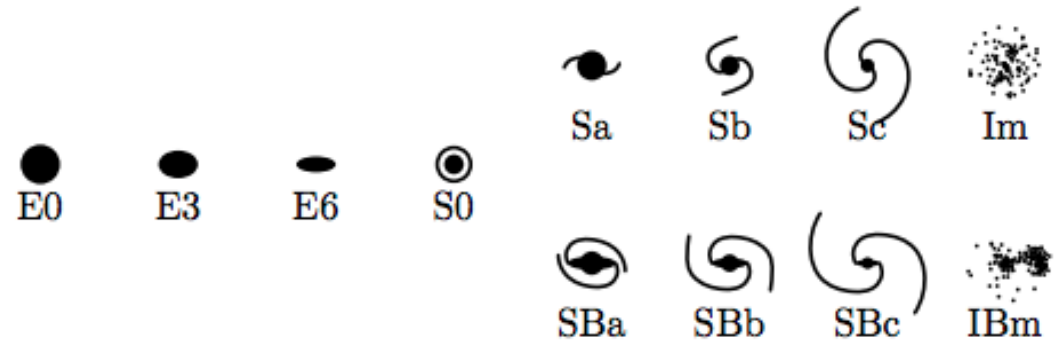

Figure 1.1: Hubble tuning fork showing galaxy morphology (Abraham 1998).

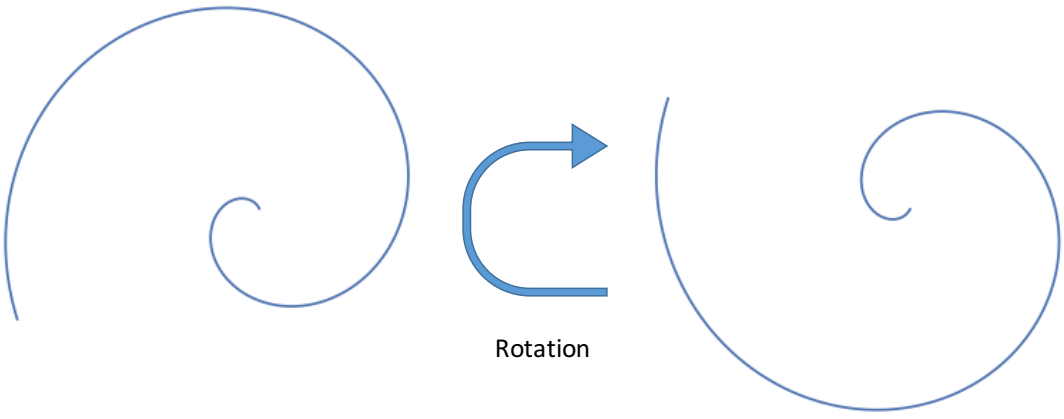

Figure 1.2: Trailing (left) and leading (right) spiral arms. The sense of disc rotation is clockwise.

making up the spiral arms is constantly changing and therefore is not subject to winding and can also explain the increase in star formation on the leading edge of spirals, where gas is compressed to higher density. Further evidence that spirals are density waves first came from Zwicky (1955) and later Schweizer (1976), who observed that the underlying red and old spiral arms are at similar locations to the blue star forming arms, but are less concentrated. They postulated that star formation occurs at the leading edge of the spiral, where the gas compression occurs, and these stars are then smoothed over time, explaining why we see featureless red spirals and more distinct blue ones.

The second breakthrough came from the works of Goldreich & Lynden-Bell (1965) and Julian & Toomre (1966) who independently found that disturbances in a differentially rotating disc are amplified (by a factor of ten or more) and are then sheared into a spiral pattern by the differential rotation. This mechanism is termed swing amplification (Toomre 1981). This occurs when there is a temporary match between the epicyclic motion of the star and the motion of the spiral perturbation, resulting in an enhancement of the spiral by the star. The parameter, Q, known as Toomre's parameter (Toomre 1964) allows us to assess the stability of a disc to perturbations. If κ is the epicyclic frequency, σ_R is the radial velocity dispersion and Σ is the surface density, then

$$Q \equiv \frac{\sigma_R \kappa}{3.36 G \Sigma}. \tag{1.1}$$

If this value is greater than unity, a disc is stable to axisymmetric perturbations. Swing amplification is most dominant when Q is greater than unity, but not by a large amount (Binney & Tremaine 2008). Toomre's stability criterion may be thought of as a temperature scale for galaxies. Discs with large velocity dispersions are 'hot' and have a large value of Q, whilst discs with small velocity dispersions can be considered 'cool' and have a small Q. This also means that spirals are self-limiting, they will fade without gas dissipation because they heat the disc.

However, Sellwood & Carlberg (1984) showed that in the presence of any cooling mechanism, such as dissipation or gas accretion, spirals may reform repeatedly, giving rise to those we observe. Furthermore, when each spiral dissipates it will leave behind an altered density distribution which will provoke further instabilities allowing for future spirals to develop (Sellwood 2000).

Some spiral arms are also seen to connect to the ends of bars (for example NGC 1300) suggesting that bars may drive perturbations leading to spirals (Elmegreen & Elmegreen 1982), however Sellwood & Sparke (1988) demonstrated that the bar and spirals do not have the same pattern speed. It is also possible that interactions with a companion may cause instabilities that lead to spiral arms (Toomre & Toomre 1972).

In Section 1.2 we described the classification system of spirals, where tightness of the spiral arms runs from Sa/SBa, the most tight, to Sc/SBc, the least tight. This tightness is defined in terms of the pitch angle, α, the angle between a circle at radius, R, and the tangent to the spiral arm as shown in Figure 1.4. In the simplest case, the logarithmic spiral, α is independent of radius and is given by

$$\alpha = \arctan \frac{m}{f_o} \tag{1.2}$$

where m is the number of spiral arms, and f_o is a constant that describes how tight the spiral is (Mo et al. 2010). Tightly wound spirals tend to have pitch angles $\alpha \sim 10^\circ$ whilst loosely wound arms tend to be in the region of $\alpha \sim 30^\circ$ (Garcia Gomez & Athanassoula 1993). The Milky Way's spirals have a mean pitch angle of 13.1 ± 0.6^o (Vallée 2015).

1.2.2 Lenticular galaxies and ram pressure stripping

Lenticular (S0/SB0) galaxies have the disc-like morphology of spirals, whilst often being red and dead like the majority of elliptical galaxies. As such, they are

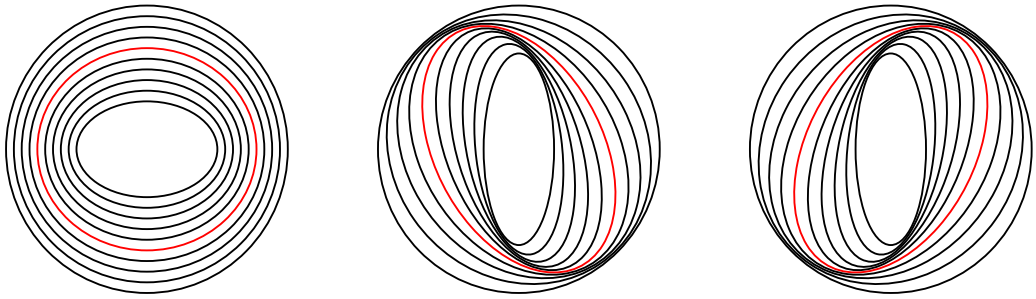

Figure 1.3: Density perturbations due to orbit crowding. The red line shows the same orbit in each plot. *Left:* Bar-like perturbation. *Middle and right:* Spiral patterns where the orbit orientation changes as a function of radius, giving rise to a natural spiral pattern.

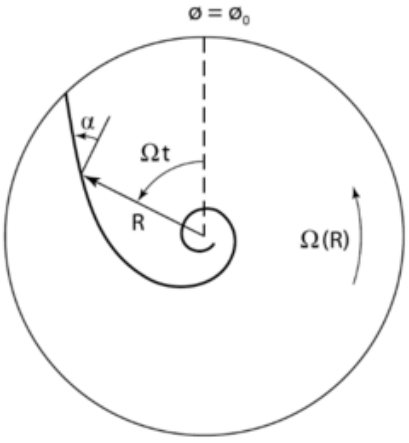

Figure 1.4: Pitch angle, α, at radius, R. Figure 6.8 from Binney & Tremaine (2008).

often seen as an evolutionary transition between spirals and ellipticals. As discussed in Section 1.2 they tend to be found more frequently in clusters, whilst the field environment tends to favor spiral galaxies (Dressler 1980). Furthermore, the fraction of lenticulars decreases with look-back time, whilst the fraction of spirals increases (Dressler et al. 1997; Couch et al. 1998; Postman et al. 2005), implying that environment plays an important role in lenticular galaxy formation.

Lenticulars are characterised by their lack of young stars and smooth appearance which results from a lack of cold gas (van Woerden 1977; Chamaraux et al. 1986). Many mechanisms have been proposed to explain this quenching of star formation including ram pressure stripping (Gunn & Gott, J. Richard 1972; Quilis 2000), strangulation (Larson et al. 1980; Bekki et al. 2002), harassment (Moore et al. 1996, 1999) and minor-merger triggered starbursts leading to gas depletion (Mihos & Hernquist 1994; Bekki 1998). Whilst it is not clear which of these dominates, in this thesis we will primarily consider the effect of ram pressure stripping and so limit our discussion to that mechanism. As a galaxy moves through the intracluster medium (or through any gas rich medium) it will experience an external pressure, first derived by Gunn & Gott, J. Richard (1972), given by

$$P_{\rm RAM} = \rho_{\rm ICM} v_{\rm rel}^2 \tag{1.3}$$

where $P_{\rm RAM}$ is the ram pressure, $\rho_{\rm ICM}$ is the intracluster medium density and $v_{\rm rel}$ is the relative velocity of the infalling galaxy. Ram pressure stripping has been seen observationally in clusters such as Virgo (Koopmann & Kenney 2004; Crowl et al. 2005) and Fornax (De Rijcke et al. 2010) and has been tested via N-body simulations (e.g. Roediger & Brüggen (2007) and Kronberger et al. (2008a,b)). For a review on ram pressure stripping see van Gorkom (2004). A galaxy's rotation velocity is correlated with its absolute magnitude, an empirical relation known as the Tully-Fisher relation (Tully & Fisher 1977). Bedregal et al. (2006) showed that lenticular galaxies lie systematically below this relation, which they attribute

to fading due to a lack of star formation. If the process transforming spirals into lenticulars is hydrodynamical (e.g. ram-pressure stripping or strangulation) then the number of globular clusters should remain constant (Ashman & Zepf 1992). Aragon-Salamanca et al. (2006) found that the specific globular cluster frequency (the number of globular clusters per unit V-band luminosity) in lenticular galaxies increases, indicating that a passive, non-merging formation scenario is the most plausible.

Johnston et al. (2012, 2014) observed 21 Virgo lenticular galaxies and performed a bulge+disc decomposition. They found that the bulges are relatively younger and more metal-rich than their outer discs, and concluded that this is because the last bout of star formation was concentrated at the centre fueled with gas enriched from the disc. They also found no evidence for a star formation burst, implying that ram pressure stripping is a gentle process. Other works have found that some lenticular galaxies show negative metallicity gradients and positive age gradients (Prochaska Chamberlain et al. 2011; Bedregal et al. 2011).

1.2.3 Profile types

Since galaxies form inside-out (e.g. Nelson et al. (2012) and Patel et al. (2013)) the outer parts probe the characteristics of current disc formation and may hold vital information for understanding lenticular formation mechanisms. It has long been known that all disc galaxies show an exponentially declining surface density (or surface brightness profile) (de Vaucouleurs 1959), however some profiles have a change in scale length at a "break-radius", as shown in Figure 1.5. The first of these, type I (Freeman 1970), are purely exponential and have been observed up to 10 scale-lengths from the inner regions (Bland-Hawthorn et al. 2005; Erwin et al. 2008; Vlajić et al. 2011). Type II profiles (Freeman 1970) show a decrease, or truncation, in scale-length past the break-radius. These breaks have been shown to

originate from a decrease in cold gas surface density in the ISM leading to a star formation threshold (Kennicutt 1989; Schaye 2004; Roškar et al. 2008b). The outer disc is then populated by stars migrating outward due to transient spiral structure, via the corotation resonance mechanism proposed by Sellwood & Binney (2002) which we discuss in Section 1.3. This leads to a type II profile with a break radius that moves outwards as gas cools into the disc (Roškar et al. 2008b). Alternatively type II profiles have also been predicted to occur without a star-formation threshold, instead resulting from coupling of multiple patterns, such as bars and spirals (Debattista et al. 2006; Minchev & Famaey 2010). Objects that show a break in their stellar disc have also been shown to have minima in their colour profile close to this radius (Bakos et al. 2008; Azzollini et al. 2008). Type III profiles (Erwin et al. 2005) show an increase in scale-length past the break-radius (anti-truncated). Herpich et al. (2015a) find a correlation between the initial halo angular momentum parameter and the resulting disc profile classification, with a low spin parameter causing type III and a high spin parameter causing type II. They conclude that this link is due to the anti-correlation between radial distribution of stellar mass and the halo spin parameter, which may be a result of bar induced heating (Herpich et al. 2015b). Type III profiles have also been seen in N-body simulations with moderate (~ 5 $M_{\odot}$/yr) gas inflow. This causes the disc to become unstable and the velocity dispersion in the outer disc to increase, which in turn leads to a type III profile and a signature up-turn in the stellar velocity dispersions at post-break radii (Minchev et al. 2012). Minor gas-rich prograde mergers (Younger et al. 2007) and major mergers (Borlaff et al. 2014; Querejeta et al. 2015) have also been shown to cause type III discs.

Erwin et al. (2012) found that the behavior of light profiles depend on the environment, with type I and type II lenticulars being found equally in field galaxies. However they found virtually no type II profiles amongst cluster galaxies and double

the frequency of type I profiles. This finding was also seen by Roediger et al. (2012) who found no type II profiles amongst Virgo lenticulars. Gutiérrez et al. (2011) found 33% of their sample of lenticulars showed a type I profile, whilst only 10% of spirals in the field do, and that the frequency of type II profiles increases from 25% to 80% for the lenticular and spiral samples, respectively. However, Maltby et al. (2015) find remarkably similar frequencies of type I/II/III profiles in both the cluster and field environments surrounding Abell 901/902 and conclude that the stellar distribution in S0 galaxies are not drastically effected by environment. Nevertheless they did find a weakening of breaks in the sense that the ratio of inner to outer scale-length decreases and suggest that the transformation of spirals to lenticulars may entail the disappearance of breaks. These studies imply that environmental processes driving the evolution of lenticulars may also be responsible for the light-profile properties, which may give insight into which formation mechanism is more important.

1.2.4 Warps

One of the more interesting phenomena occurring in the outer regions of spiral discs is warping, where when viewed edge-on the galaxy is not a flat disc. Warps generally fall in two categories, S-type (sometimes also referred to as integral shape), where one side rises above the plane and the opposite side declines, and U-type, where both sides rise. There are some cases of warps that may not affect both sides of a galaxy equally and instead form an L-shape (Sánchez-Saavedra et al. 2003).

Our galaxy has been known to be warped since the mid-1950s when Burke (1957) and Kerr (1957) demonstrated, using 21-cm surveys, that the plane tilts towards the Large Magellanic Cloud in the southern hemisphere. Similarly Newton & Emerson (1977) found M31 is also warped into an S-shape and surveys outside of the Local Group have suggested that virtually all spiral galaxies are warped to some

extent (Sancisi 1976; Bosma 1978; Sanchez-Saavedra et al. 1990; Reshetnikov et al. 2002). Many extended spiral galaxies exhibit warped structure, including 20 out of 26 galaxies in the WHISP survey (García-Ruiz et al. 2002) and all of the Local Group disc galaxies (Kuijken & Garcia-Ruiz 2001).

Briggs (1990) used observational data from twelve warped galaxies and constructed three rules for warp behavior:

1. The warp develops between R_{25} and R_{Ho}, the Holmberg radius, where the B-band surface brightness is 26.5 mag/arcsecond^2.

2. The line-of-nodes is straight within R_{Ho} and

3. Outside of R_{Ho} the line-of-nodes forms a loosely wound, leading spiral.

One of the key findings from Brigg's work is that gas only exhibit strong warps when they extend past the optical region of the galaxy. Warps are thought to form through torquing of the disc due to cosmic infall (Ostriker & Binney 1989; Quinn & Binney 1992; Jiang & Binney 1999; Shen & Sellwood 2006), from misalignment of angular momentum between the disc and the dark matter halo (Debattista & Sellwood 1999), from satellite perturbations (Weinberg & Blitz 2006) or from halo torquing of in-falling gas (Roškar et al. 2010). The exact formation mechanism is likely dependent on a variety of factors and it is unlikely that one of these mechanisms is solely correct.

Observations have shown that the star-formation in the outer regions of disc galaxies is generally very low, but extended ultraviolet (XUV) discs have been detected in the outskirts of many galaxies (for examples see Verdes-Montenegro et al. (2002); Thilker et al. (2005, 2007); Sancisi et al. (2008); Bush et al. (2014)), implying that there must be some star formation past the Hα cutoff (Kennicutt 1989), which may be triggered by minor interactions (Bush et al. 2014) or by cold gas

inflows (Holwerda et al. 2013). Due to inside-out growth, these extended regions probe current disc assembly and so are invaluable for studying galaxy evolution.

1.3 Radial migration

At their time of birth stars inherit the properties of their parent gas clouds and thus their orbits are nearly circular, because gas can dissipate excess energy efficiently. Orbits of young stars were thought to be nearly circular, only deviating due to eccentricity arising from heating. Under the epicyclic approximation, the change in radius about the guiding centre is given by $\Delta R \simeq \sqrt{2}\sigma_R/\kappa$ (equation 3.99 Binney & Tremaine (2008)), where σ_R is the radial velocity dispersion and κ is the epicycle frequency. Velocity dispersion increases with age (Holmberg et al. 2009), so the oldest stars will have the greatest radial excursions. Typically for stars in the Solar neighborhood $\sigma_R \sim 50$ kms^{-1} (Holmberg et al. 2009) and thus the largest excursions, given $\kappa \simeq 37$ km s^{-1}kpc^{-1} (Binney & Tremaine 2008) are $\simeq 2$ kpc.

Sellwood & Binney (2002) showed that a relationship existed between a change in angular momentum and the induced change in guiding radius of stars interacting with transient spiral structures. Importantly, at corotation resonance this relationship, known as radial migration, allows stars to increase or decrease their galactocentric radii without causing an increase in eccentricity, allowing for a large redistribution of stars without heating the disc. Since disc galaxies have a multitude of transient spirals with a wide range of pattern speeds (Hockney & Brownrigg 1974; Sellwood & Carlberg 1984; Roškar et al. 2012), this allows for a large redistribution of the stellar content across the disc.

In a rotating frame of a spiral perturbation there is an invariant known as Jacobi's integral, E_J, defined as [equation 3.112 (Binney & Tremaine 2008)]:

$$E_J = E - \Omega_p L \tag{1.4}$$

where E is the specific energy, L is the specific angular momentum and Ω_p is the pattern speed of the perturbation. Changes in angular momentum and energy must therefore be related as

$$\Delta E = \Omega_p \Delta L. \tag{1.5}$$

For a certain increase in energy, a fraction will cause changes in the random motion, and the remaining will change the circular motion. If we define J_R as any parameter that quantifies radial kinetic energy then

$$dE = \frac{\partial E}{\partial J_R} dJ_R + \frac{\partial E}{\partial L} dL. \tag{1.6}$$

Following the arguments by Sellwood & Binney (2002), if J_R is chosen to be the radial action, the partial derivatives above become the frequencies, ω_R and Ω, of a star's radial and azimuthal motion. So

$$\Delta E = \omega_R \Delta J_R + \Omega \Delta L. \tag{1.7}$$

Combining Equations 1.5 and 1.7 gives

$$\Delta J_R = \frac{\Omega_p - \Omega}{\omega_R} \Delta L. \tag{1.8}$$

At corotation resonance, where $\Omega = \Omega_p$, changes in angular momentum do not cause changes in J_R. We show in Figure 1.6 the classical Lindblad diagram, which helps understand this phenomenon. The solid line shows orbits that are perfectly circular, whilst moving away from this line into the white region shows increasingly eccentric orbits. The grey area shows orbits that are inaccessible. It is clear from Equation 1.7 that changes in energy move stars on trajectories that have slope Ω_p (dashed line). At corotation, this change does not move away from the circular orbit line to first order, whilst exchanges in energy away from corotation do.

In essence, stars exchanging angular momentum and energy at corotation remain on nearly circular orbits, which differs from traditional heating mechanisms. It is important that the star is traveling at the same rotational velocity as the spiral

(i.e. in corotation with the spiral), otherwise it will overtake the density wave or be overtaken by it and no energy will be transferred. It is also important that the spirals causing this exchange are transient, otherwise the star would be trapped. A star on the inside of the corotation radius will gain angular momentum where it will pass outwards, where the over-density will then pull the star back into the inside. Radial migration leaves no imprint on the in-plane kinematics, so observationally quantifying the amount of migration is difficult from purely kinematical data. Furthermore, reconstructing the galactic history is also difficult since we can no longer consider each radial annulus to evolve in isolation.

An important implication of migration may be that the picture of inside-out growth may be more complex than first thought. Roškar et al. (2008a) showed that the post-break region of a MW-like simulation was populated by stars that formed interior to the break, and migrated outwards. This results in an upturn in the average age. Interior to the break, age decreases with increasing radius as expected, but at the break radius a strong upturn in average age is seen. Migration is a random walk and as such older stars have more time to move further away from their birth location, resulting in the outer disc being predominantly populated by the older stars. These age upturns have been confirmed observationally by integral field spectroscopy of NGC 6155 (Yoachim et al. 2010), and via HST/ACS resolved stellar photometry of NGC 7793 (Radburn-Smith et al. 2012) and M33 (Williams et al. 2009).

Other mechanisms for radial migration have also been suggested. An overlap in the resonances between bars and spiral arms (Debattista et al. 2006; Minchev & Famaey 2010; Minchev et al. 2011) or disc perturbation from cosmologically accreted satellites (Quillen et al. 2009; Bird et al. 2012) have been shown to cause large changes in radial distribution of stars born at a given radii. Whilst these mechanisms have been shown to cause migration, Sellwood & Binney (2002), Roškar et al. (2008b,

2010) and Solway et al. (2012) have shown that even without bars, and in an isolated context, the redistribution of stars is efficient. It is most unlikely that a single mechanism is dominant and instead a combination is prevalent in nature. However, migration via accretion has been shown to heat the disc beyond observed limits in the Milky Way (Roškar et al. 2012). The velocity dispersion of stars in the local neighbourhood is a necessary constraint on any model of galactic evolution.

It has long been established that there is a correlation between age and the velocity dispersion of stars (e.g. Carlberg et al. (1985); Nordström et al. (2004)). Young stars are kinematically cold, whilst older stars are hotter. There are many mechanisms proposed to explain this heating, but the two main ones are from scattering from giant molecular clouds (Spitzer Jr. & Schwarzschild 1951, 1953) or scattering via spiral arms (Barbanis & Woltjer 1967; Carlberg et al. 1985). The relative importance of these mechanisms is not well understood, however Jenkins & Binney (1990) reproduced with acceptable agreement the Solar neighbourhood velocity dispersion. Understanding the causes of such increases can give insight into the history of the Milky Way.

1.4 Thick disc formation

A thick disc component has been found in our own galaxy (Gilmore & Reid 1983) and in external galaxies (Burstein 1979; Pohlen et al. 2004; Comerón et al. 2011), where it is necessary to fit two exponentials to the vertical density profile, with the thick component having a longer scale height (Chen et al. 2001; Larsen & Humphreys 2003). The thick disc also manifests as an older (e.g. Bensby et al. (2005)), kinematically hotter (e.g. Chiba & Beers (2000)), α-enhanced population (Fuhrmann 1998; Prochaska et al. 2000; Lee et al. 2011) that is seen to lag behind the rotation of the thin disc. However, work by Bovy et al. (2012b) has argued that the MW

may have no distinct thick disc and is instead a continuous superposition of single-exponential mono-abundance populations. This leads to a regime where the disc grows "inside-out" and "upside-down". Similar mono-abundance sub-populations have been found in other N-body studies (Bird et al. 2013; Stinson et al. 2013; Roškar et al. 2013). The origin of the thick disc is still largely unknown, with many mechanisms seemingly able to reproduce the observational trends. It is possible that it formed via an accreted population from tidally stripped satellites (Abadi et al. 2003) or is an older disc component that has been heated via minor mergers (Quinn et al. 1993; Kazantzidis et al. 2008). Outwardly migrating stars have been shown analytically (Schönrich & Binney 2009a,b) and through N-body simulations (Loebman et al. 2011) to reach larger heights above the plane, creating a thicker disc component. Stars migrating outwards feel a decreased vertical restoring force because, on average, they conserve their vertical actions (Solway et al. 2012). Minchev & Famaey (2010) argued that migrating particles change their properties to match the local population, and thus cannot form a thick disc population. Migration has been shown to be reduced by vertical motions but the maximum changes in radius are similar for thick and thin disc stars (Solway et al. 2012). Finally, Brook et al. (2004) formed a thick disc component from accreted stars during a period of gas rich merging at high red-shift which match observations of the Milky Way thick disc.

It is not clear which of these formation mechanisms is dominant and it is possible that all are capable of producing a thick disc which matches observation. Sales et al. (2009) studied four published simulations of discs with varying formation mechanisms; accretion from satellites (Abadi et al. 2003), heating via minor mergers (Villalobos & Helmi 2008), radial migration (Roškar et al. 2008a,b) and in-situ formation during a gas-rich merger (Brook et al. 2004). They found that there is a difference in orbital eccentricities dependent on which mechanism forms the thick disc. If it formed via migration, heating or the gas-rich merger scenario, then the

distribution of eccentricities will peak at low values. In comparison, this distribution is broader and tends towards higher eccentricities if the thick disc has formed from an accreted population. This study was followed up observationally by Wilson et al. (2011) using the Radial Velocity Experiment (RAVE) dataset, who found that the observed eccentricity distribution peaked at lower eccentricities, thus favouring a non-accretion scenario.

1.5 Chemical evolution

Stars fuse hydrogen and helium into heavier metals (Burbidge et al. 1957) that are ejected back into the interstellar medium via stellar winds and supernovae. The next generation of stars form with the metallicity of this enriched gas and the overall metal content of stars will increase as a function of time. The rate at which this enrichment occurs will depend on a variety of factors including the initial mass distribution, the gas inflows and outflows, and the specific rate at which supernova explode. Since stars only undergo nuclear fusion in their cores, their surface (and thus observed) metallicity is indicative of their formation properties. Being able to model the chemical evolution within our Galaxy is an important constraint on the history of the Milky Way. The first models used a closed-box approach, in which material can neither enter or escape the model, leading to few metal-poor stars, known as the G-dwarf problem. These models in fact also under produce K-dwarfs (Casuso & Beckman 2004) and M-dwarfs (Woolf & West 2012) as well. This is solved by opening up one side of the "box" and allowing gas-infall (Tinsley 1975, 1977). For the simulations contained within this thesis, the gas cools from the large halo surrounding the disc, which approximates the cosmological context that real galaxies form in, alleviating this problem, whilst allowing us to keep the resolution high. Furthermore, the galaxies analysed have been shown to match the metallicity distribution function of the Milky Way as observed by APOGEE (Loebman et al.

2016).

A further constraint on galactic chemical evolution models is the age-metallicity relation (AMR). Under the premise that each annulus of a galaxy evolves in isolation we would expect the gradual enrichment of the interstellar medium to build an AMR. In essence, the oldest stars should be metal poor, having formed in the early universe, whilst young stars should show the most metal enrichment. Observational surveys have shown that the AMR is flatter and broader than expected (Edvardsson et al. 1993; Nordström et al. 2004; Haywood 2008). In all these spectroscopic surveys the limiting uncertainty is in the age estimation, with errors usually of the order $\pm 1.5 - 2.0$ Gyr, given that it requires an accurate knowledge of the stellar mass. Recently, Casagrande et al. (2015) used asteroseismology data from Kepler to age red giants, dramatically decreasing the uncertainty (typical errors on age are 20%), and found a similarly flat and broad AMR. Nordström et al. (2004) investigated whether eccentricity alone could account for the broadened AMR, but concluded that it could only contribute up to 50% of the observed scatter. The AMR is flattened due to contamination of annuli, bringing stars of different metallicity into a region, and polluting the inherent AMR.

Observations of M31 have shown that the warped region displays a strong relation between age and metallicity (Bernard et al. 2012, 2015), implying that the warp either lowers the efficiency of migration, or does not experience migration at all. It is the inclusion of a warp and its effect on the AMR we address in this thesis.

1.6 Simulations

Galaxy simulations are broken up into two major categories, N-body, where only the gravitational interaction of particles is considered, and hydrodynamical, where as well as gravitation, the evolution of gas into stars, feedback and enrichment must also be accounted for.

CHAPTER 1

The first N-body simulations were carried out by Holmberg (1941) using arrangements of 37 lightbulbs to understand the tidal interaction of two merging spiral galaxies. It took 3 decades for von Hoerner (1960) to implement the first fully computational N-body simulation with a paltry $N = 16$ particles, closely followed by Aarseth (1963) at $N = 100$. Ever since then we have approximately doubled the number of particles every two years in accordance with Moore's Law (Moore 1965) and now we find it possible to run collisionless simulations of the order $N = 10^9$.

By adapting code to approximate the gravitational calculation, it is possible to reduce computation times without increasing the number of processors. One of the most popular currently is the tree algorithm pioneered by Barnes & Hut (1986). Older codes such as those used by von Hoerner (1960) and Aarseth (1963) used direct integration between each particle, which is $\mathcal{O}(N^2)$. Instead the tree algorithm begins by creating a structure which is recursively sub-divided into eight equally sized cubes until only one particle is in each cell. The code then traverses this tree and at each stage checks if an "opening angle" criterion is satisfied where $l/D < \theta$ where l is the cell length, D is the distance between the particle and the cell centre of mass and θ is an accuracy parameter usually ~ 1. If the criterion is not satisfied, then the box is opened up into its sub-cells, and conversely if it is satisfied the particles contained within the cell are grouped into a pseudo-particle with centre of mass equivalent to the constituent particles. This essentially serves, for particles at a large distance and close together, to reduce the number of calculations that have little effect based on their relative separation. This new calculation is $\mathcal{O}(N \log N)$.

Even with the major increases in computing power over the past decades, simulations still have resolution limitations. In most cases a single particle will actually represent a larger mass, for example in the simulations discussed in this thesis, a typical particle will have mass $\sim 10^6 M_\odot$. This causes two problems when simulating

galaxies. Firstly, short-range interactions between particles can create binary systems, which is unphysical given that each particle represents something of the order of a globular cluster. Furthermore, close encounters between particles can lead to large-angle scattering, which is unphysical, as well as needing a short integration time, which would cause the simulation to be computationally very expensive and time consuming. One popular way to overcome this is to apply a Plummer softening, ϵ, into the gravitational force calculations. The force then becomes:

$$F \propto \frac{1}{(r+\epsilon)^2} \tag{1.9}$$

where F is the force and r is the separation between particles. This serves to reduce the force during close encounters, and suppresses these large-angle interactions. The minimum softening needed to prevent large deflections is given by White (1979) as:

$$\epsilon \sim \frac{G\mu}{\sigma^2} \tag{1.10}$$

where μ is the average particle mass and σ is the typical velocity dispersion.

1.6.1 Smoothed particle hydrodynamics

To properly trace the metal content of galaxies, we also include the effects of gas, using smoothed particle hydrodynamics (SPH) (Monaghan 1992). One of the key reasons to use SPH is that it explicitly conserves angular momentum, making it particularly useful for modelling astrophysical discs (Wadsley et al. 2004). SPH was first developed by Lucy (1977) and Gingold & Monaghan (1977). In the simulations in this thesis our SPH smoothing kernel length, h, is set so there are a fixed number of particles, $N_{\rm smooth}$, in twice the smoothing length, where $N_{\rm smooth}$ is set to 32 (Stinson et al. 2006).

One particularly interesting addition to SPH is the inclusion of feedback mechanisms. As stars form, only a fraction of the gas is used up, whilst the remaining gas is blown into the interstellar medium via the pressure from the stellar wind.

Supernova also provide a source of feedback into the interstellar and intergalactic medium. They can heat the gas to temperatures in excess of $T \gtrsim 10^6$ K, which is sufficient enough for it to be ejected from the galaxy (Dekel & Silk 1986) and also serve to regulate star formation, since they heat the surrounding gas around the star forming region, preventing further gas from collapsing (Silk 2003). Because of resolution limitations, feedback cannot be modelled specifically, and instead a sub-grid prescription must be used. Early simulations attempted to model supernova feedback by injecting the 10^{51} ergs of energy into the surrounding particles (e.g. Katz et al. (1992)), however this is quickly radiated away, leaving no effect on the ISM and meaning star formation rates were higher than observations indicated (Katz et al. 1996). Early attempts to overcome this problem tried preventing the surrounding gas particles from cooling (e.g. Thacker & Couchman (2000)), allowing the supernova energy to heat the surrounding gas and regulating the star formation rates (Brook et al. 2004). Extending this, Stinson et al. (2006) applied a blastwave approximation based on Chevalier (1974) and McKee & Ostriker (1977). This calculates the maximum blastwave radius, and uses this as the radius in which to prevent cooling. The cooling time is determined based on the phases of the supernova. Realistically this phase should last as long as the Sedov phase, where there is no efficient radiation, however this only lasts a few thousand years (Padmanabhan 2001), far below our time resolution. Instead we use a cooling time equivalent to the snowplough phase of the supernova, where momentum is conserved as the blastwave expands (McKee & Ostriker 1977), and has been shown to produce realistic galaxies (Stinson et al. 2006). Other mechanisms may also be used, such as adding the SN energy as a kinetic component (Navarro & White 1993) or by using a multiphase ISM (Yepes et al. 1997; Hultman & Pharasyn 1999; Springel & Hernquist 2003).

1.7 Context for this thesis

Whilst the mechanisms driving migration have been investigated, both theoretically (e.g. Sellwood & Binney (2002)) and through simulations (e.g. Roškar et al. (2008b); Minchev & Famaey (2010); Loebman et al. (2011)), its impact is not yet fully understood. These works showed that migration can have significant influence on the chemical and structural properties of the galaxy and that we can no longer consider each radial annulus to be distinct from its neighbours. This thesis intends to address whether the inclusion of a warp has any impact on these properties. Of particular interest is the HST observations of the M31 warp (Bernard et al. 2012, 2015), which shows a strong correlation between age and metallicity, implying that migration does not occur in these regions. We will look for similar AMRs in N-body+SPH simulations of warped galaxies and attempt to understand how they form and investigate if this has any impact on the disc AMR. It is important to understand the implications of migration on the secular evolution of disc galaxies so that we may interpret and understand upcoming surveys such as GAIA (Perryman et al. 2001; Lindegren et al. 2008), GAIA-ESO (Gilmore et al. 2012) and the Large Synoptic Survey Telescope (LSST) (Ivezic et al. 2008).

Type II density profiles have been shown to be caused by a star formation threshold due to a drop off in the cold gas surface density. The extended profiles are then built up from migrating stars. As such the outskirts of disc galaxies are affected significantly by migration. Observations have shown that the frequency of type II profiles decreases in cluster environments. This thesis will test theoretically if these transformations are a by-product of both star formation termination due to ram pressure stripping and increased migration due to an increase in spirals induced by the cluster environment.

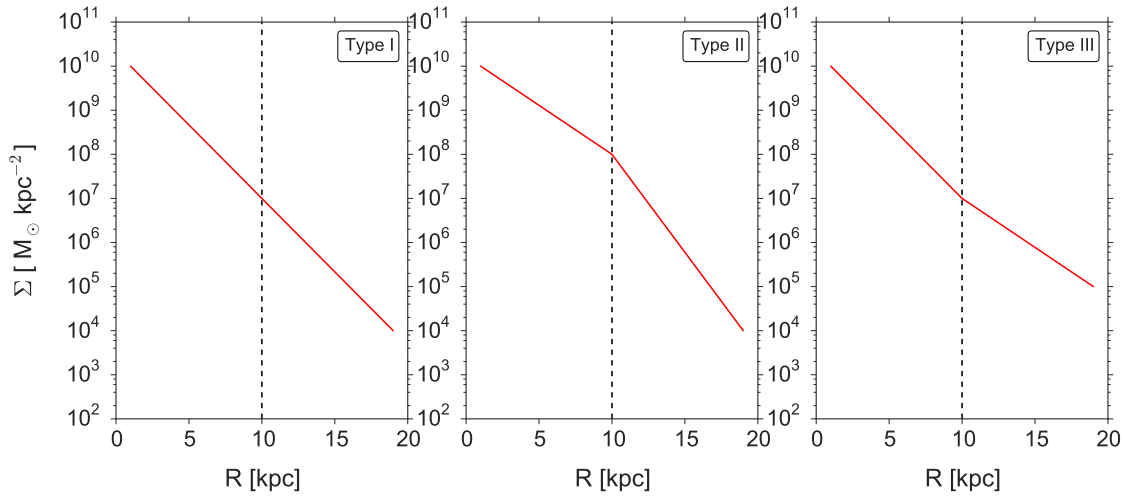

Figure 1.5: Schematic of profile types. Type I shows a single exponential out to large radii. Type II and III show breaks in their profiles with truncated and anti-truncated outer slopes respectively.

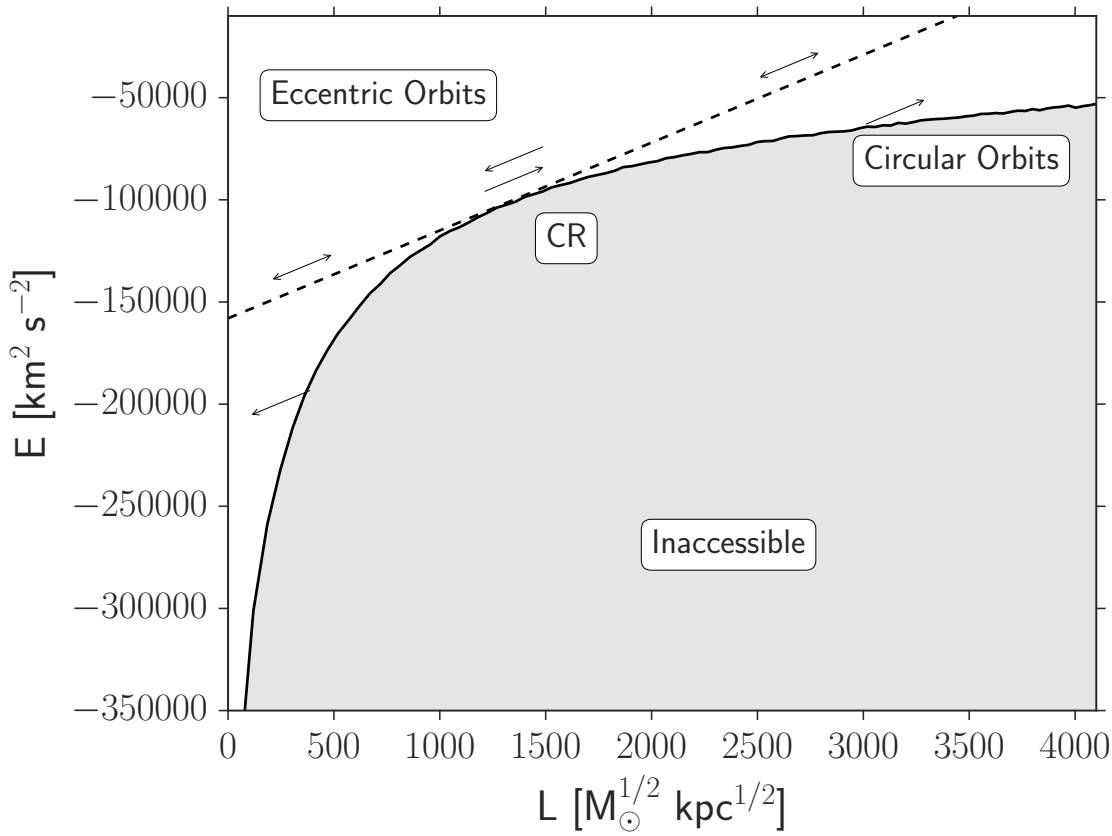

Figure 1.6: Classical Lindblad diagram. The solid line shows circular orbits and the grey region shows inaccessible orbits. The dashed line indicates a possible pattern speed for a spiral.

Chapter 2

The origin of type-I profiles in cluster lenticulars

In this chapter, we present results from N-body+SPH simulations of a spiral galaxy falling into a cluster, where it experiences ram pressure stripping, eventually quenching the star formation in the disc. We consider the changes to the density profile compared to the same galaxy evolving in isolation. We demonstrate that the mechanism driving the differences is radial migration, and consider the effect this has on the age and metallicity profiles.

2.1 Simulations

Our simulation consists of an infalling galaxy embedded within a cluster sized halo including its hot gas corona. The initial conditions for the galaxy are the same as those used in Roškar et al. (2008a,b), beginning with a spherical NFW dark matter halo (Navarro et al. 1995) and an embedded spherical corona of gas with a temperature approximating hydrostatic equilibrium. We impart an angular momentum, $j \propto R$, to the gas to promote disc formation, with a spin parameter of $\lambda = 0.065$ (Bullock et al. 2001). The dark matter consists of two shells, the inner

containing 9×10^5 particles of mass 10^6 $M_\odot$ extending to 200 kpc and the outer containing 1×10^5 particles of mass 3.5×10^6 $M_\odot$. There are 10^6 gas particles, each with mass 1.4×10^5 $M_\odot$. The total mass within the virial radius (R_{200} = 200 kpc) is 10^{12} $M_\odot$. We use a softening of 50 pc for the gas and stars, and 100 pc for the dark matter. Roškar et al. (2008b) tested these parameters for numerical robustness and concluded that they represented a compromise between resolution and computational cost, whilst producing realistic Milky Way analogues (e.g. Roškar et al. (2008a, 2012); Loebman et al. (2011, 2016)).

The cluster environment is set up to mimic the Fornax cluster. The virial radius is set to 0.7 Mpc and the virial mass enclosed is 6×10^{13} $M_\odot$ (Ikebe et al. 1992; Drinkwater et al. 2001; Nasonova et al. 2011). We model the cluster with 9×10^6 dark matter particles of mass 4×10^6 $M_\odot$ in the inner shell, extending to 700 kpc, and 10^6 dark matter particles of mass 2×10^7 $M_\odot$ in the outer shell. There are 2×10^7 gas particles in the cluster, each of mass 2.3×10^5 $M_\odot$. The softening lengths are set to match the infalling galaxy. We prevent the cluster gas from cooling to mimic the episodic AGN feedback which prevents star formation in the centres of massive clusters (Binney 2004). This also prevents star formation in the cluster, reducing computational expense, since we are only interested in the effect the hot gas environment has on the infalling galaxy.

We initially place the galaxy at three times the cluster virial radius, to allow the galaxy to form a disc before the ram pressure stripping commences. We give the galaxy a velocity of 190 kms^{-1}, directed at 60° to the cluster centre, targeting periapsis at 150 kpc. We refer to this simulation as the "cluster" model. We use the isolated simulation of Loebman et al. (2011) as a comparison model, which is similar to the models of Roškar et al. (2008b,a), but includes the effects of metal diffusion between gas particles (Shen et al. 2010). We refer to this simulation as the "isolated" model. We do not include the effects of diffusion in our cluster model. Finally we

present a third simulation, which we refer to as "quenched", where we turn off the star formation by hand in the isolated model, at $t = 6$ Gyr, corresponding to the time of peak stripping in the cluster model. This provides us a control simulation to test whether quenching alone causes profile transformations.

We evolve the simulations for 10 Gyr with the N-body + smooth particle hydrodynamics (SPH) code GASOLINE (Wadsley et al. 2004). We adopt star formation criteria where the gas density and temperature have to be greater than 0.1 cm^{-3} and less than 15000 K, respectively. The star formation and feedback cycles are initiated as described in Stinson et al. (2006), including the effects of both Type II and Type Ia supernovae. The energy is injected into the interstellar medium in the form of a sub-grid modeled blast-wave as described in Stinson et al. (2006). Stars form with 1/3 of the gas particle mass, corresponding to 4.6×10^7 M$_\odot$, and each gas particle can form multiple star particles. The minimum gas mass is set at 1/5 of its original mass. Once gas particles drop below this mass it is removed, and its mass is distributed to the surrounding particles. We refine our timesteps using $\delta t = \Delta t/2^n < \eta(\epsilon/a_g)^{1/2}$, where ϵ is the softening length and a_g is the particle acceleration at the current position. We use a refinement parameter $\eta = 0.175$ and a base time-step of 0.01 Gyr. The tree code opening angle $\theta = 0.7$. The SPH kernel is defined using the nearest 32 neighbours. These parameters have been previously shown to lead to realistic late-type galaxies (Roškar et al. 2012, 2013).

2.2 Profile changes

We show in the top panel of Figure 2.1 the mass enclosed within the inner 20 kpc of the cluster galaxy (solid lines) as a function of time compared with the isolated galaxy (dotted lines). Initially, the cluster and isolated models evolve in parallel. At ~ 4 Gyr the galaxy reaches a location in the cluster environment dense enough for ram pressure stripping of the cool gas to become strong, after which, the star

formation rate drops rapidly. A significant fraction ($\sim 10\%$) of dark matter is also lost from the inner 20 kpc. The vertical dashed line shows the time at which the galaxy is at periapsis, as shown in the bottom panel.

In the top panel of Figure 2.2 we compare the evolution of the surface density profiles of the isolated and the cluster galaxies. The isolated galaxy develops a type II profile due to the star formation threshold and outwardly migrating stars moving past the break radius (Roškar et al. 2008b). In comparison the cluster simulation loses the majority of its cold gas and exhibits a remarkably flatter, nearly type I profile. At early times the cluster galaxy exhibits a type II profile, with the break moving outwards, as is the case also in the isolated galaxy. Between 4 Gyr and 5 Gyr, when the galaxy is at periapsis and ram pressure stripping is strongest (as shown in Figure 2.1), the galaxy starts to transition from a type II to a type I profile. To verify that this transition is not related solely to a termination of star formation, we also show the hand quenched model's final surface density profile (solid thick black line). Simply turning off star formation does not cause a transition from type II to type I profile, although the break does become weaker, similar to the findings of Maltby et al. (2015), indicating that the termination of star formation may be responsible for the break weakening, but does not cause the transformation from type II to type I.

We show in Figure 2.3 the formation radius versus the final radius for our cluster simulation. Almost no stars form exterior to $\sim$ 10 kpc, yet the disc extends to around 18 kpc. Thus, some mechanism must be redistributing stars from the inner disc to the outer disc.

The bottom panel of Figure 2.2 shows velocity dispersions of the cluster galaxy (black) and the isolated galaxy (red). The cluster galaxy is not substantially hotter and has little to no additional vertical or tangential heating. Without a heating mechanism to move stars from the inner to the outer disc, we therefore look to

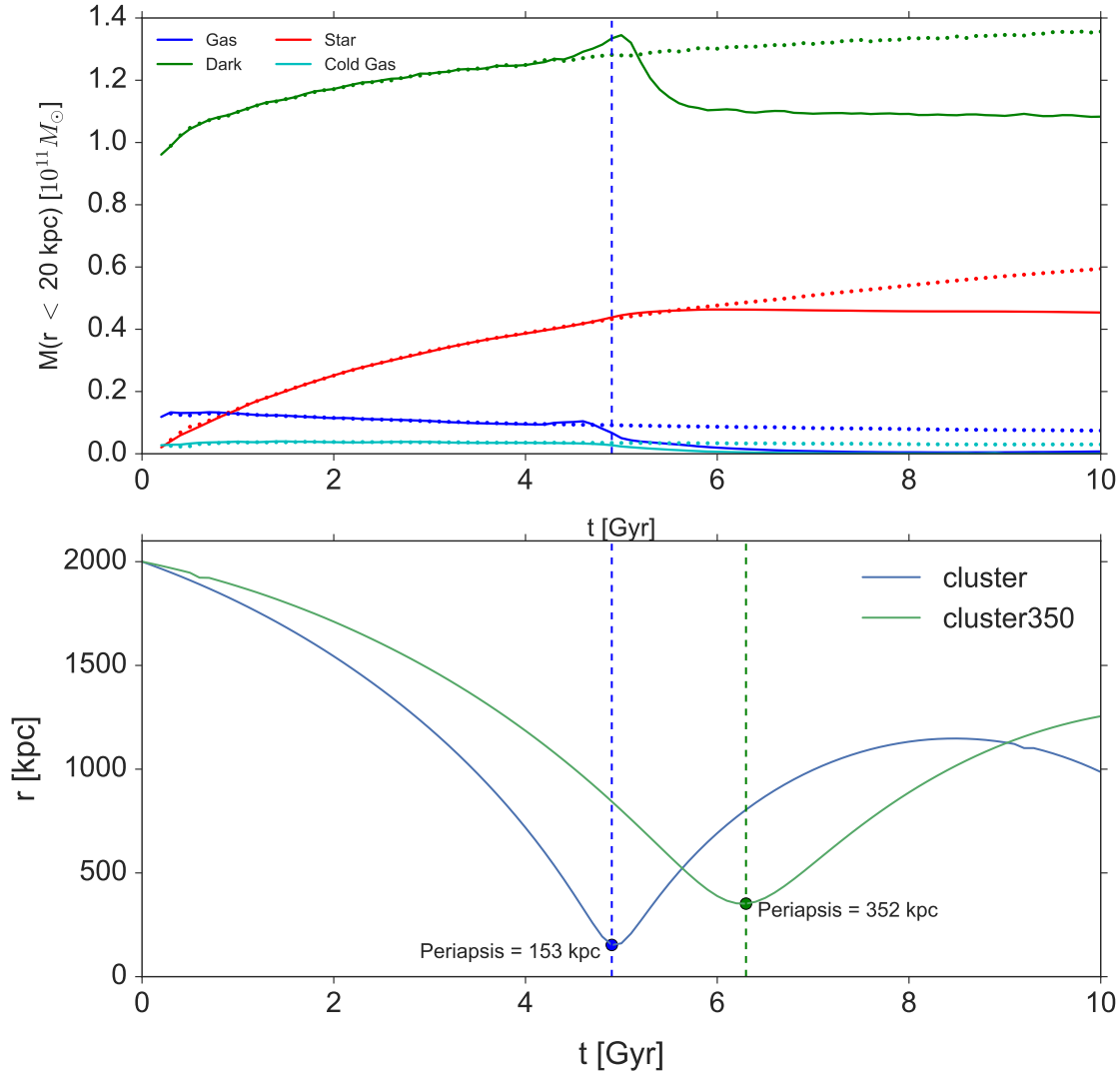

Figure 2.1: *Top*: Evolution of the mass enclosed within 20 kpc of the centre of the cluster galaxy (solid) as it falls into the cluster environment compared with the isolated galaxy (dotted). The blue line shows all gas particles whilst the cyan line shows only cool (T < 15000 K) gas. Green and red show the dark matter and stellar content respectively. *Bottom*: Cluster-centric radius as a function of time for the cluster galaxy (blue) and cluster350 galaxy (green). The vertical lines correspond to the time at which the galaxies are at periapsis.

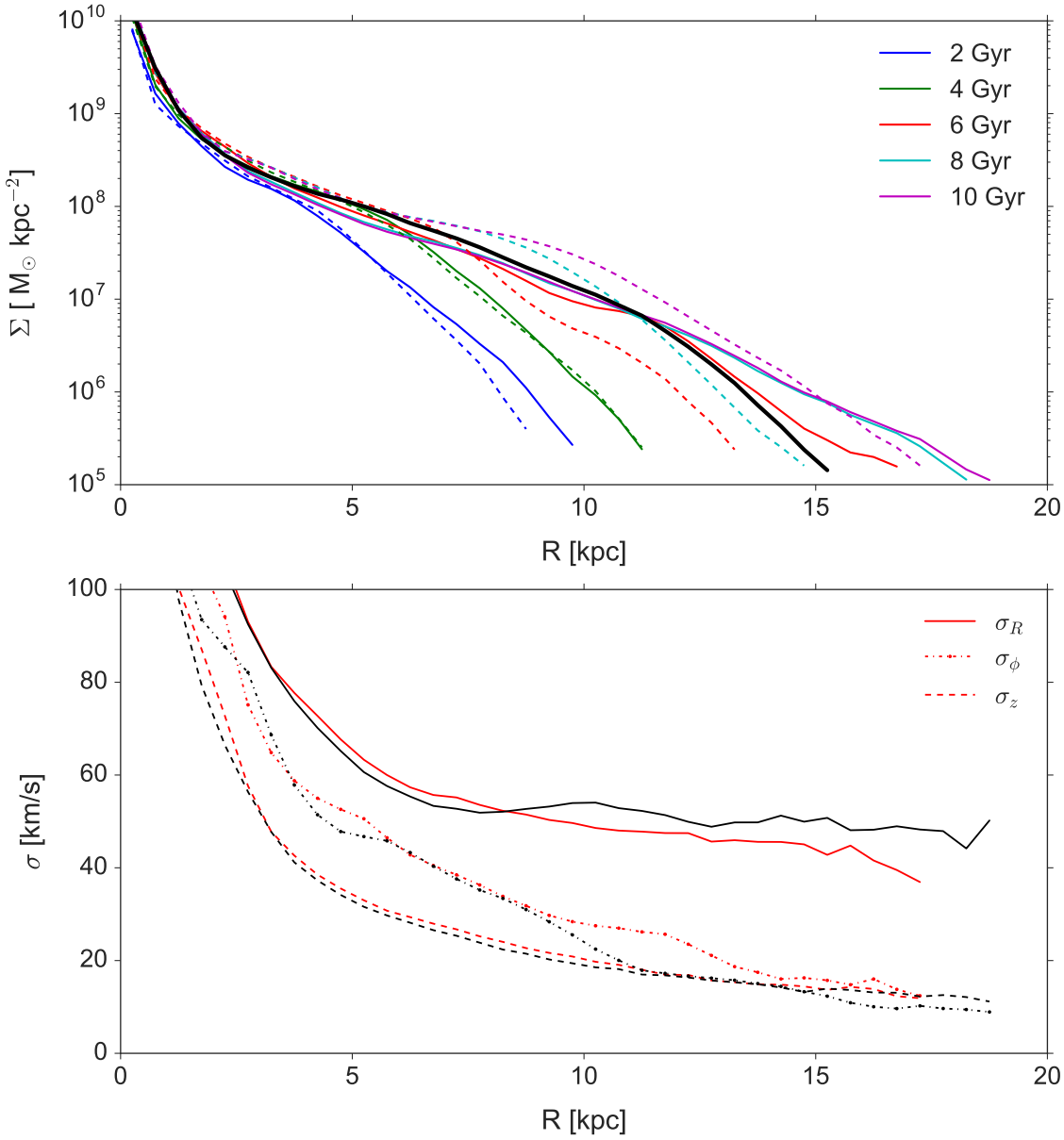

Figure 2.2: *Top*: Evolution of the surface density profile for the cluster galaxy (solid lines) and isolated galaxy (dashed lines). We also show the final surface density profile for the quenched model (solid thick black line). *Bottom*: Velocity dispersions in cylindrical coordinates for the cluster galaxy (black) and the isolated galaxy (red).

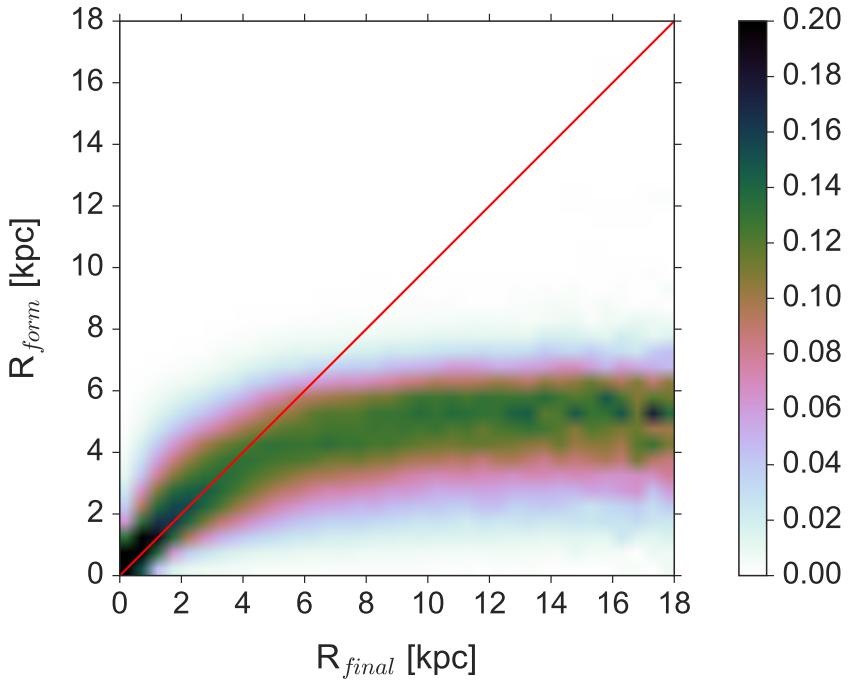

Figure 2.3: Mass weighted $R_{\rm form}$ versus $R_{\rm final}$ for our cluster simulation. Each column is normalised to unity by dividing by the total mass in each column. This helps to highlight the structure in the outer disc. The colour then represents the probability that a star will have that value of $R_{\rm form}$ given $R_{\rm final}$.

the transient spiral migration mechanism of Sellwood & Binney (2002) to explain the presence of stars at large radii. We define migrated particles as those with $|\Delta R| \geq 2.0$ kpc and non-migrating particles as those with $|\Delta R| < 2.0$ kpc.

In Figure 2.4 we show the mass profiles of migrated (solid lines) and non-migrated (dashed lines) populations for the cluster model (black) and the isolated model (red). At a radius of larger than ~ 10 kpc and ~ 12 kpc in the isolated model and cluster model respectively, the migrated population fraction is almost 100%. This implies that radial migration is an important mechanism to consider and will significantly change the properties of outer discs.

In Figure 2.5 we show the change in angular momentum for stars with a given starting angular momentum between t = 4.7 and t = 5.3 Gyr. In this space, strong spiral-driven migration manifests as a line of negative gradient (Sellwood & Binney 2002; Roškar et al. 2012). Particles with a positive Δj_z have moved outward, whilst particles with negative Δj_z migrate inward. Figure 2.5 shows that at the time corresponding to periapsis, there is a lot of outward migration induced in the cluster simulation that is not present in the isolated simulation. In the bottom panel we show a difference map between the cluster and isolated simulations, showing large ($\Delta j_z > 600$ kpc kms^{-1}) changes in j_z not seen in the isolated simulation. The outer feature cuts the x-axis at $j_z \sim 1850$ kpc kms^{-1} corresponding to a corotation radius of ~ 8 kpc; a $\Delta j_z \sim 600$ kpc kms^{-1} will then move stars out to a $R_{\rm final} \sim 12$ kpc. At this time, this is the extreme outer disc, so this mechanism can provide a plausible explanation for the profile transitioning from type II to type I. Figures 2.6 and 2.7 show further examples of strong outward migration between $t = 5.3 - 5.9$ Gyr and $t = 5.9 - 6.5$ respectively, corresponding to the time at which the ram pressure stripping is the most extreme. In Figure 2.8 we show the final output, showing that migration continues even after the galaxy has lost a significant fraction of its cold gas.

In the top panel of Figure 2.9 we show the age profile for the cluster simulation (black) and the isolated simulation (red). As shown by Roškar et al. (2008a), the age profile for the isolated simulation shows a decrease of mean age up to the break radius, and then an upturn in average age due to the migration of the older stars into the outer disc. In comparison, the cluster simulation shows a quite flat average age across the entire disc. An upturn is indicative of a star formation threshold and migration, whereas in the cluster simulation, the star formation has been quenched everywhere except in the very inner regions. Without star formation, migration will continue to mix the populations, flattening the age profile. In the bottom panel of Figure 2.9 we show the evolution of the metallicity profile for the cluster galaxy, where we find that the metallicity gradient becomes shallower everywhere at the time of the major stripping. The redistribution of the stars due to migration leads to a flattening of the <[Fe/H]> profile.

2.3 A second model

In order to assess whether parameters such as impact angle and galaxy orientation make a difference to the ram pressure stripping and induced spiral activity, we have run a suite of simulations, similar to our cluster model, but with varying initial orientation, and with different infall angles. We place the galaxy offset in the z-axis from the cluster centre. We vary the initial orientation of the galaxy by placing the disc in in the $x-y$, the $x-z$ or the $y-z$, planes. For each of these orientations we target three periapsis distances of 150, 350 and 450 kpc, by angling the galaxy velocity tangentially or inclined at $30°/60°$ respectively toward the cluster centre. Our previously discussed cluster model is in the $x-y$ plane with periapsis at 150 kpc. We show in the bottom panel of Figure 2.1 the cluster-centric radius for this model in green, indicating that periapsis occurs further out in the cluster and at a later time, when compared with the cluster model.

We present results from the $x - y$, 350 kpc model, which has been evolved for 10 Gyr, which we shall refer to as the "cluster350" model. Since this simulation has the same infall velocity, but is angled at a shallower angle we expect that the ram pressure stripping and tidal forces will be less severe, allowing us to test the importance of the disc stripping.

We show in Figure 2.10 the star formation histories for all the models discussed so far. We see that in both cluster galaxies, prior to significant mass loss, there is an increase in star formation, which we attribute to shock-compression of the gas. This is strongest in the fiducial model, but is also apparent in the cluster350 model. We find that star formation in the latter model, is quenched much more gently, but by 10 Gyr is forming stars at roughly half the rate ($\sim 2 M_{\odot} yr^{-1}$) as the isolated simulation.

The surface density profiles are shown in Figure 2.11, which compares our two cluster galaxies and the isolated galaxy at 10 Gyr. The cluster350 galaxy shows an extended profile compared with the isolated galaxy, yet still exhibits a type II profile with a break at $R \sim 9$ kpc. Nevertheless, the break appears to be weaker, implying that the mechanism for transforming from type II to type I profiles was not as strong, which we relate to the larger periapsis driving less induced spiral structure. Similarly to the cluster model and the isolated model, the cluster350 model is not substantially hotter in any direction.

The age profile shown in Figure 2.12 for the cluster350 model is not flattened to the same extent as the cluster model, instead showing a U-shape similar to the isolated galaxy. However, we find that the profile is intermediate between the isolated and cluster models further indicating that this galaxy is somewhere between evolving from a type II to a type I profile. The quenched model shows a flatter mean age profile than the isolated model, demonstrating that quenching and migration alone results in a flat age profile, without necessarily having a type I profile.

Recent CALIFA observations have observed minima in age profiles in both type I and type II galaxies (Ruiz-Lara et al. 2016), whilst previous studies have focused solely on galaxies with type II profiles.

These findings lead us to suggest that the orbital parameters are important to the profile transformations. Galaxies that fall closer to the centre of the cluster exhibit type I profiles and flat age gradients, whilst those with larger periapsides display properties that are intermediate between our two extreme cases. Since we have demonstrated that the galaxies that fall closer to the cluster centre are not substantially hotter, this relationship is a consequence of the increased tidal forces inducing spiral redistribution at smaller radii. There is also the possibility that infall orientation may also affect the induced spiral frequency and strength, but we cannot address that question with the pair of simulations presented here. The full suite of simulations is designed to address this question.

2.4 Conclusions

Using an N-body+SPH simulation of galaxies falling into a gas rich environment, we have shown that gas stripping and an increase in spirals causes a transition from a type II to a type I profile. Evolved in isolation, the model galaxy develops a type II, truncated, surface density profile, whilst the cluster galaxy evolves from a type II to a type I profile. Although the radial velocity dispersion is increased very slightly, it is not large enough to account for radial excursions of $\Delta R > 10$ kpc. Instead, we show that there is an increase in spiral activity induced by the environment causing larger radial migration. This serves to efficiently redistribute the material from the inner disc to the outer disc, whilst retaining nearly circular orbits.

This readily explains why type I profiles are found more commonly amongst cluster lenticulars, but does not explain how they occur in the field. We speculate that interactions between group galaxies may also induce strong spiral structure,

increasing the efficiency of migration in these galaxies too.

Finally, we have shown that in galaxies transitioning from type II to type I profiles, the age profile does not show the large upturn expected from star-formation threshold and migration (Roškar et al. 2008a). Instead the age profile becomes approximately constant across the disc, as does the metallicity profile.

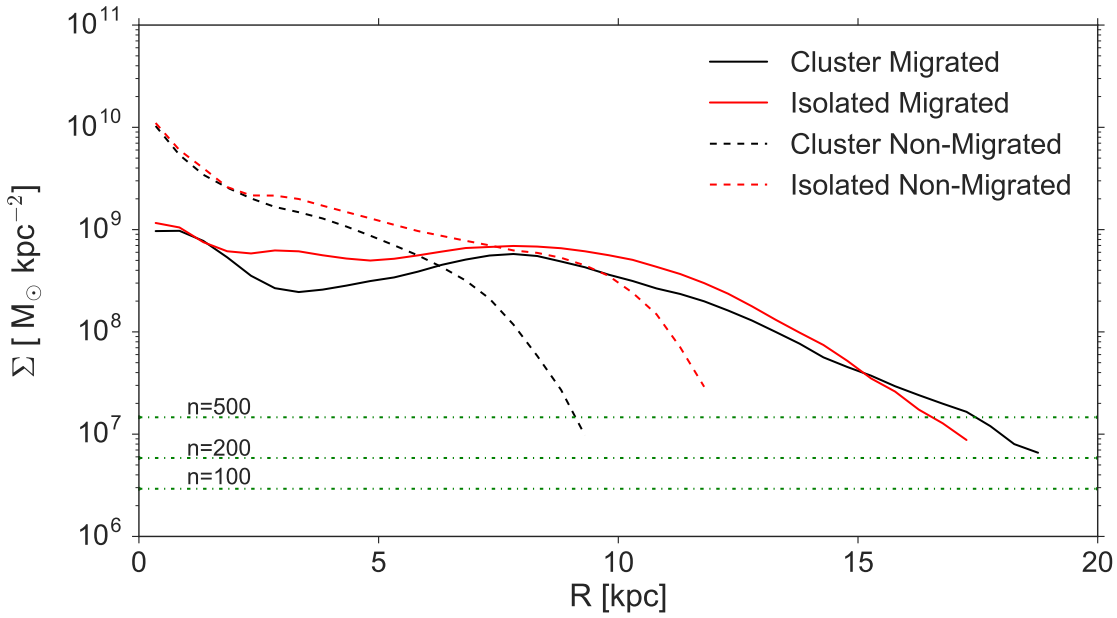

Figure 2.4: Mass distribution for migrating ($|\Delta R| > 2.0$ kpc) and non-migrating ($|\Delta R| < 2.0$ kpc) particles. The lines are described in the inset. The horizontal green lines indicate where 100, 200 and 500 particles with average mass would lie.

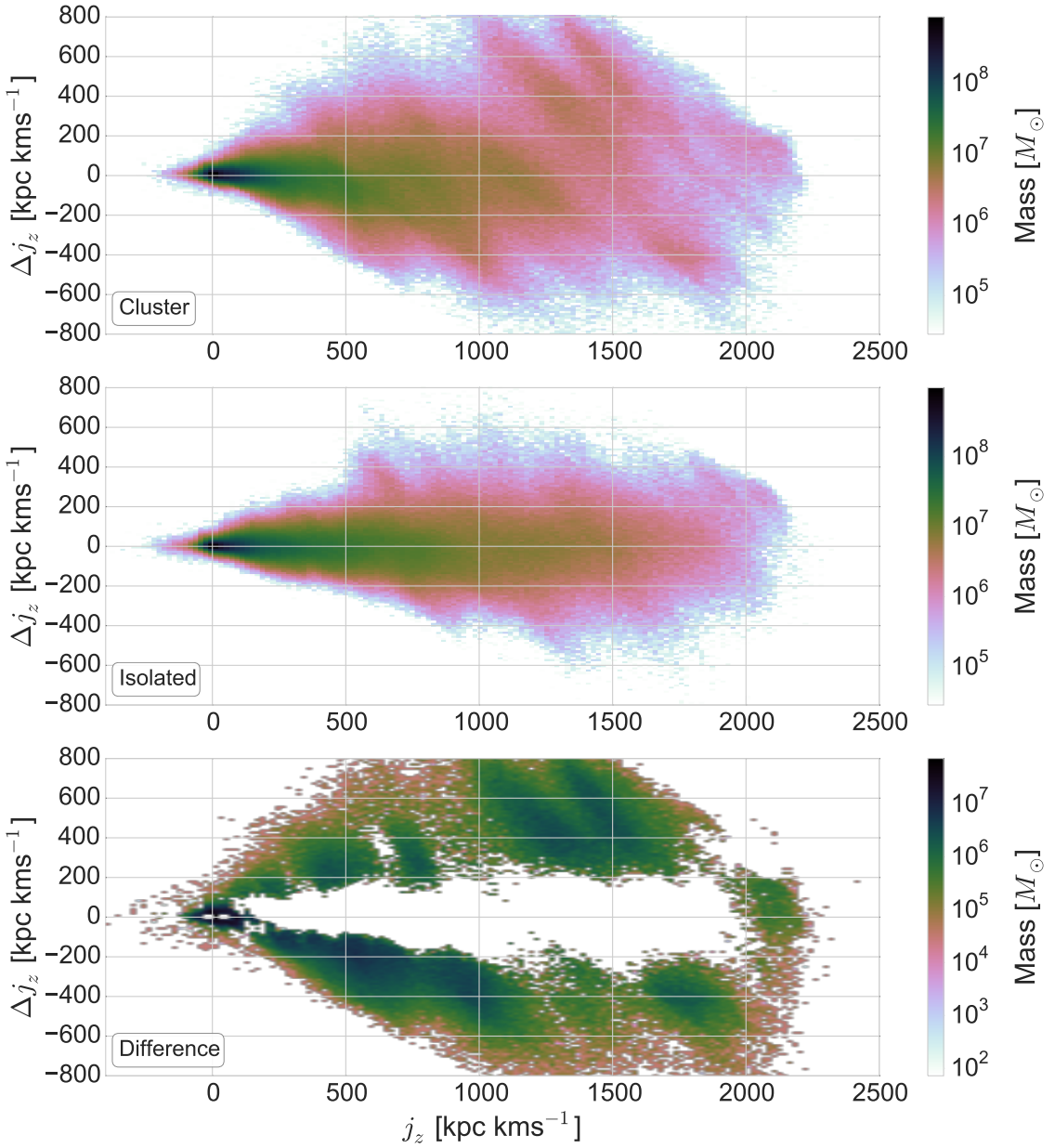

Figure 2.5: Mass weighted distributions of Δj_z given starting j_z between $t = 4.7 - 5.3$ Gyr for the cluster simulation (top), isolated simulation (middle) and the difference between the two (bottom).

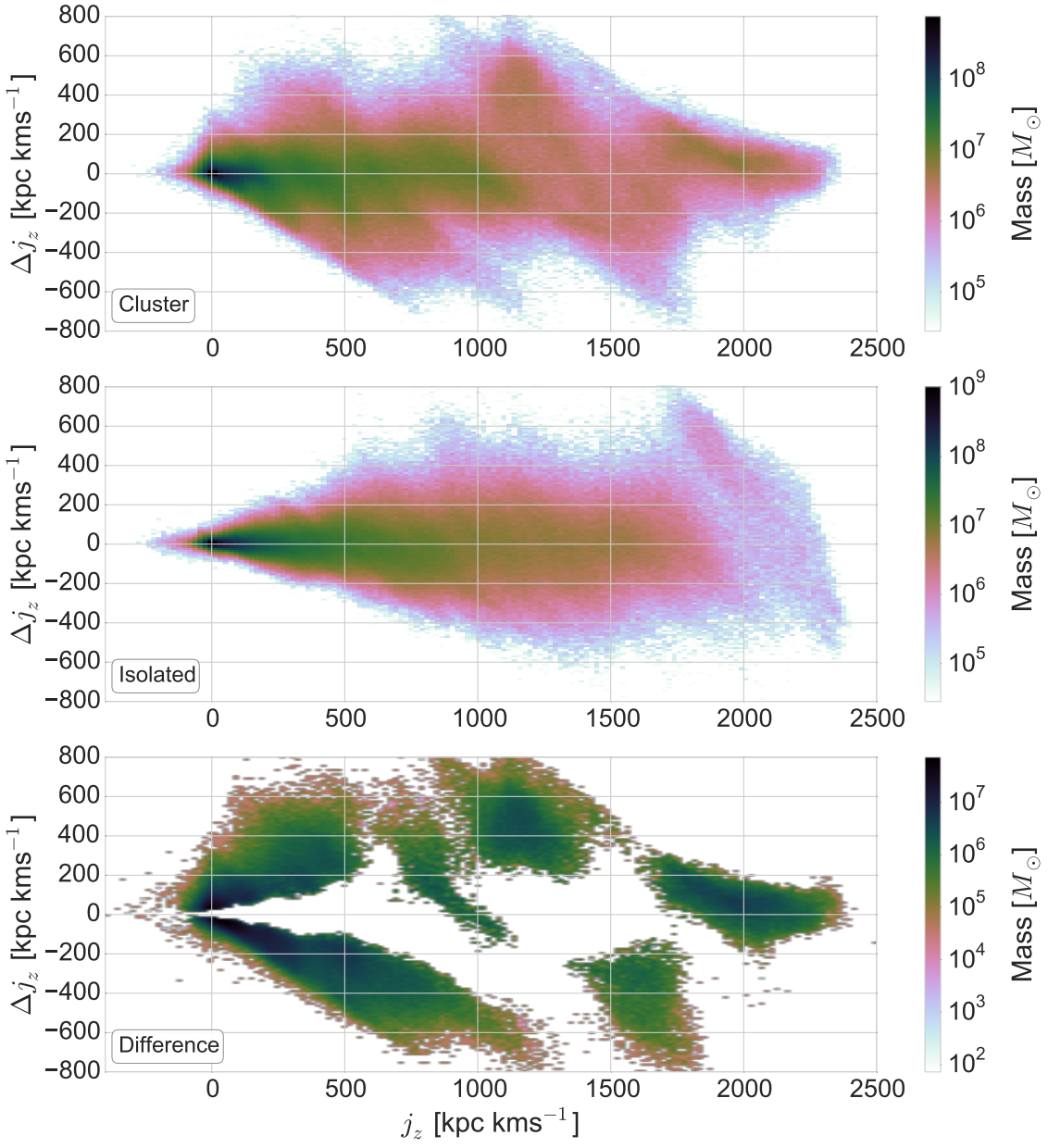

Figure 2.6: Same as Figure 2.5 but for $t = 5.3 - 5.9$ Gyr.

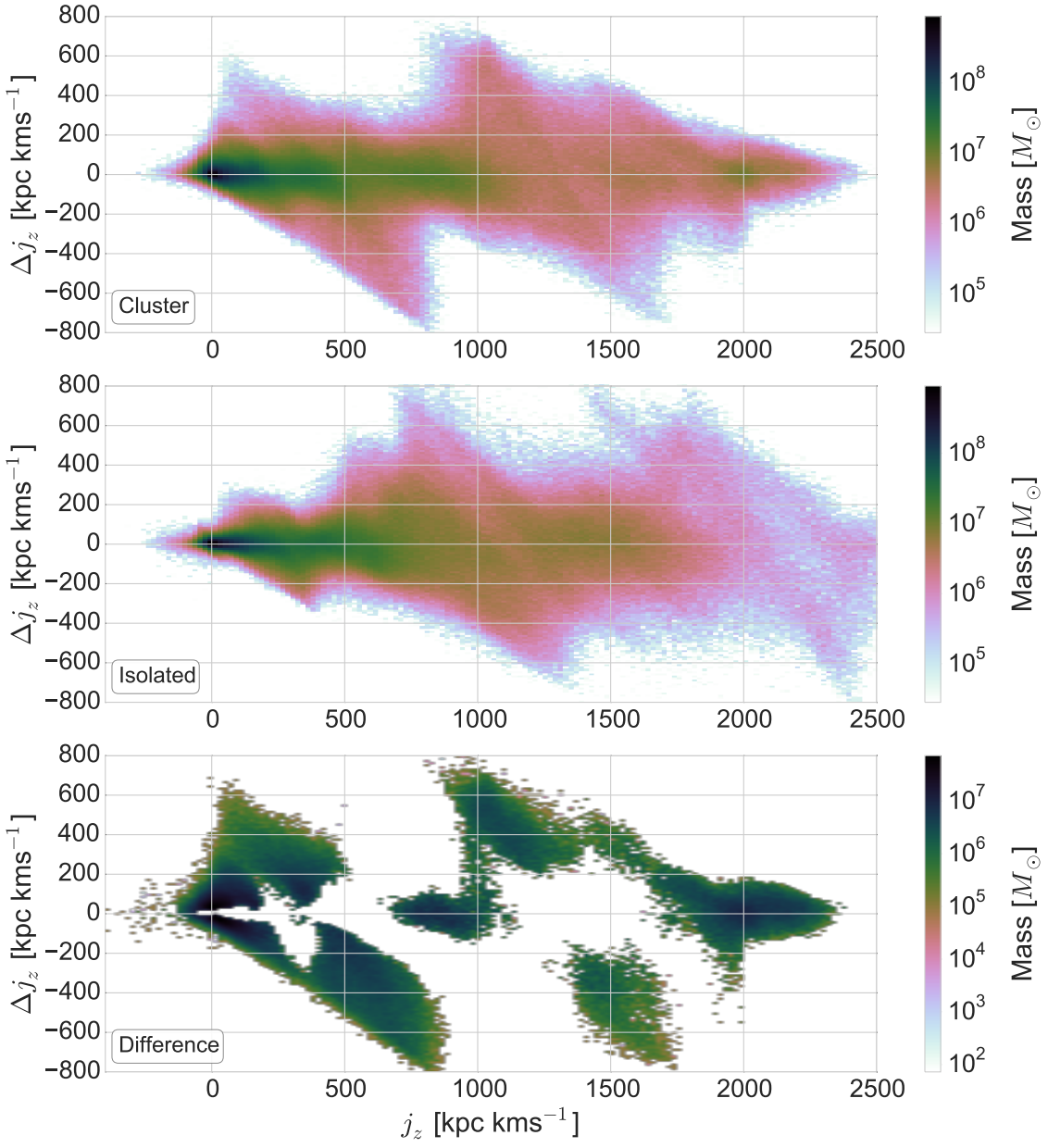

Figure 2.7: Same as Figure 2.5 but for $t = 5.9 - 6.5$ Gyr.

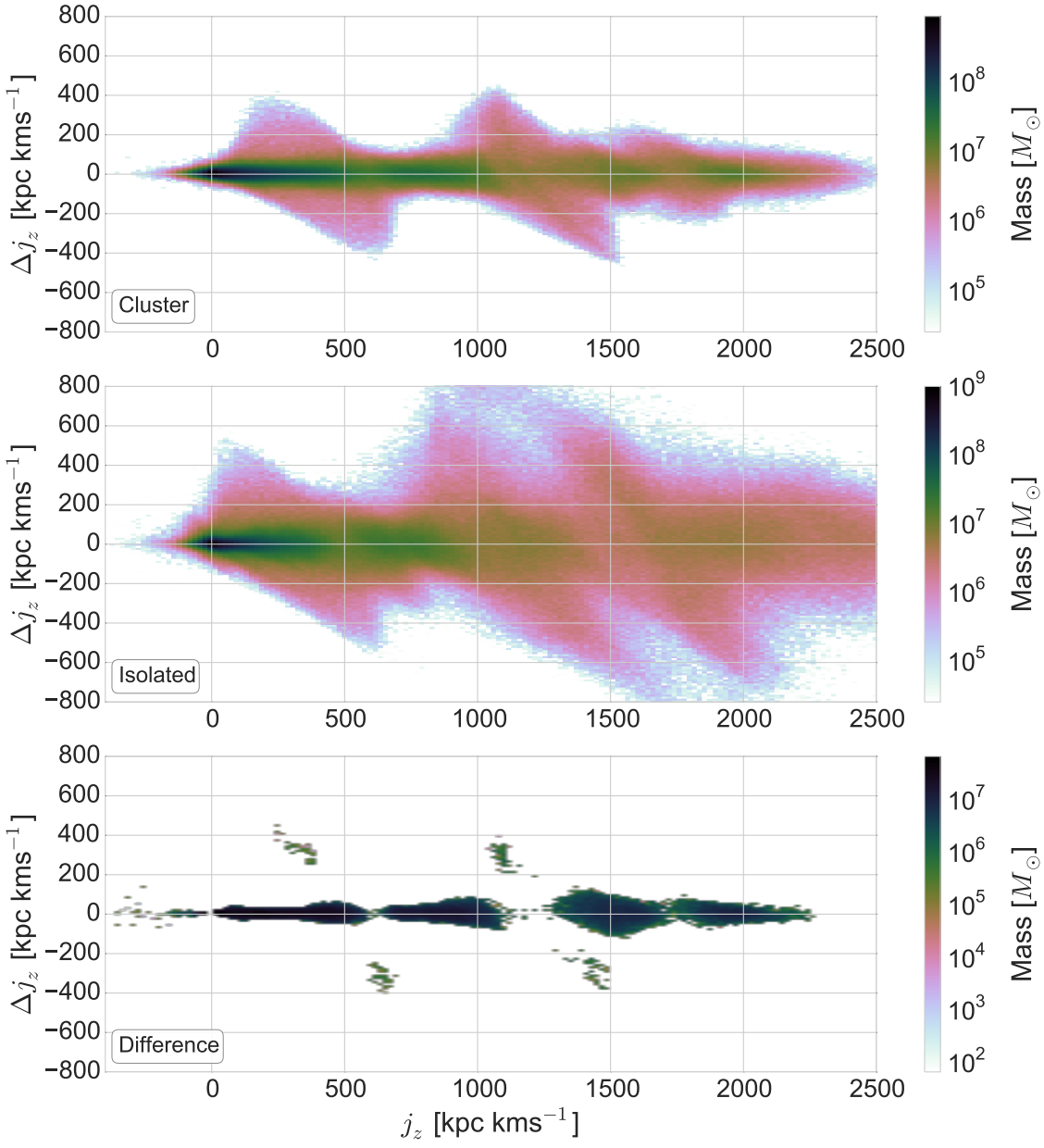

Figure 2.8: Same as Figure 2.5 but for $t = 9.4 - 10.0$ Gyr.

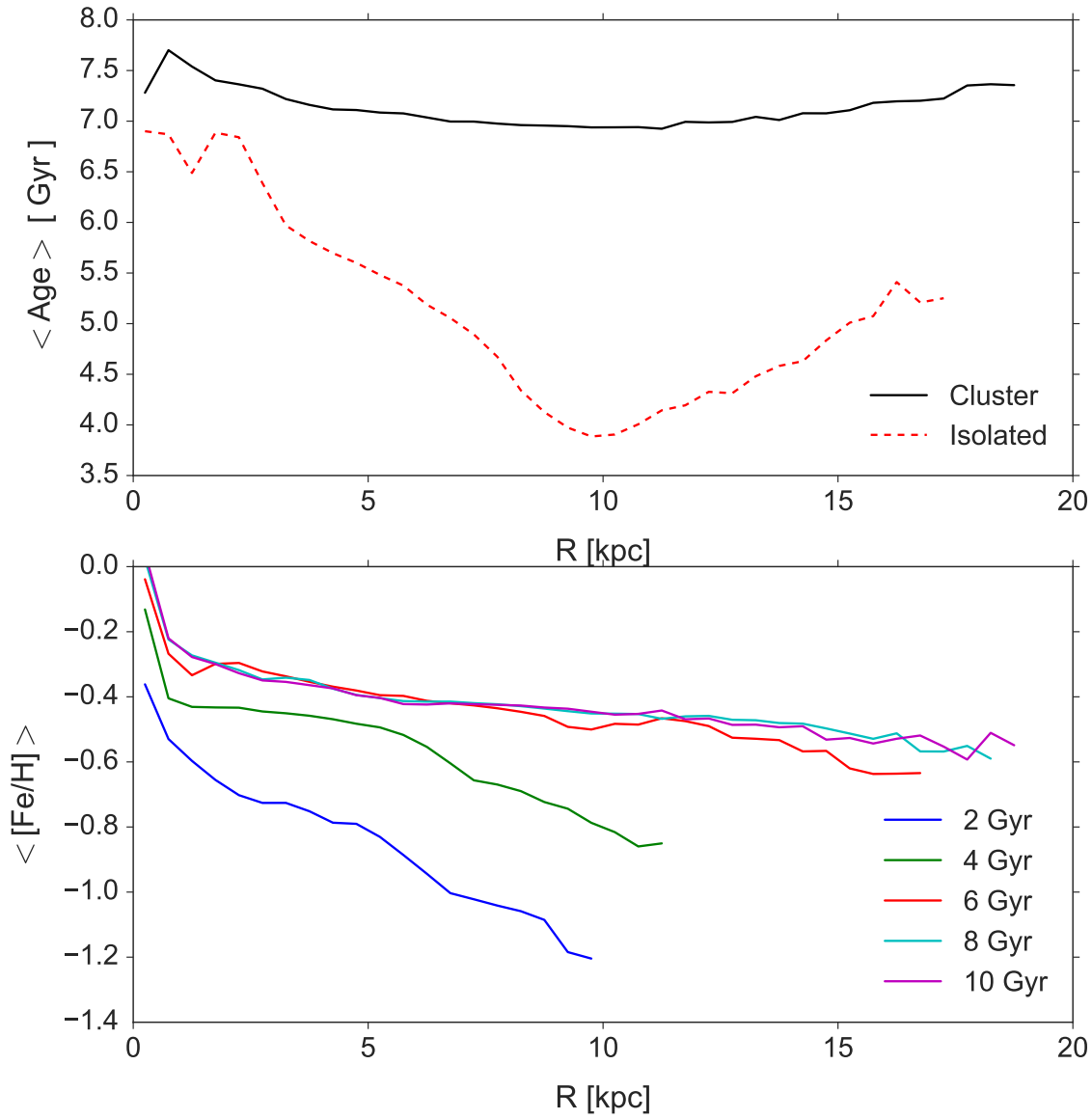

Figure 2.9: *Top*: Mean age profile for the final cluster model (black solid) and the final isolated model (red dashed). *Bottom*: Mean [Fe/H] profile for the cluster model.

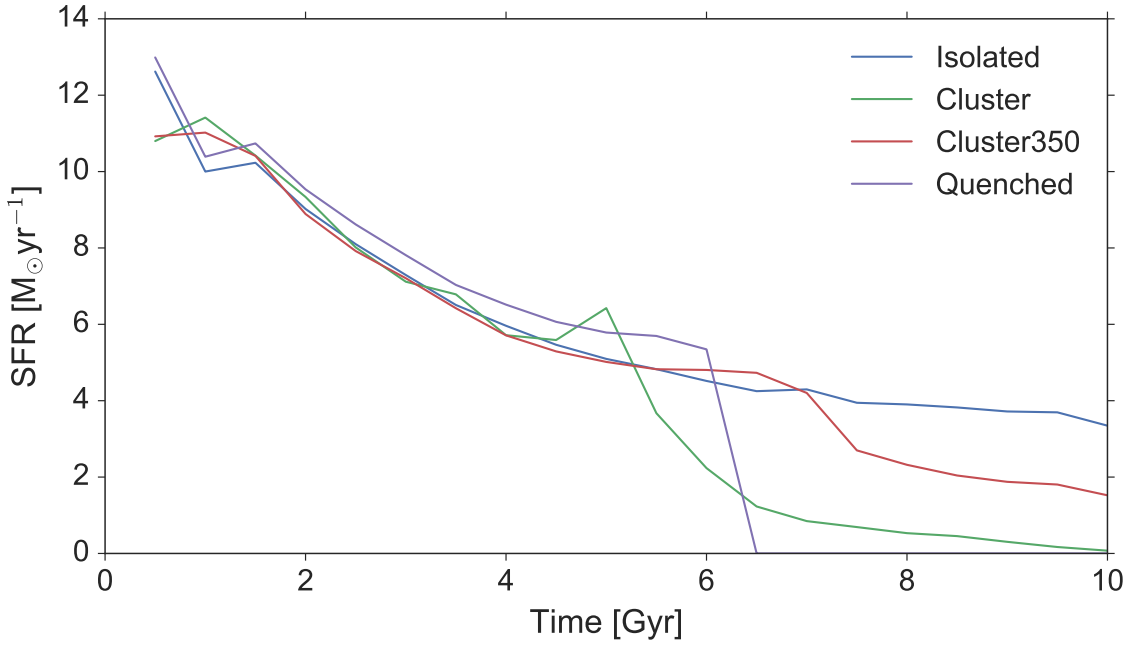

Figure 2.10: Star formation histories for our models, as detailed by the inset.

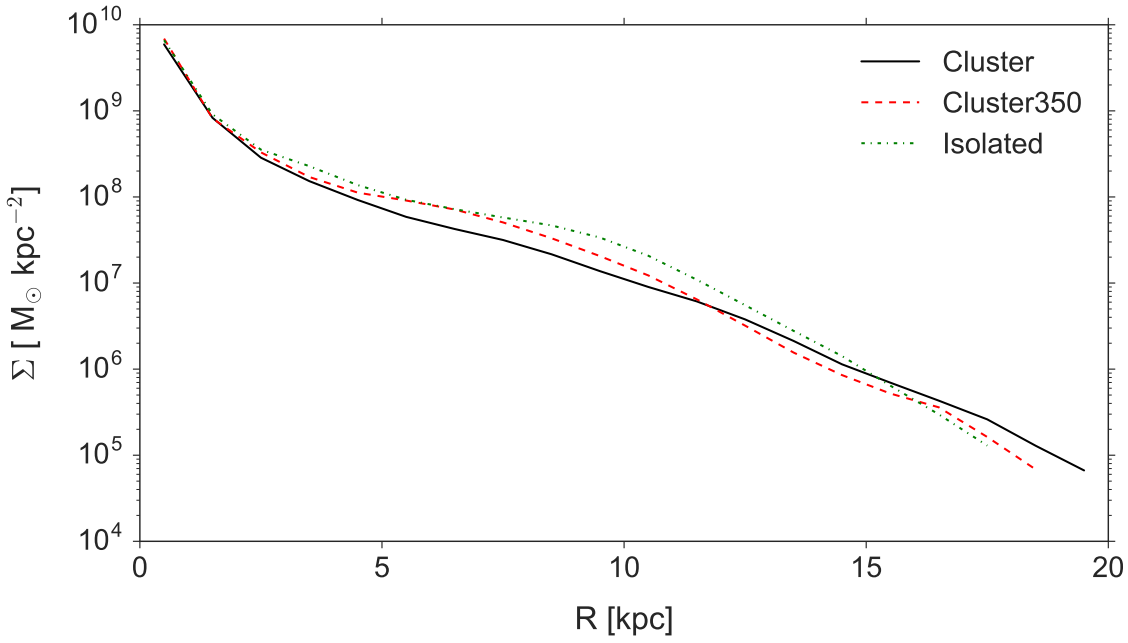

Figure 2.11: Surface density profiles of the cluster model (black solid) and the cluster350 model at (red dashed). We also show the isolated model profile at (green dot dashed).

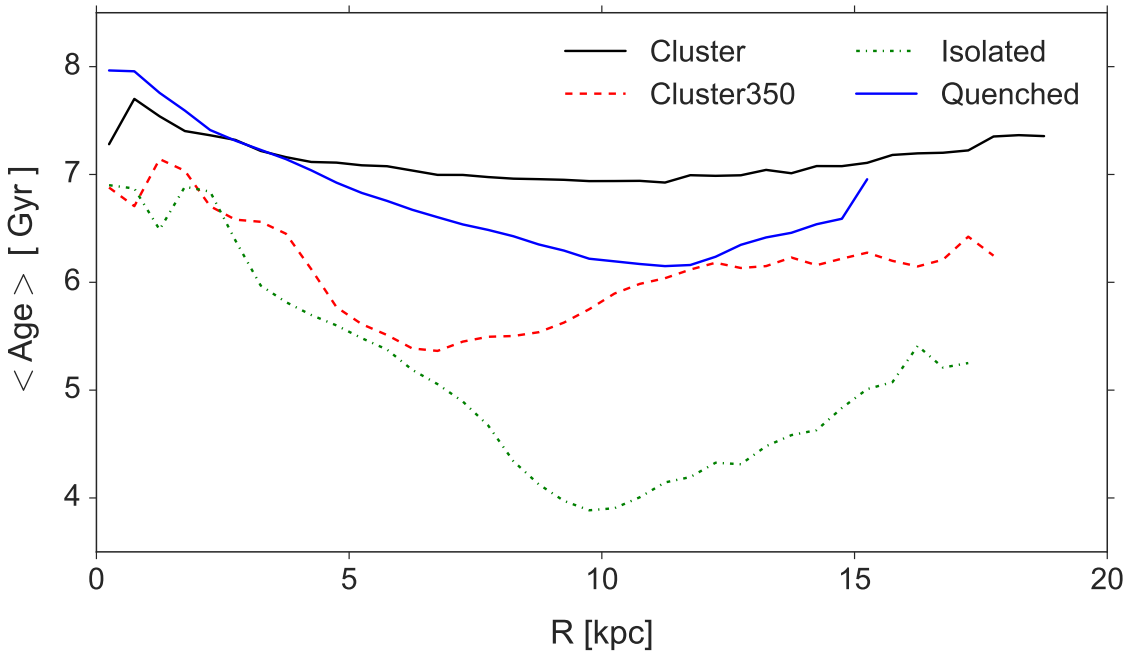

Figure 2.12: Age profiles for the four models at 10 Gyr.

Chapter 3

Colour changes during the transition from spiral to lenticular

In this chapter we consider the simulations discussed in Chapter 2, and present their colour profiles and demonstrate that quenching causes a spiral galaxy to evolve into a lenticular. We measure the star formation rate before, during and after stripping and discuss the observational implications, particularly the effect this quenching has on the position of the galaxy in the colour-mass diagram.

3.1 Methodology

The models analysed are the isolated and cluster galaxies from Chapter 2. We use these simulations as input for a 3D radiative transfer code. If a star emits light with specific intensity (surface brightness), I_λ, an observer with no medium between the source and themselves will observe the star with the same intensity. However, the interstellar medium (ISM) is not obstacle free. We have to consider emission from sources in the path, absorption and re-emission from dust and scattering via dust. Dust has been shown to permeate the ISM (Zhukovska et al. 2008) and is found in galaxies (Dunne et al. 2011) and molecular clouds (Martel et al. 2012) and as such

it is an extremely important factor to include when considering radiative transfer calculations.

We use DART-ray (Natale et al. 2014) a 3D ray-tracing radiative transfer code to calculate the propagation of light through simulated galaxies, allowing us to estimate their colours and magnitudes. For a detailed description of applying DART-RAY to an N-body simulation see Natale et al. (2015). Here we describe the salient features. DART-RAY begins by separating the simulation into a three dimensional Cartesian grid. This master grid is 40 kpc per side and the grid is divided further into a series of 3×3×3 child cells based on the following rules:

1. the minimum cell subdivision level is equal to 4 (cell size = 0.494 kpc)
2. the maximum cell subdivision level is equal to 5 (cell size = 0.165 kpc)
3. the maximum cell optical depth $\tau_B = 0.01$
4. the maximum cell stellar luminosity equal to 10^{-4} times the galaxy total stellar luminosity.

Criteria (3) and (4) are not guaranteed to be fulfilled in each cell if they are in conflict with rule (2). For each of the cells we need to calculate the extinction coefficient, κ_λ, and the stellar emissivity, j_λ. The extinction coefficient is given by the equation

$$\kappa_\lambda = C_\lambda^{\rm gas} \rho_{\rm gas} \tag{3.1}$$

where $C_\lambda^{\rm gas}$ is the dust cross section per unit mass. The intensity of a light ray once it has crossed a cell, i, is then given by

$$I_{\lambda,i+1} = I_{\lambda,i} e^{-C_\lambda^{\rm gas} \rho_{\rm gas} l_c} \tag{3.2}$$

where l_c is the ray crossing path length within a cell and $\rho_{\rm gas}$ is the gas mass density. The exponent in this equation is equivalent to the optical depth, τ_λ. DART-RAY

assumes the dust cross-section from the model of Draine & Li (2007) and assumes that these correlate linearly with metallicity, a reasonable assumption since dust is made of metals. Therefore to calculate $C_\lambda^{\rm gas}$ we have to know the metallicity of the gas in each cell, which produces two complications. Firstly, the gas metallicity can vary by large amounts even in relatively small regions, so we take the cell metallicity as a mass weighted average. Secondly, GASOLINE only traces the abundance of iron and oxygen. Since

$$[\mathrm{Fe/H}] = \log_{10}\left(\frac{\mathrm{Fe}}{\mathrm{H}}\right) - \log_{10}\left(\frac{\mathrm{Fe}}{\mathrm{H}}\right)_\odot \tag{3.3}$$

where Fe and H are the abundances, we can assume that [Fe/H] and overall metallicity, Z, are related by

$$Z = Z_\odot 10^{[\mathrm{Fe/H}]} \tag{3.4}$$

where $Z_\odot = 0.018$ (Anders & Grevesse 1989; Grevesse & Noels 1993). This metallicity is then used to derive the dust cross-section per unit mass, using a linear dust-gas mass relation, which holds well for massive galaxies (Rémy-Ruyer et al. 2014), therefore

$$C_\lambda^{\rm gas} = C_\lambda^{\rm gas,\odot}\frac{Z}{Z_\odot}. \tag{3.5}$$

The final quantity needed is the stellar volume emissivity j_λ, which encapsulates the total emissivity of stellar sources in each cell. First, DART-ray derives the sum of the luminosities of each stellar particle in each cell and using a mass-luminosity relation, converts this to the wavelength-specific luminosity, using the Starburst99 library (Leitherer et al. 1999). Since the stellar particles are not individual stars, we treat each is a single-age stellar population, with age equivalent to that of the particle, given by the simulation output.

3.2 Transformation from spiral to lenticular

In the previous chapter we examined the changes in profile classification of a spiral galaxy falling into a gas rich cluster environment, where it underwent strong ram pressure stripping. In Figure 3.1 we show $u - r$ colour images of the cluster model (top) and isolated model (bottom) at $t = 2$ Gyr. Both galaxies show similar characteristics, a redder outer disc component with blue star-forming spiral arms and a redder bulge.

Figure 3.2 shows $u - r$ colour images of the cluster model (top) and isolated model (bottom) at $t = 10$ Gyr. Here we find large differences between the cluster and isolated galaxies. The isolated galaxy shows a red outer disc component with blue star forming spiral arms and redder bulge and inter-arm regions. The dashed black line corresponds to the break radius ($\sim$ 10 kpc) and shows clearly that the majority of the star formation occurs interior to this radius, with stars outside being an older, redder population that has migrated outward (Roškar et al. 2008b,a). The lenticular galaxy shows an almost constant colour across most radii with a redder bulge component and could easily be mistaken, face on, for an elliptical galaxy. The centre of the lenticular galaxy is redder for two reasons. Firstly, the colour is dominated by the flux from the older population. Comparing the u-band shows there is $\sim$ 10 times more flux in the older (age $>$ 2 Gyr) population compared with the younger population. Secondly, the young stars are $\sim$ 1.0 dex higher in [Fe/H] compared with their older counterparts. This demonstrates that care must be taken when using colour analysis alone to determine potential locations of young stars in recently stripped lenticular galaxies.

Johnston et al. (2014) found that when performing a bulge-disc decomposition of lenticulars in cluster environments that the bulges were younger than the discs. In this sample, they suggest that the stripping occurs outside-in, meaning that the last bout of star formation would be in the centre, fueled by gas that has been funneled

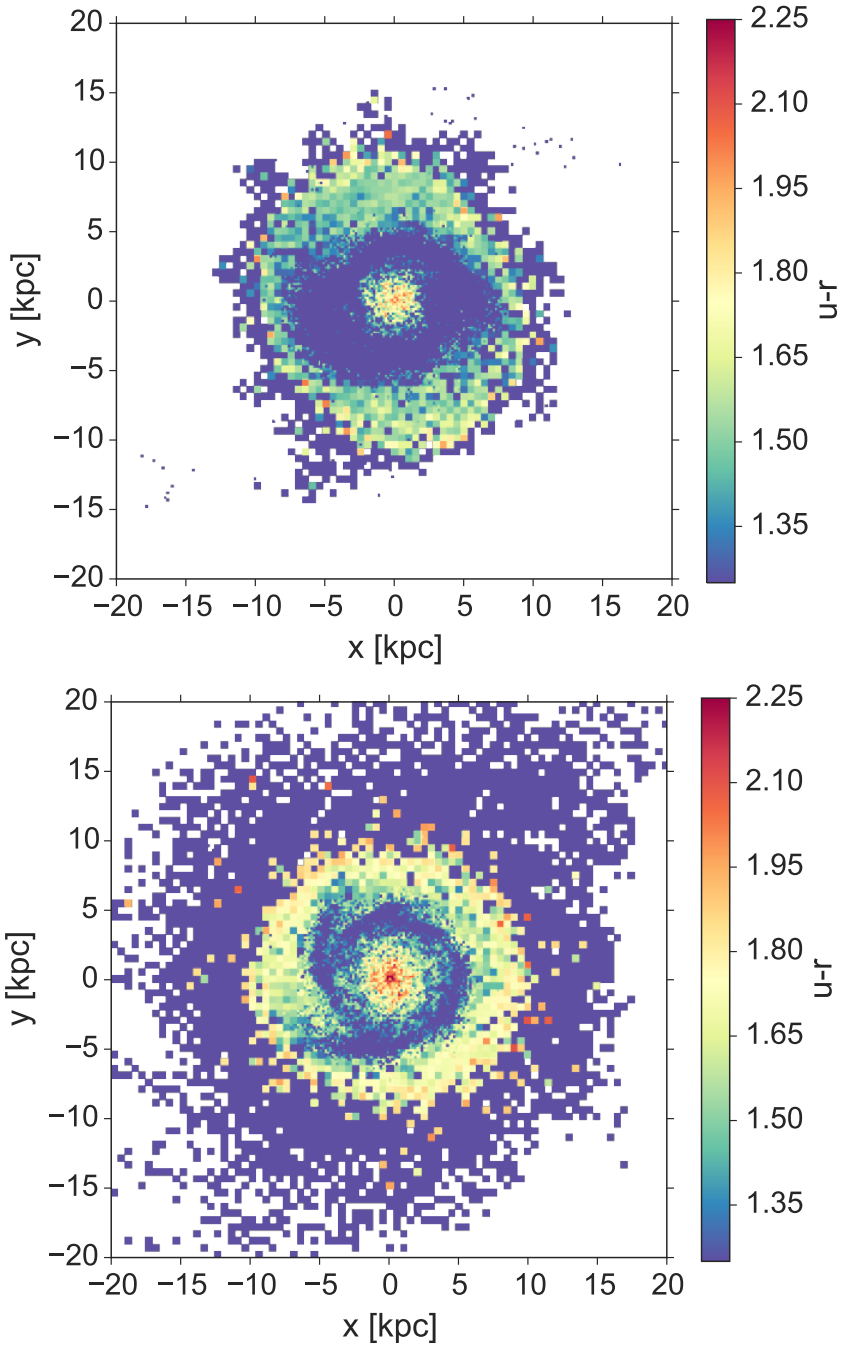

Figure 3.1: $u-r$ maps of the cluster galaxy (top) and the isolated galaxy (bottom) at t=2 Gyr.

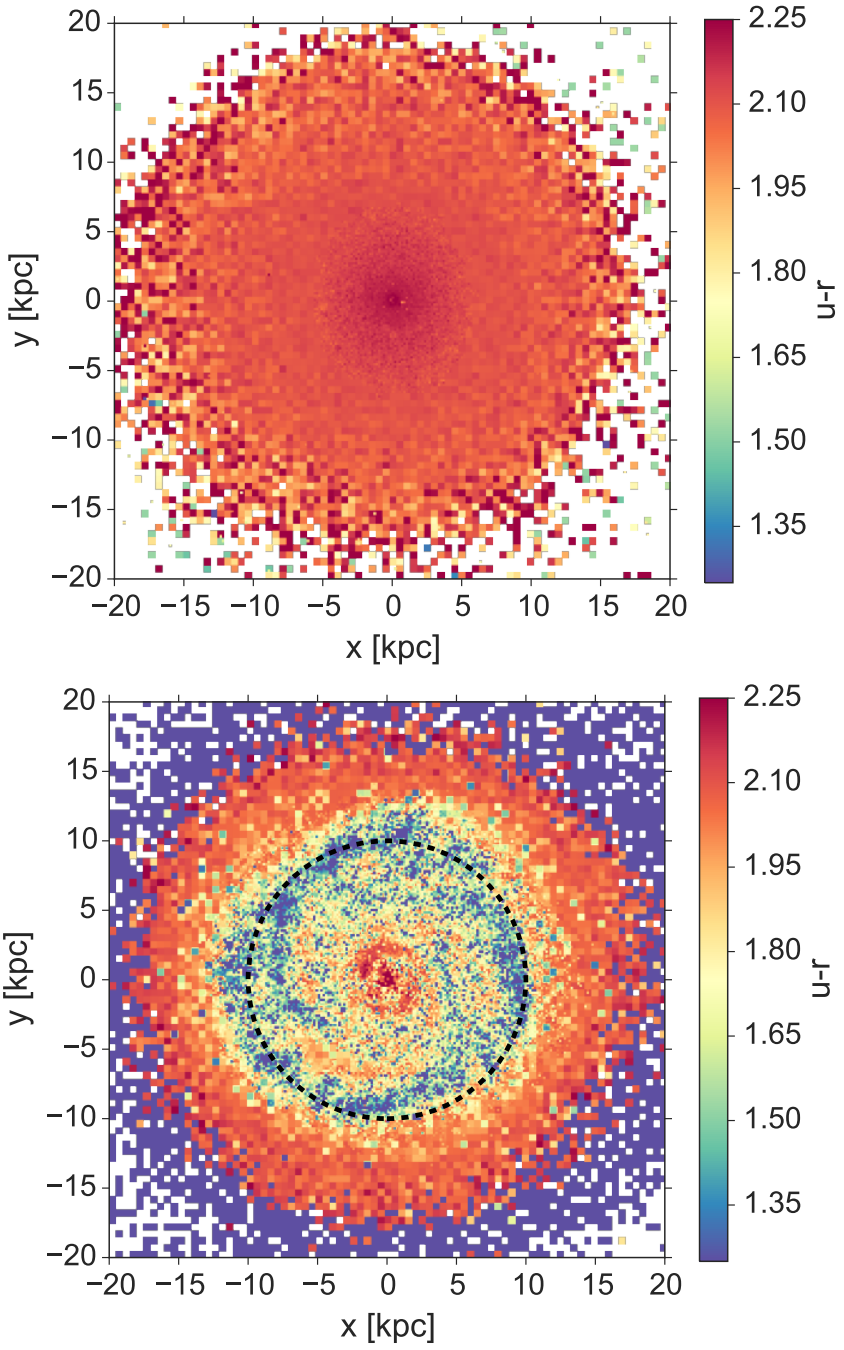

Figure 3.2: $u-r$ maps of the cluster galaxy (top) and the isolated galaxy (bottom) at t=10 Gyr. The dashed circle in the bottom panel indicates the break radius.

into the centre. In Figure 3.3 we show the mass distribution of young stars (age ≤ 0.5 Gyr) as a function of formation radius at different epochs. It is evident that up to the beginning of ram pressure stripping the star formation grows outwards as more gas cools into the disc, similar to the picture of inside-out growth. Once the strong stripping begins, the star formation moves inward as gas is stripped from the outside in. At $t = 8$ Gyr, the star formation is terminated across the whole disc, except the inner 1.5 kpc.

These findings, along with those demonstrated in Chapter 2 allow us to conclude that the ram pressure stripping of gas from the disc due to the cluster environment, causes the evolution from a spiral galaxy to a lenticular galaxy. This can explain the increase in lenticular galaxies seen in cluster and group environments, but does not explain how field lenticulars could be formed.

3.3 Evolution in the mass-colour plane and mass-metallicity plane

Observations from SDSS have shown that there is a distinct bimodality in galaxy distribution in the colour-mass diagram (Schawinski et al. 2014). Early-type galaxies are distributed in a "blue-cloud", whilst late-type galaxies form a "red-sequence." In between these regions appears a sparsely populated "green valley" which is thought to be a transition region between the red and blue regions. Since lenticulars are often considered a transition between spiral and elliptical galaxies it is possible that the quenched cluster galaxy may have either traversed this region, or remain in it. To test this we show in Figure 3.4 the colour-mass diagram. The blue points correspond to the isolated galaxy and are labelled by the time. The galaxy moves across the diagram as it converts gas into stars, yet its colour remains blue and relatively constant. The red points show that at early times ($t = 2$ Gyr) the cluster

galaxy exhibits similar colour and mass to the the isolated model. Once ram pressure stripping begins ($\sim t = 5$ Gyr) the galaxy converts less gas mass to stars and is redder than the isolated model. However the galaxy still falls within the blue cloud. There are a few possible reasons for this. Firstly, because the simulations begin with pristine gas, a fraction of the stars have extremely low metallicity. Low mass, low metallicity stars are brighter and bluer than corresponding stars with higher metallicity. Since they are also long lived, they will contribute a large amount of blue light. To test this hypothesis, we identify the stars with the lowest 25% of metals (-0.76 dex) in the cluster simulation, and exclude these from the DART-ray calculation.This is shown as the large red star and successfully moves the galaxy from the blue cloud to the middle of the green valley. Since little star formation has occurred since t = 6 Gyr we would expect the galaxy to fall well within the red sequence. Whilst this test has not alleviated the problem fully, it demonstrates that the $u - r$ colour is very sensitive to the metal content of the stellar particles. Our choice of initial mass function (IMF) may also effect these results. GASOLINE assumes a Miller & Scalo (1979) IMF whilst DART-RAY uses a Kroupa (2001) IMF. Whilst it is currently unclear how this may effect the colours, the main differences between these IMFs are at the low mass end of the distribution, the Miller-Scalo IMF flattens below solar mass, resulting in fewer low mass stars. This may solve the colour problem and it is important to be consistent between GASOLINE and DART-RAY, however this is beyond the scope of this thesis since it would require either complex changes in the DART-RAY code or rerunning the simulations with a different IMF.

Finally we show in Figure 3.5 the mass-metallicity relation overlaid with contours taken from the SDSS sample of Tremonti et al. (2004). The SDSS fibers median projected size is ~ 4.6 kpc for the sample and as such we limit our gas metallicity to the inner 5 kpc. All the galaxies match quite well with the overall distribution yet

there are some small differences between the cluster and isolated models. Firstly we can see the cluster run has lower mass, a direct consequence of the stripping and subsequent quenching of star formation. The isolated model is also more metal-rich, which can also be explained by the continual star formation enriching the cool gas further. All the galaxies are towards the lower metallicity end of the distribution given their mass, which may be a reflection that the oxygen yield implementation in GASOLINE may not be correct.

3.4 Conclusions

In this chapter we have used the simulations presented previously in Chapter 2 and DART-ray, a 3D ray-tracing radiative transfer code to calculate the changes in colours, as well as the evolution in the mass-colour plane as a spiral galaxy falls into a gas rich cluster environment. At early times, before the galaxy reaches a location in the cluster where the gas density is high enough to begin stripping of the cold gas, the two galaxies evolve in unison. Once the ram pressure stripping becomes efficient, we find that the cluster galaxy develops a redder disc, with no spiral features, when compared to the isolated model. Similarly to Johnston et al. (2014), we find that the star formation terminates outside-in, with the last bout occurring in the inner few kpc. This transformation also causes the galaxy to become much redder than the isolated model and would be considered to be at the boundary of the green valley and blue cloud. Whilst we would expect that the galaxy would be in the red sequence given the almost complete lack of star formation in the past ~ 4 Gyr, we have also demonstrated that the $u - r$ colour is sensitive to the metallicities used in the DART-ray calculation. By removing the lowest quartile of metal-poor stars in the sample, we move much closer to the red sequence. As such, we need to address the implication of these changes, but this is beyond the current scope of this thesis. Regardless, the relative change in $u - r$ colour between the isolated

and cluster galaxies shows that once ram-pressure stripping removes the cold gas and star formation ceases, the galaxy is considerably redder in colour. Furthermore, this change in colour occurs rapidly once the ram-pressure stripping begins, which could provide an explanation for the relative sparsity of galaxies in this region of the colour-mass diagram. Finally one further important point of note is that the centre of the lenticular galaxy appears redder than the surrounding disc, even though the last bout of star formation has occurred in these regions. This is due to both the flux being dominated by the older population and the young stars being metal rich. This raises an important caveat when using colours to determine the locations of potentially young stars in recently stripped lenticulars.

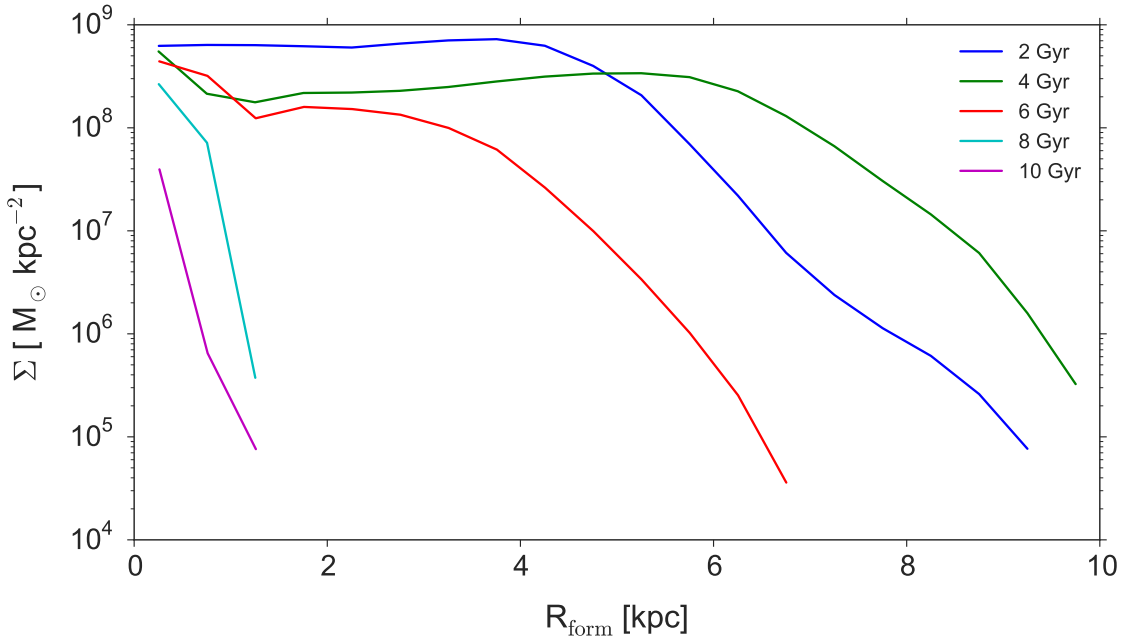

Figure 3.3: Mass surface density of young stars (age $\leq$ 0.5 Gyr) in the cluster simulation as a function of R_{form} for different epochs as detailed by the inset.

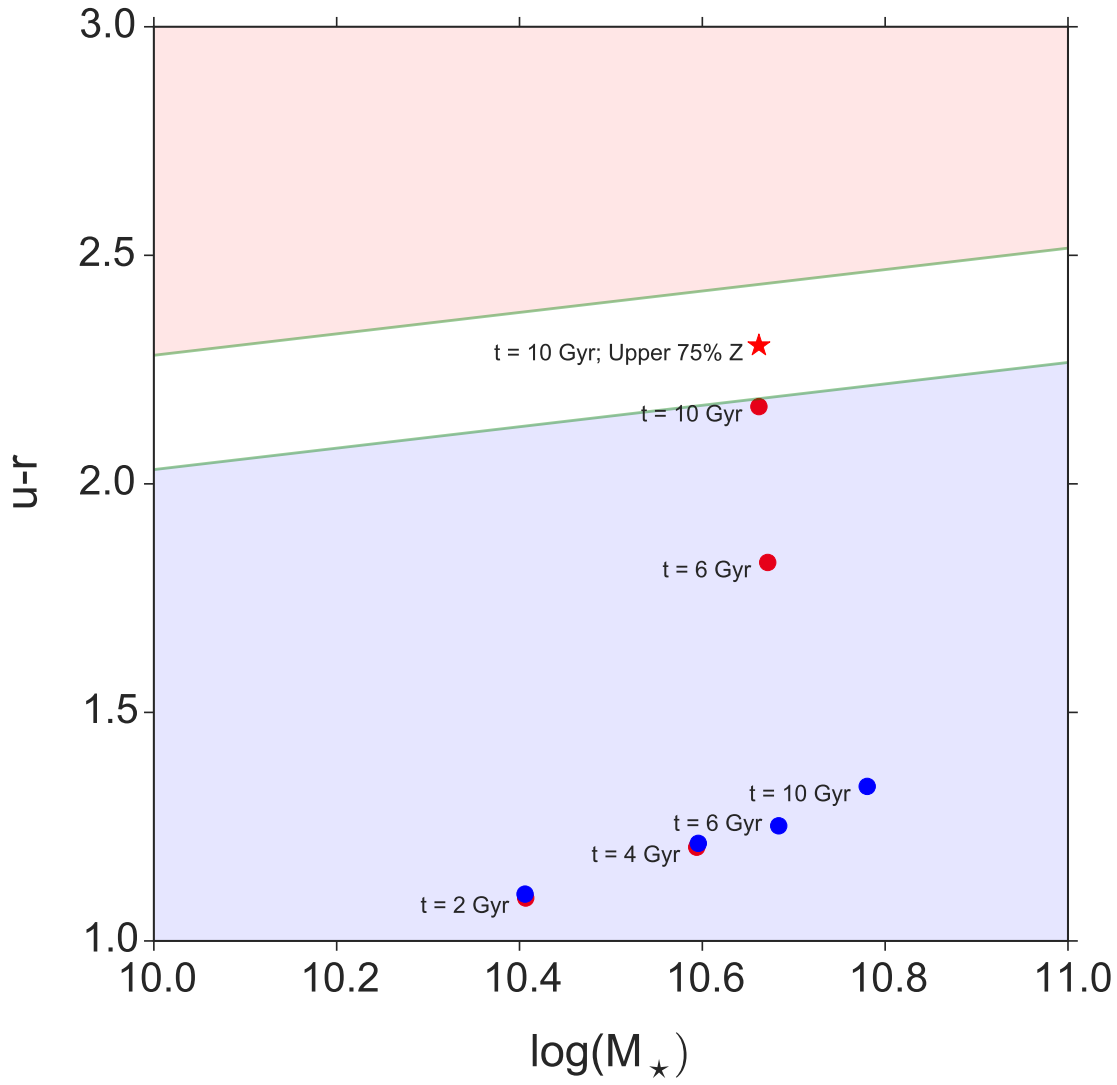

Figure 3.4: Colour-mass diagram showing the evolution of the cluster galaxy (red-points) and the isolated galaxy (blue points). The green lines show the green valley separation from Schawinski et al. (2014). The blue cloud and red sequence are shaded appropriately. The red star is the cluster galaxy at $t = 10$ Gyr with the stars in the lower 25% of the metallicity distribution function removed.

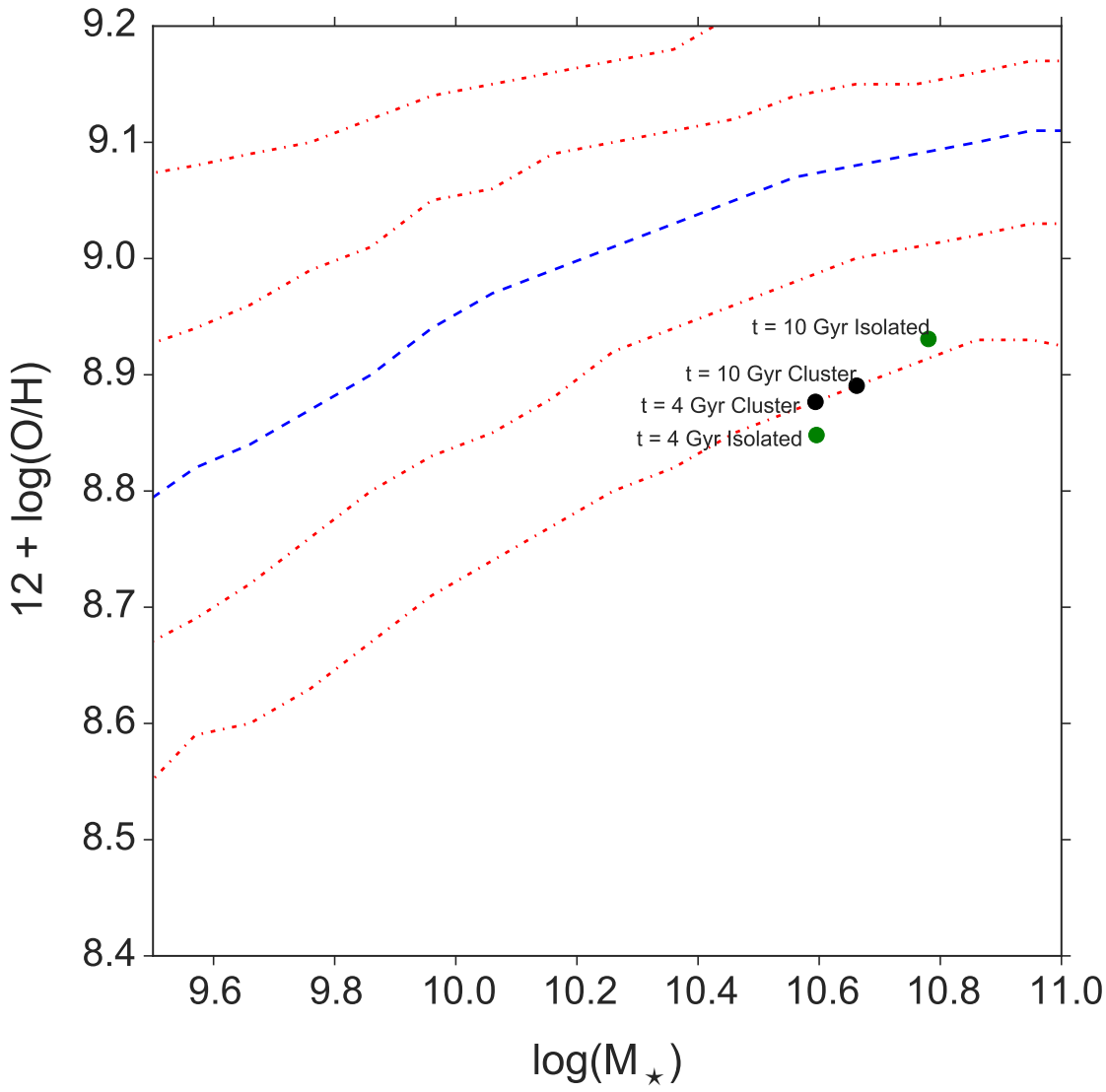

Figure 3.5: Mass-metallicity diagram showing the cluster galaxy (black) and isolated galaxy (green). The gas metallicity is calculated using the cool gas (T $<$ 15000 K). The blue dashed line indicates the median of the distribution of metallicity in bins of 0.1 dex in stellar mass taken from Tremonti et al. (2004). The dot-dashed red lines represent the contours of 2.5, 16, 84, and 97.5 percentile.

Chapter 4

The distinct populations of warps

In this chapter we present results from N-body+SPH simulations of a warped spiral galaxy, studying how warps affect the chemical evolution, and investigate the impact this has specifically on the age-metallicity relation (AMR). We show that substructures present in the AMR are a direct consequence of the warp, and are found across all disc radii due to settling and migration. Stars formed in the main disc do not migrate into the warp, which therefore exhibits an AMR. We also find similar substructures in other observed quantities such as the [O/Fe]-age plane. Finally we look at the chemical space to study substructures and their kinematical origin.

4.1 Simulations

In order to produce a warped system, we set up initial conditions in which a prolate halo has a gas corona with angular momentum misaligned by 45° with the long axis of the halo. We do this using the method of Debattista et al. (2013) and our model is very similar to the model GP45 (Debattista et al. 2015). Two identical spherical systems are merged head-on from a separation of 500 kpc with a relative velocity of 100 km/s. The initial spherical halos have a size $r_{200} \simeq 200$ kpc and mass

$M_{200} \simeq 8.7 \times 10^{11}$ M$_\odot$. Each halo uses 1×10^6 particles in each of the gas and dark components. Gas particles initially have masses 1.4×10^5 M$_\odot$ and softening 50 pc, the latter inherited by the star particles, while dark matter particles come in two mass flavours (10^6 M$_\odot$ and 3.6×10^6 M$_\odot$ inside and outside 200 kpc, respectively) and with a softening of 100 pc. The gas corona in each halo has an angular momentum parameter (for the gas only) of $\lambda = 0.16$. Each halo is inclined by 45° relative to the initial separation vector between the two halos. Thus the final merger remnant has angular momentum tilted relative to the merger major axis, ensuring that gas cools onto the disc via a warp. After the merger the gas has $\lambda = 0.11$, $r_{200} \simeq 240$ kpc and $M_{200} \simeq 1.6 \times 10^{12}$ M$_\odot$. As shown by Debattista et al. (2015), gas from the corona cools onto a warp, as a result of which the disc remains tilted relative to the dark matter halo, never settling into one of the symmetry planes of the halo.

We evolve the simulation for 10 Gyr with GASOLINE (Wadsley et al. 2004) the smooth particle hydrodynamics (SPH) extension to the N-body tree-code PKDGRAV (Stadel 2001). This length of simulation can be considered comparable to disc formation and evolution since the time of the last major merger as suggested by cosmological simulations (Brook et al. 2004). The gas cools and settles into a disc and once the density and temperature are higher than 0.1cm^{-3} (low threshold model) or 100cm^{-3} (high threshold run) and less than 15,000 K respectively, star formation and supernova feedback cycles are initiated as described in Stinson et al. (2006). By taking the galaxy out of a cosmological context we increase the resolution, and our simulations have no *a priori* assumptions. We evolve two versions of the simulation for comparison, a low star formation threshold run and a high star formation threshold run. The high threshold run requires greater gas density before star formation begins, which particularly lowers the star formation in the warp, allowing us a test-case with which to compare the effect warps have on the efficiency of migration and its implications. Both simulations adopt a supernovae feedback

coupling to the ISM where 40% of the traditional 10^{51} erg per SN is injected as thermal energy into the ISM, comparable to most modern implementations (Brook et al. 2012; Scannapieco et al. 2012). The remainder of the energy not transferred to the ISM is considered to radiate away (Stinson et al. 2010). We include the effects of diffusion (Shen et al. 2010) allowing the gas to mix, which has been shown to decrease the spread in the age-metallicity relation (Pilkington et al. 2012). Whilst our simulation is not designed to match any specific observed galaxy, the rotation curve of the final system presented in Figure 4.1, shows that our simulated galaxies are intermediate in mass to the MW and M31. In the Solar neighbourhood the MW circular velocity has been measured as 218 ± 6 kms^{-1} (Bovy et al. 2012a) and the rotation curve for M31 is ~ 250 kms^{-1} (Carignan et al. 2006).

4.2 Evolution of the systems

Both the low and the high threshold run form strong warps in the gas component. However, due to the increased threshold needed for star formation in the latter, there is a much less prominent stellar warp. Figure 4.2 shows line-of-sight density maps of the gas component at t=10 Gyr for the low threshold run (top) and high threshold run (bottom). The low threshold run has formed a weak bar in the last 500 Myr which has begun to sweep up the gas, causing the cavities. However the underlying stellar components for the two galaxies are both quite similar throughout the simulation, showing flocculent spiral arms and no bar. Since the bar will not have had much time to significantly affect the properties of the galaxy, we consider them to be directly comparable.

In Figures 4.3 and 4.4 we show Briggs figures (Briggs 1990) for our low and high threshold runs respectively, showing the spherical angular momentum coordinates, θ and ϕ, as the radial and angle coordinates in 2D polar coordinates (for a detailed description of these figures see Debattista et al. (2015)). In these diagrams the

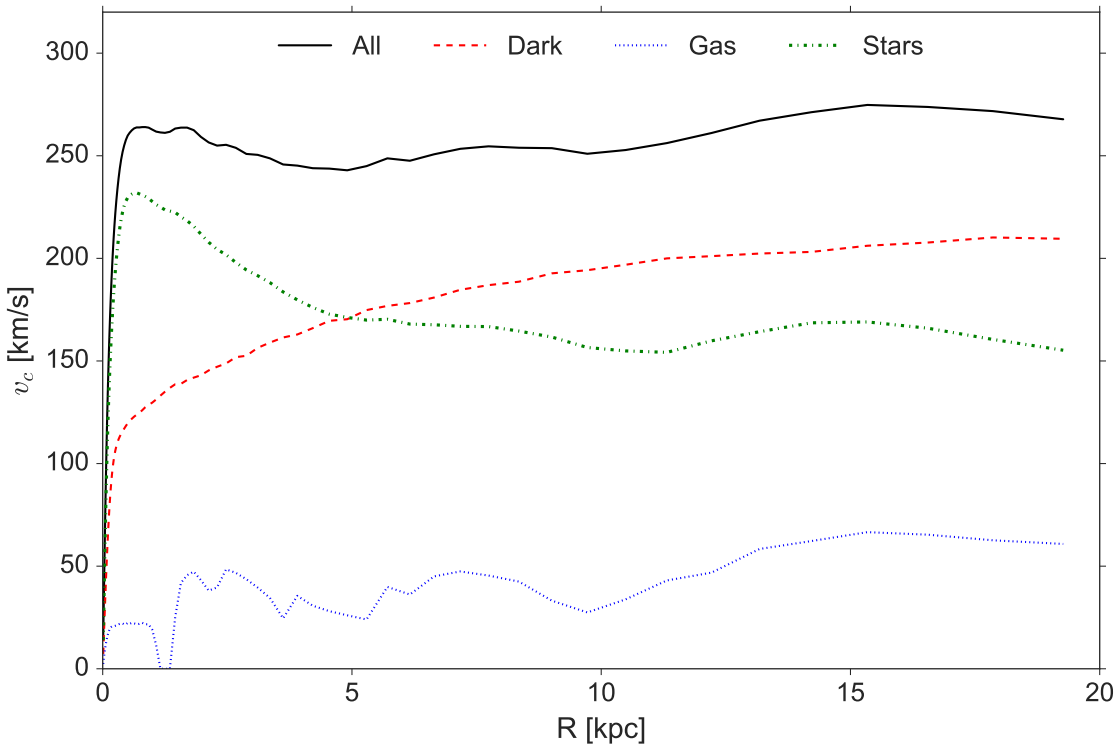

Figure 4.1: Rotation curve for our low threshold run. The relative contributions from dark matter, gas and stars is shown in red dashed, blue dotted and green dot-dashed respectively, and the total contribution from all components is shown by the black solid line.

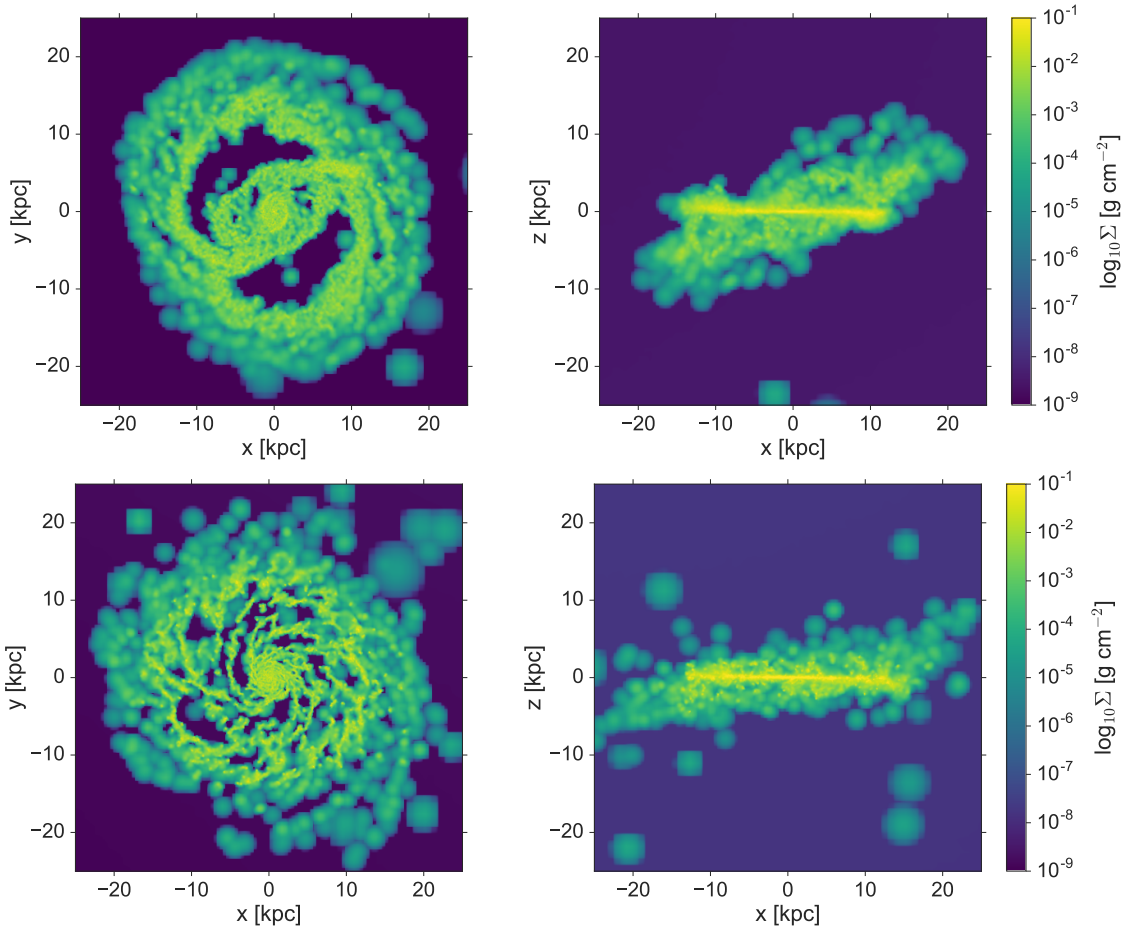

Figure 4.2: *Top*: Surface density of the gas distribution in the low star formation threshold run at 10 Gyr face-on (left) and edge-on (right). *Bottom*: As above but for the high star formation threshold run.

angular momentum vector of a warp traces out a leading spiral in the direction of disc rotation (which in our case is always set to be counter-clockwise). The inner disc is aligned in the x-y plane at each time so any tilting in the disc is a direct consequence of the warp. An unwarped disc will have all of the points clustered in the centre. The stellar component is shown in red and the gas component in green. Our low threshold run shows a prominent, long-lived warp in the gas component throughout the simulation, however the stellar warp becomes much weaker at 6 Gyr, becoming difficult to distinguish from the main star forming disc. The high threshold run shows a similar long-lived gaseous warp until 8 Gyr, after which it becomes weaker. Due to the increased threshold needed for star formation in this run, the stellar warp is much weaker, lasting only from 2 Gyr to 4 Gyr before becoming substantially weaker.

Separating the warp and the main disc component is complex, since selection purely on radius and height will either be contaminated by the main thick disc, or will miss other parts of the warp. We therefore define $\theta_{\rm form}$, the angle between the angular momentum vector of stellar particles at formation, and the angular momentum vector of the inner disc. Particles forming in the main disc have $\theta_{\rm form}$ close to zero, whilst stars forming in the bulge have large values due to their small radius. Particles with intermediate $\theta_{\rm form}$ form in the warp. We have visually verified this by checking these stars do in fact form in the warp. In the top panel of Figure 4.5 we plot formation radius, $R_{\rm form}$, versus $\theta_{\rm form}$ for the low threshold run. The majority of stars form at an angle less than 10°, whilst the warp produces a structure at angles from $10^\circ - 40^\circ$ in the outer disc. In comparison the high threshold run (bottom panel), has fewer stars forming with $\theta_{\rm form} \geq 10^\circ$. Therefore we define two regimes: stars forming with $\theta_{\rm form} \leq 10^\circ$ are predominantly main disc stars, whilst those forming with $\theta_{\rm form} \geq 10^\circ$ and $R_{\rm form} \geq 10$ kpc are warp stars. By restricting the formation radius we prevent contamination from the bulge and we set the $\theta_{\rm form}$

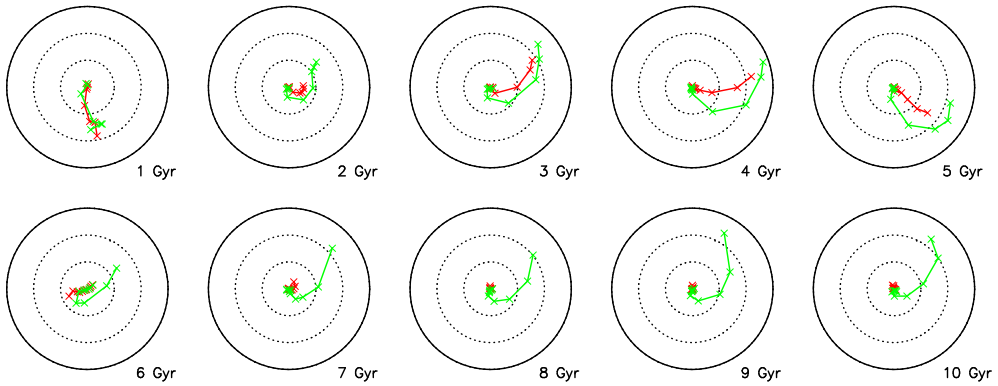

Figure 4.3: Briggs figures for the low threshold run, of stars (red) and cold (T $<$ 15000 K) gas (green). There are 10 evenly spaced radial bins from 0 kpc to 20 kpc. The dotted lines show increments of 10°, with the maximum at 30°. The main disc is aligned in the $x - y$ plane and disc rotation is counter-clockwise. The radial and angle coordinates in the plot correspond to the disc's angular momentum coordinates θ and ϕ respectively.

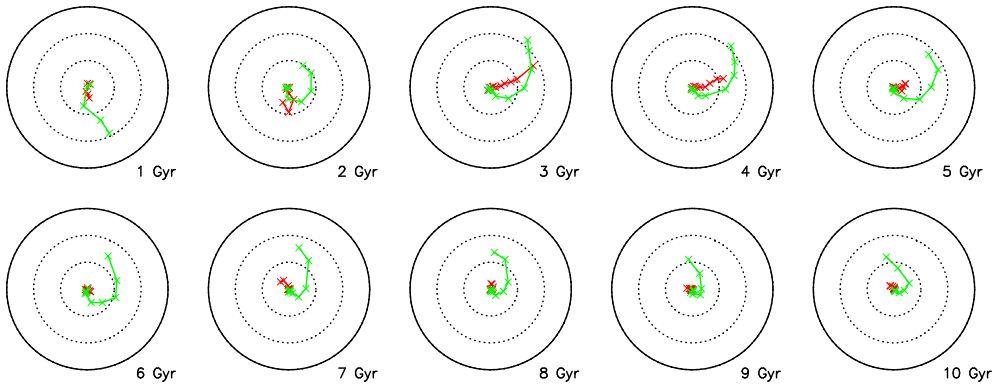

Figure 4.4: Same as Figure 4.3 but for the high threshold run.

cut conservatively to prevent contamination of the warp population from the main disc. These cuts are indicated in the figures. Both the high and low threshold runs show a secondary structure at $3 \leq R_{\rm form} \leq 5$ kpc, which we attribute to a short-lived warp in the first 1–2 Gyr of evolution. We have chosen not to include this in our selection criteria for the warp, since it does not last long enough to have a strong impact on the disc stellar populations.

Now we can isolate stars forming in the warp from those forming in the main disc we can verify the differences in star formation between the high and low threshold runs warps. We plot in Figure 4.6 the star formation rate for stars forming in the warp, in the low threshold (black-solid) and high threshold (red-dashed) simulations. Using Simpson's rule to calculate the total star formation in the warp, we find that there is $\sim 50\%$ less star formation in the high threshold run compared with the low threshold run. This demonstrates that whilst Figures 4.3 and 4.4 indicate that the warp weakens, star formation continues in the warp throughout the simulations.

In the top panel of Figure 4.7 we show the metallicity profile of cold gas ($T \leq$ 15000 K) in the main disc of the low threshold run (solid lines) and in the main disc of the high threshold run (dashed lines). The angle and radius of gas particles are instantaneous. As the disc ages and star formation enriches the ISM with metals, the metallicity in the disc increases in both runs. At all times and all radii, the low threshold run is more metal rich than the high threshold run, a natural consequence of the lower star formation rate. In the bottom panel, we show the same, but for cold gas in the warp, with $10^\circ \leq \theta \leq 40^\circ$ and $R_{\rm form} \geq 10$ kpc. In both runs, the warp is enriched less and has a steeper gradient compared with the inner disc.

4.3 Age-metallicity relations

If migration is efficient we expect that the AMR across the disc should be broad and flat, as seen in the Solar neighbourhood. We find that the AMR of the Solar

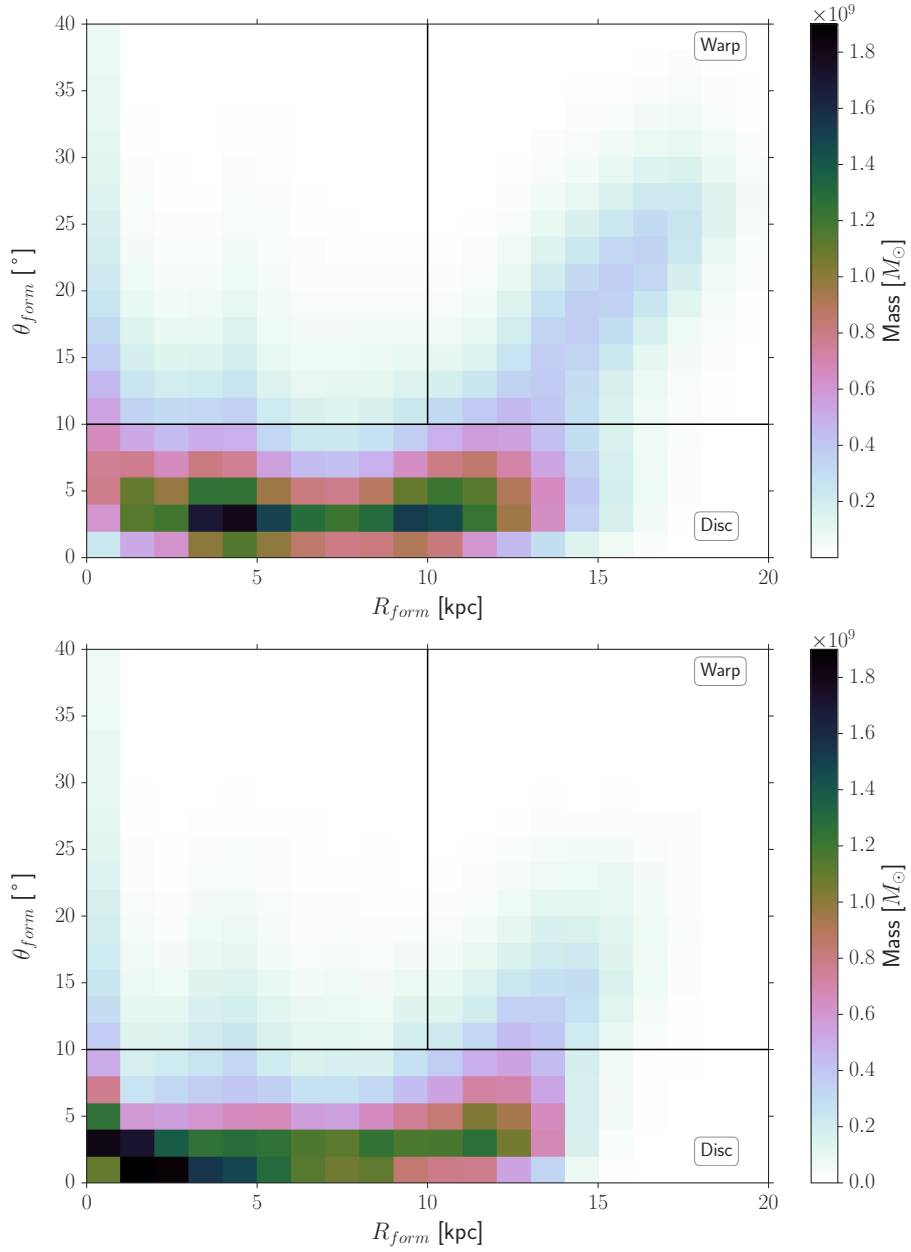

Figure 4.5: Mass weighted distribution of all stars in the $R_{\text{form}} - \theta_{\text{form}}$ plane, for the low threshold run (top) and the high threshold run (bottom). Black lines show our separations between the disc and warp components as labelled.

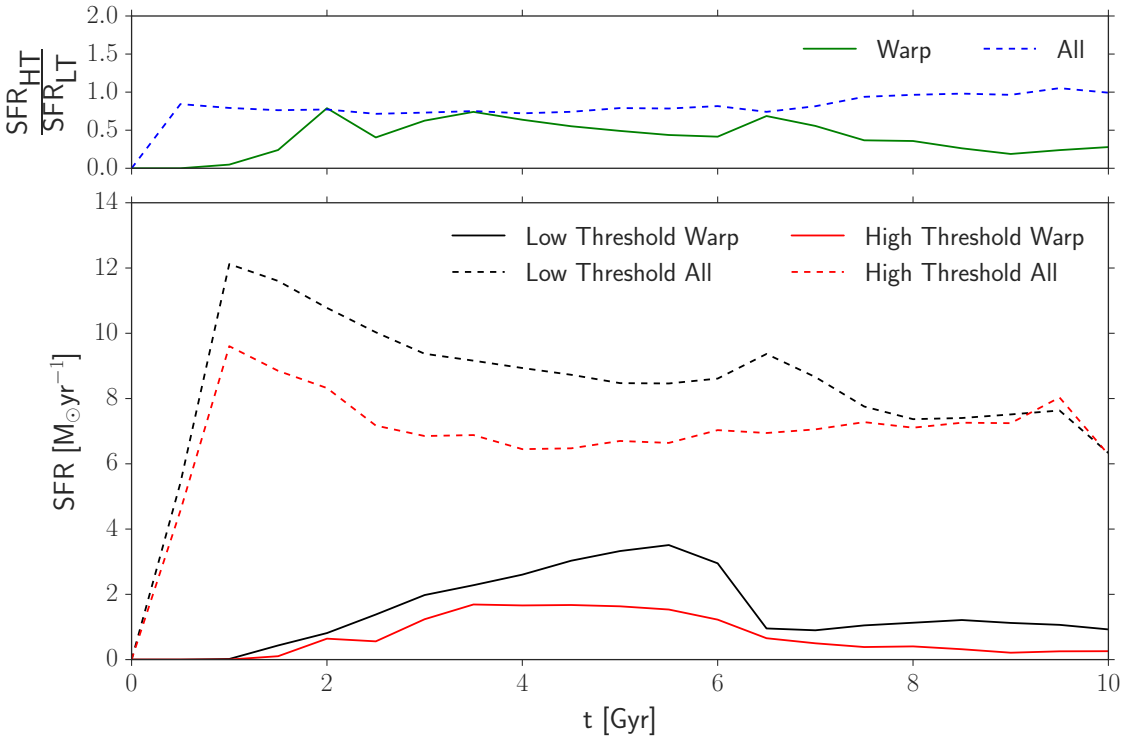

Figure 4.6: A comparison of the star formation rates in the low threshold run (black) and the high threshold run (red) globally (dashed) and for stars forming in the warp (solid). The top panel shows the ratio of the star formation rate between the two runs as a function of time for the warp (green) and globally (blue).

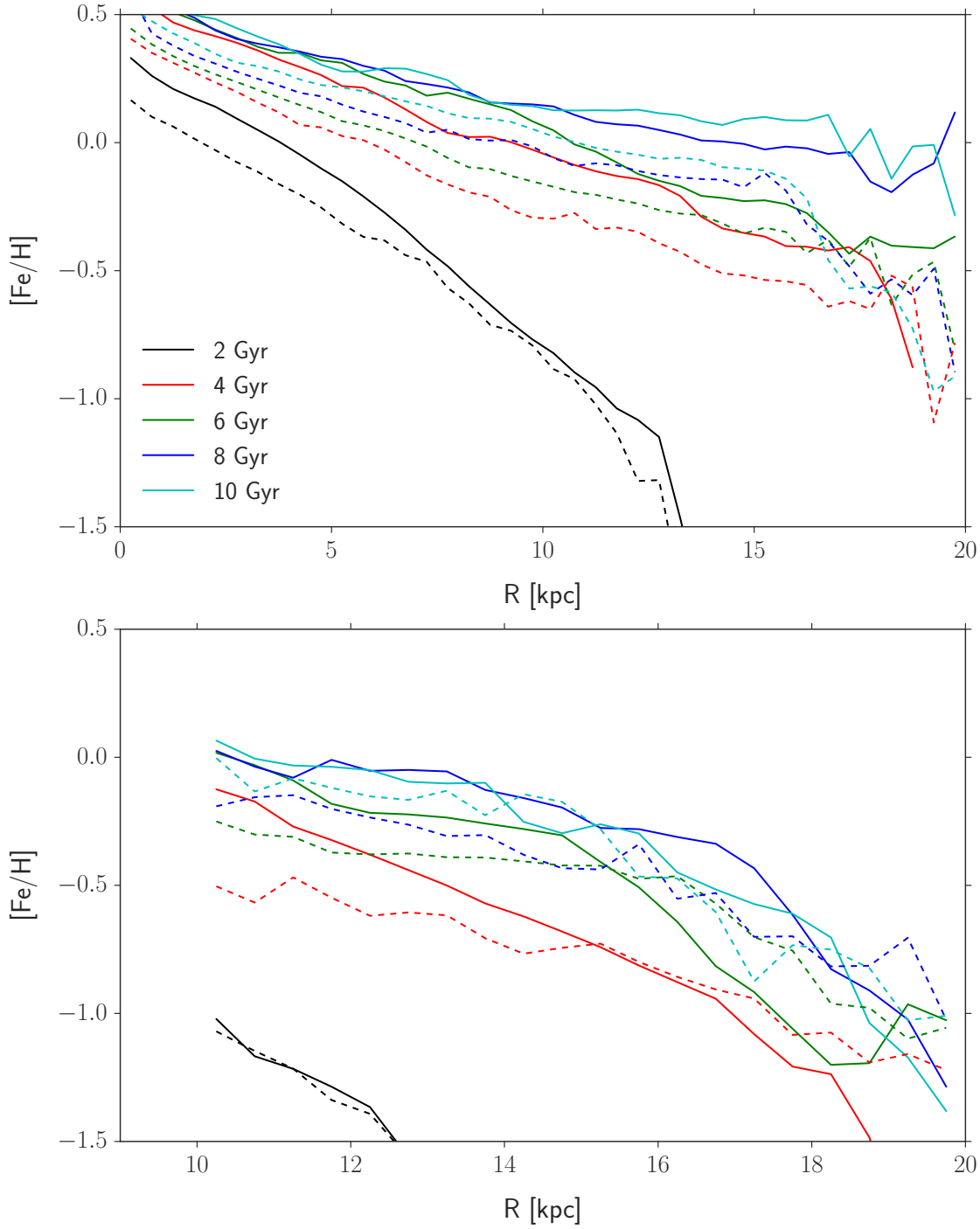

Figure 4.7: *Top*: Evolution of cool gas ($T \leq 15000$ K) metallicity as a function of radius. The solid lines correspond to gas in the low threshold run main disc, whilst the dashed lines correspond to gas in the high threshold run main disc. The different colours correspond to profiles at different times, as indicated in the inset. *Bottom*: As above, except for gas in the warp, with $10° \leq \theta \leq 40°$ and $R \geq 10$ kpc.

neighbourhood (7.0 kpc $\leq R \leq$ 9.0 kpc) for the low threshold run exhibits the broad, flat characteristics of migration, but also contains substructures, as shown in the top panel of Figure 4.8. This substructure is also present in AMRs taken all over the disc. The sharp decrease in metallicity at old age is due to the pristine initial conditions. The bottom panel of Figure 4.8 shows the AMR of the high threshold run which also shows a similarly broad and flattened AMR, but lacks the well-defined substructure. We have also verified that the late forming bar has not had enough time to affect the stellar chemistry.

Figure 4.9 shows the metallicity distributions for stars of different ages forming in the warp and in the main disc. The disc stars enrich faster than their warped counterparts. Stars in the main disc become super-solar whilst most particles that were born in the warped region are sub-solar even after 10 Gyr.

The substructure in the AMR appears to be strongest in the age range 4–7 Gyr, corresponding closely to the time where the star formation in the warp is strong in the low threshold simulation, as indicated by Figure 4.3. This suggests that the warp may be responsible for this feature in the AMR. We use our previous definition of $\theta_{\rm form}$ and $R_{\rm form}$ to isolate star particles forming in the warp, which we show in the top panel of Figure 4.10. This excludes the flat, broadened AMR and isolates the substructure successfully. The slope of this substructure is calculated by least-squares fitting as -0.30 ± 0.01 dex/Gyr, which is comparable to the AMR of the warped region of M31 found by Bernard et al. (2012, 2015). For this substructure to be present at all radii, some mechanism must be moving the stars that form in the warp into the main disc. We demonstrate below that the stars born in the warp eventually settle into the disc and are then subject to migration via transient spirals, causing the substructure to manifest throughout the disc. To demonstrate that the stars do settle, we show in Figure 4.11 $\theta_{<j>}$ versus $\theta_{\rm form}$ for particles forming in the warp, where $\theta_{<j>}$ is the angle between the stellar angular momentum vector averaged

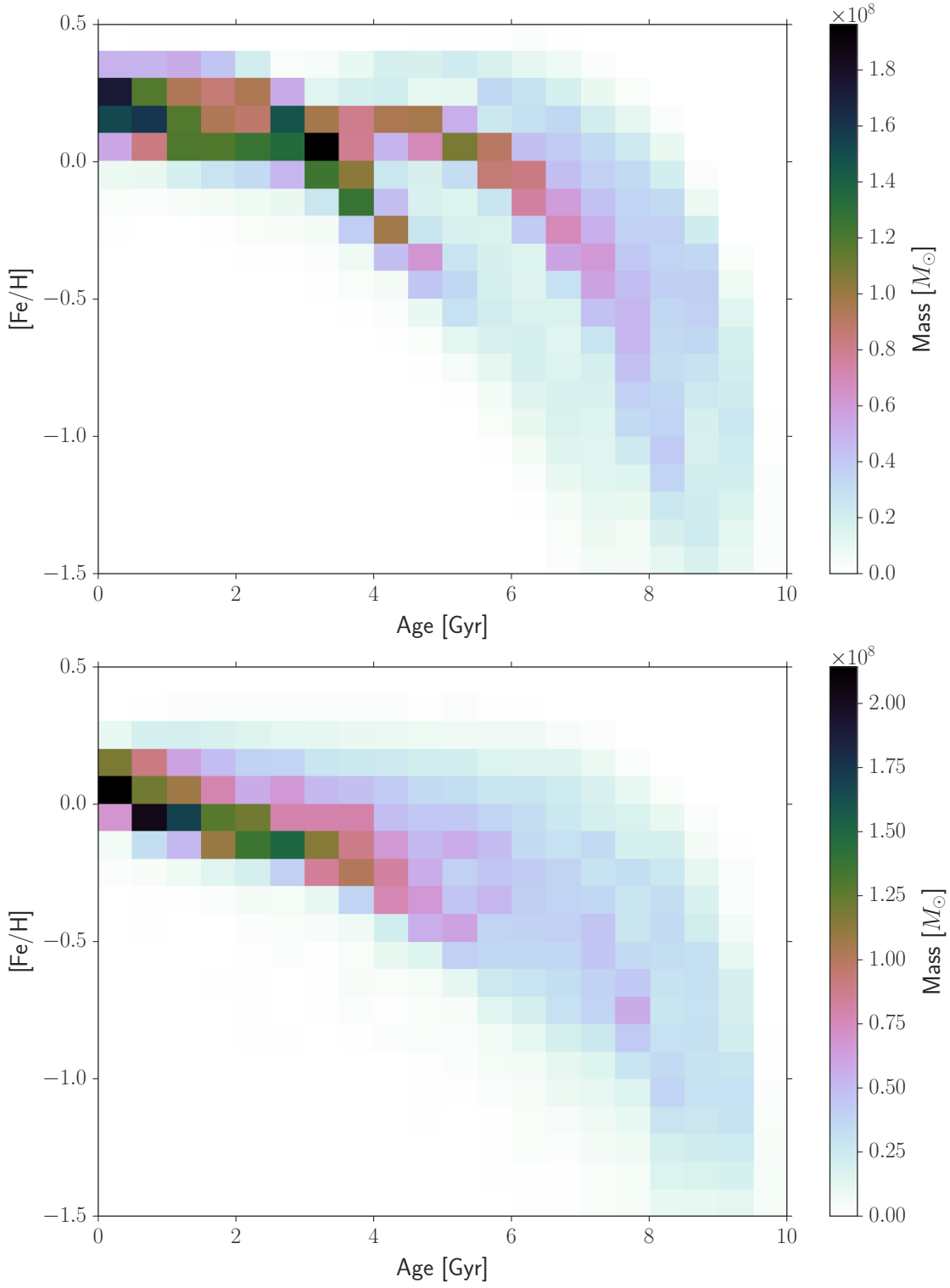

Figure 4.8: Mass-weighted AMR for the Solar neighbourhood ($7.0 \leq R \leq 9.0$ kpc) for the low threshold run (top) and the high threshold run (bottom).

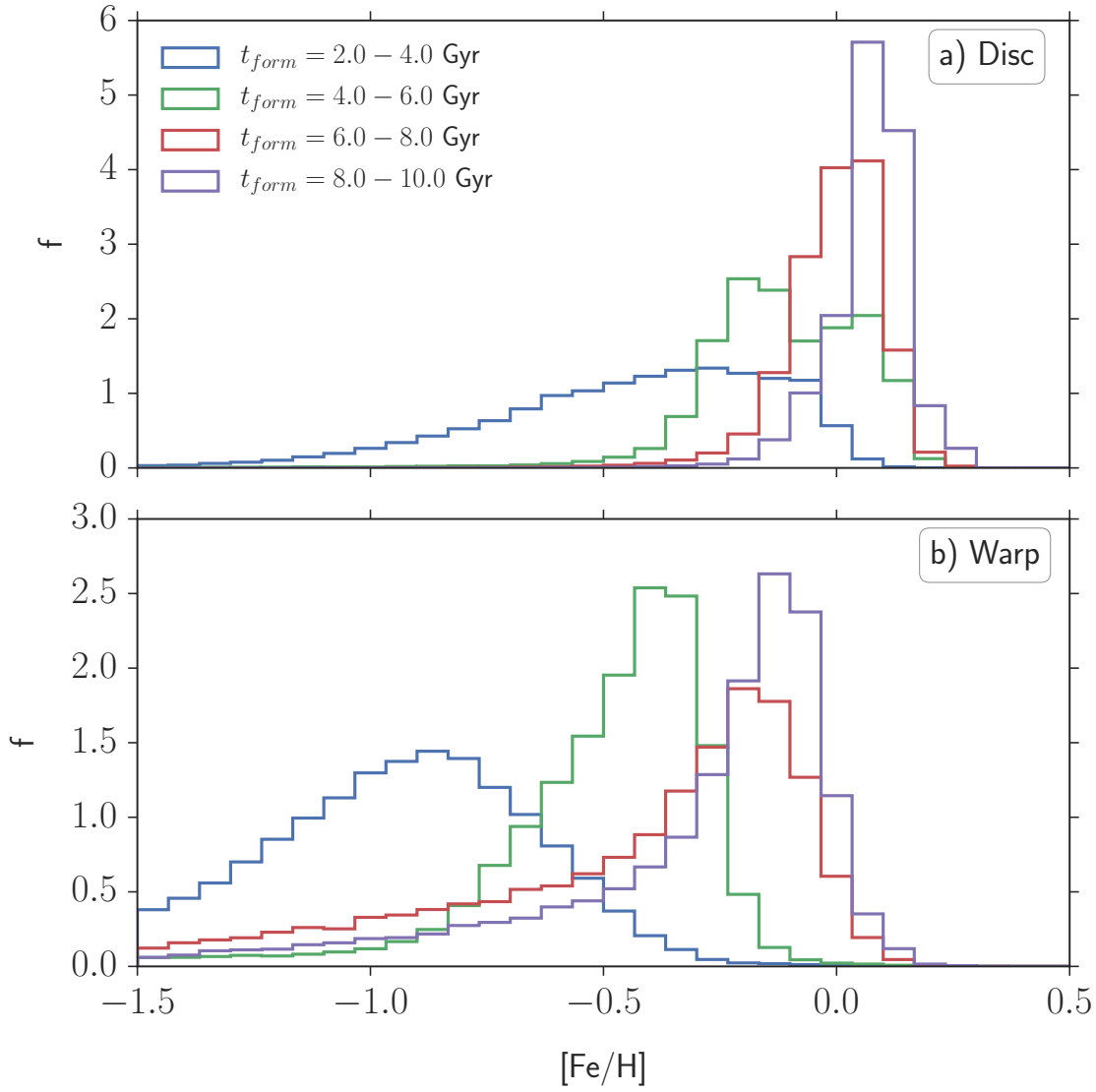

Figure 4.9: (a) Normalised Histogram of [Fe/H] for stars in the low threshold run born at different times in the disc. (b) Normalised Histogram of [Fe/H] for stars born in the low threshold run at different times in the warp. Both use the previously defined cuts for θ_{form} and R_{form}.

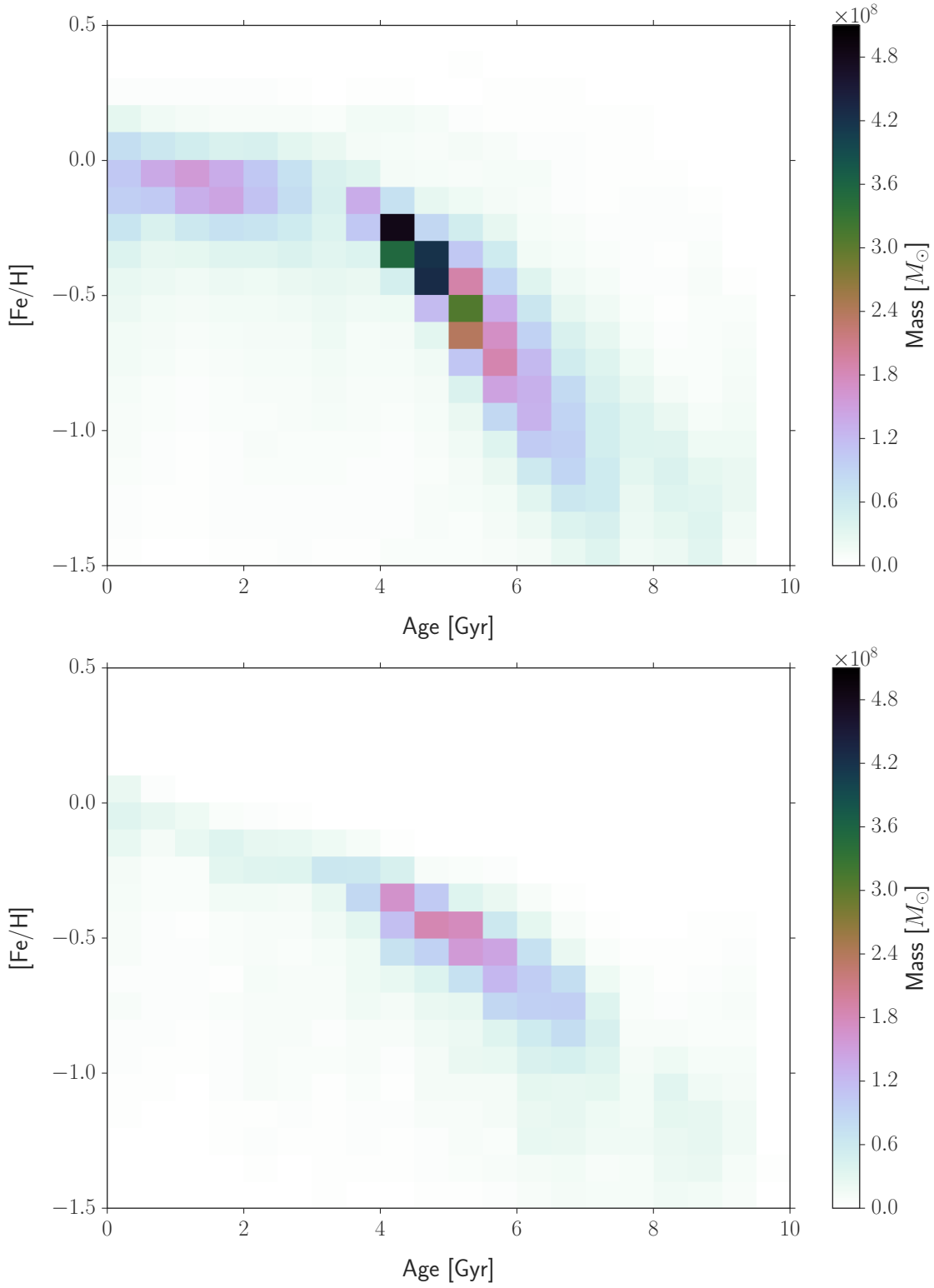

Figure 4.10: AMR of stars that form in the warp, selected by taking a cut of $10^\circ \leq \theta_{\rm form} \leq 40^\circ$ and $10 \leq R_{\rm form} \leq 20$ kpc, for the low threshold run (top) and the high threshold run (bottom).

over the last 1 Gyr, and the disc. The majority of the stars have $\theta_{<j>} << \theta_{\rm form}$ indicating that they settle into the disc during their evolution.

Therefore we postulate that stars forming in the warp do so in an environment that remains isolated from the effect of migration, settle into the disc, and then migrate across all radii where they imprint the warp AMR over the broad, flattened AMR of the main disc. This superimposes the warp AMR over the disc AMR, leading to that seen in the top panel of Figure 4.8. In the bottom panel of Figure 4.8 we show the AMR of the high threshold run warp. This shows a similar substructure but it is much weaker, which is to be expected, since there is less star formation in the warp at all times. The slope of the AMR is sensitive to the fraction of feedback energy coupled to the ISM, the rate of gas infall and the star formation rate. Assuming that the infall rate of the high and low threshold runs are approximately the same, the shallower substructure is due to less feedback in the warp as a consequence of the lower star formation.

These findings demonstrate that the substructures present in the global AMR are a result of the warp settling into the disc and imply that the warp remains chemically isolated from the mixing effects of migration. To demonstrate this is the case, we plot in Figure 4.12 $\theta_{<j>}$ versus R. We find that stars do not substantially populate the warp, implying that there is little to no migration into the warp. This explains why the AMR of the warp stars does not show the flattened, broad characteristics expected if the disc stars contaminated the warp with the higher metallicities found in the disc. Whilst not shown, we have verified that this is the case for all 1 Gyr samples. This provides an explanation for why AMRs are not flattened in observations of warps, as first shown by Bernard et al. (2012, 2015) and in our simulations. Since the stellar warp has largely dissipated ~ 4 Gyr prior to the final output, we cannot test if the warp would have a strong AMR at the present time.

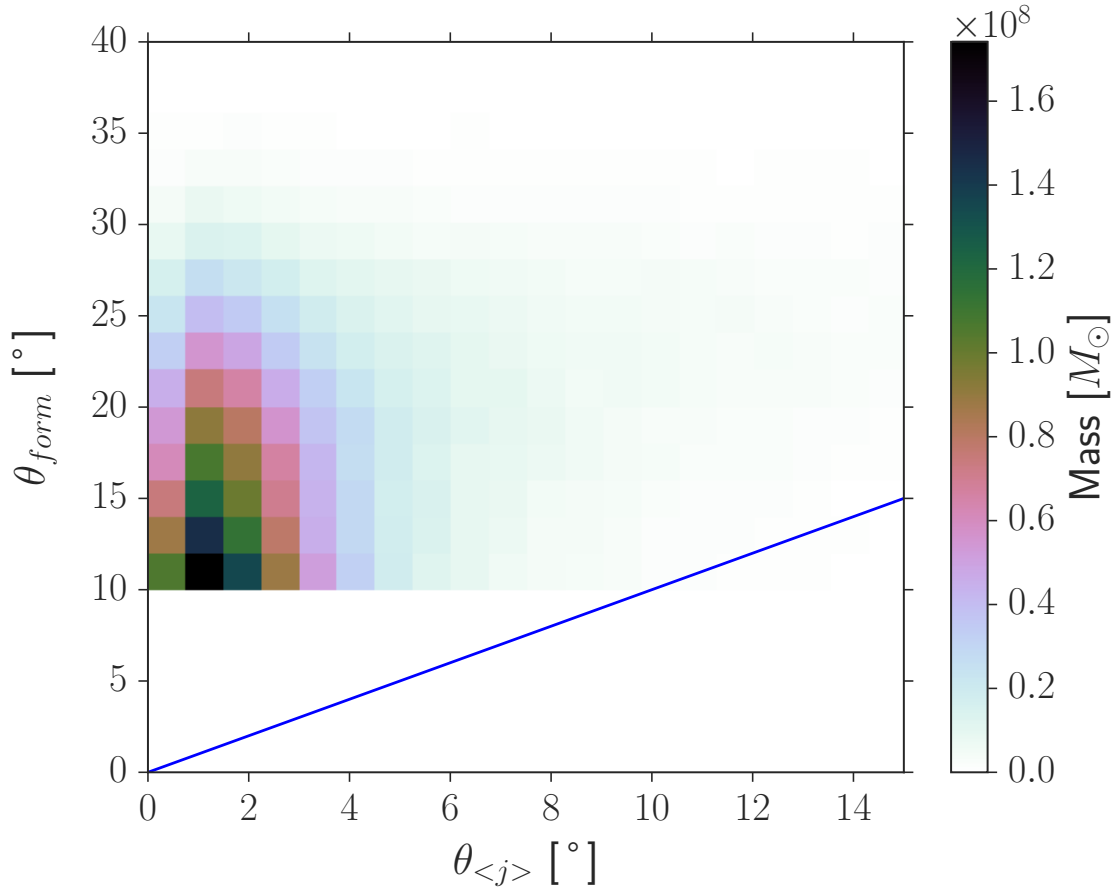

Figure 4.11: Mass weighted $\theta_{\rm form}$ versus $\theta_{<j>}$ for stars born in the warp of the low threshold run. The diagonal line indicates $\theta_{\rm form} = \theta_{<j>}$.

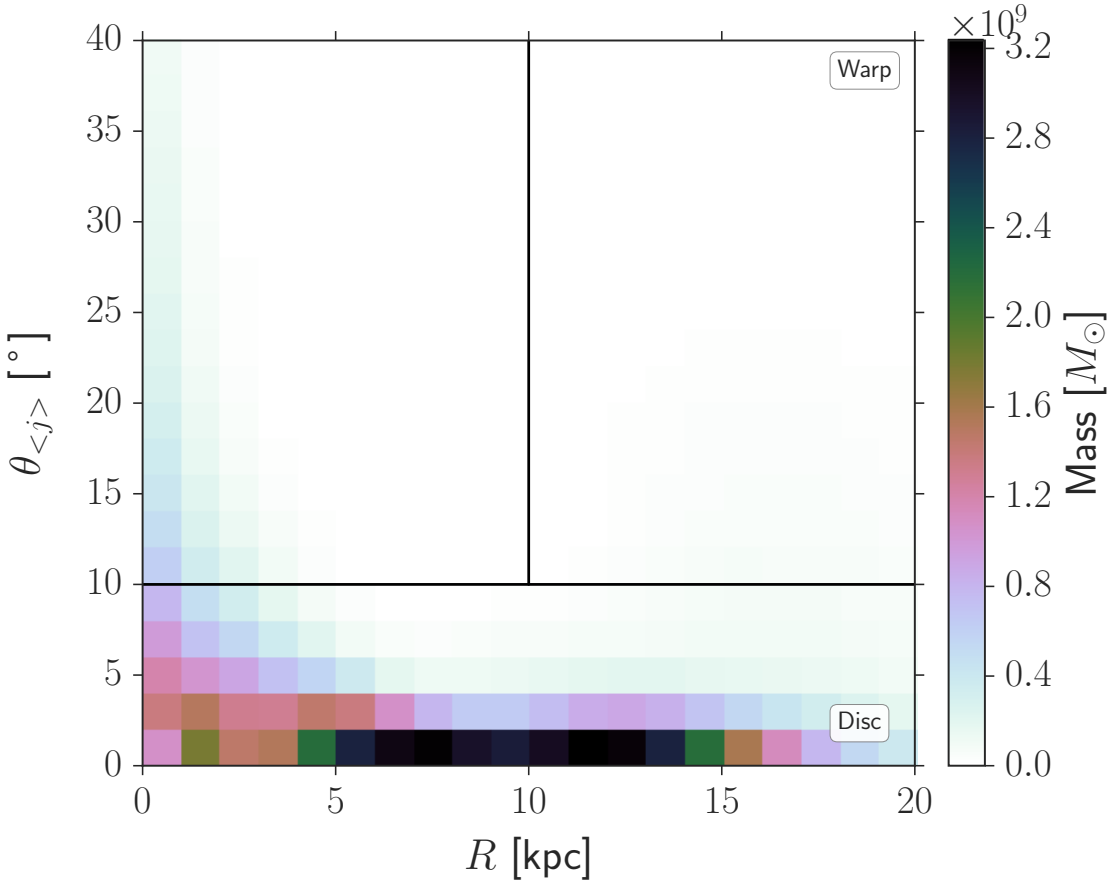

Figure 4.12: Final radius versus $\theta_{<j>}$ for stars in the low threshold run.

This raises the question whether we should be able to infer the presence of star formation in the warp of our own Galaxy solely from substructures present in the AMR. It has been known for a long time that the MW is warped in both the gas (Burke 1957; Oort et al. 1958; Levine et al. 2006), and the stellar disc (Momany et al. 2004, 2006). Our findings imply that the warp should leave a detectable imprint on the local AMR whilst it has been forming stars. To test whether this is true we take our model metallicity and age, and convolve them with a Gaussian, with full width half maximum comparable to typical errors in observations (typically $\pm$0.1 dex in [Fe/H] and $\pm$1.5 Gyr in age Edvardsson et al. (1993); Haywood et al. (2013)). The top left panel of Figure 4.13 shows the mass-weighted AMR for the Solar neighbourhood of the low threshold galaxy. In the top right panel we show the AMR convolved with $\pm$0.1 dex in [Fe/H] and the bottom left panel shows the AMR convolved with $\pm$1.5 Gyr in age. The bottom right panel shows that when both of these observational errors are considered, the AMR lacks the substructure present as a result of the warp and would therefore not likely be detectable in the Solar neighbourhood AMR, given current uncertainties in age and metallicity. Repeating this exercise with asteroseismic age uncertainties of 20 % (Casagrande et al. 2015) similarly masks the substructure and it remains masked for all tests until the uncertainty is $\sim$ 5% or lower. As such we conclude it is unlikely that these substructures will be detectable with current observational techniques.

The observations of Bernard et al. (2012, 2015) indicate that we can see an AMR in M31. Given that we have demonstrated that the warp remains isolated from the effects of migration, an AMR is expected. Figure 4.14 shows the AMR for stars forming in the warp of the low threshold run, similarly convolved with normal observational errors. This causes the AMR to be less defined and "blurred", yet there is still a general decrease in [Fe/H] with age.

In Figure 4.15 we show surface density profiles as a function of both $R_{\rm form}$ and

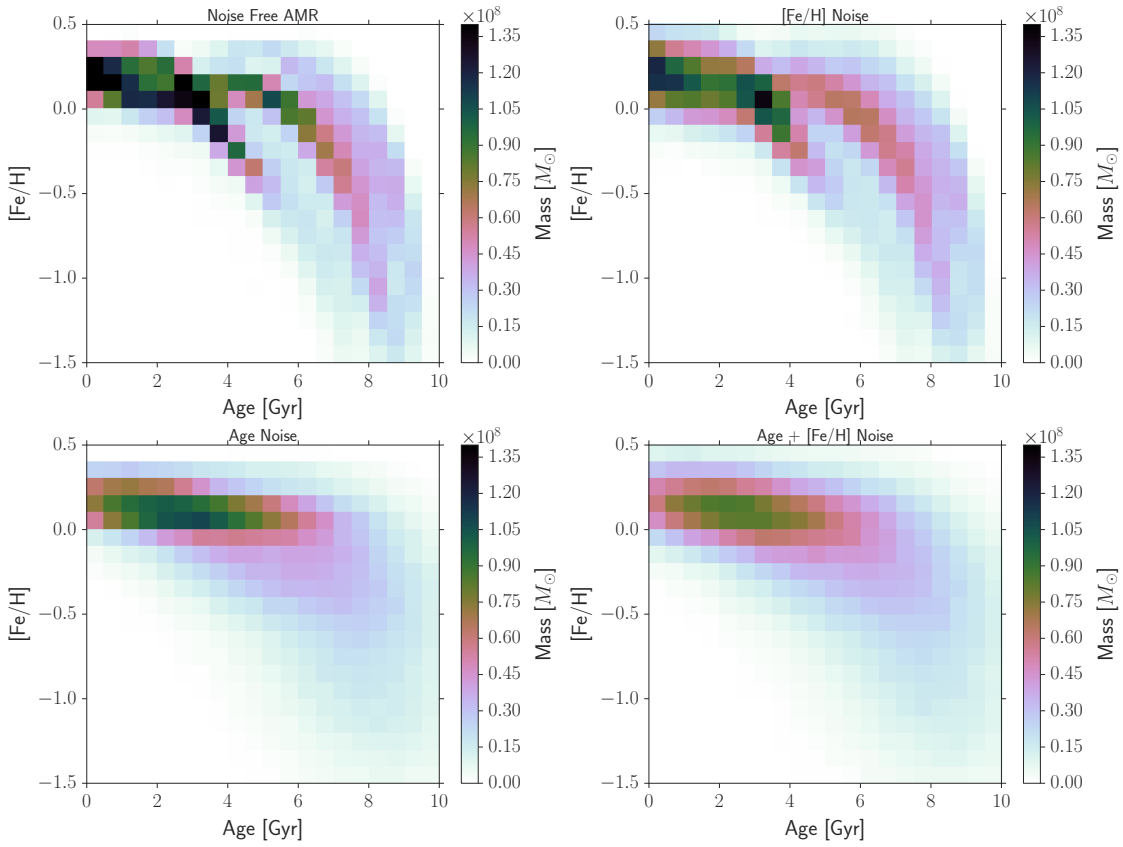

Figure 4.13: *Top Left*: Mass-weighted AMR for the Solar neighbourhood of the low threshold galaxy. *Top Right*: AMR with ±0.1 dex noise added to [Fe/H]. *Bottom Left*: AMR with ±1.5 Gyr noise added to age. *Bottom Right*: AMR with both age and [Fe/H] noise added.

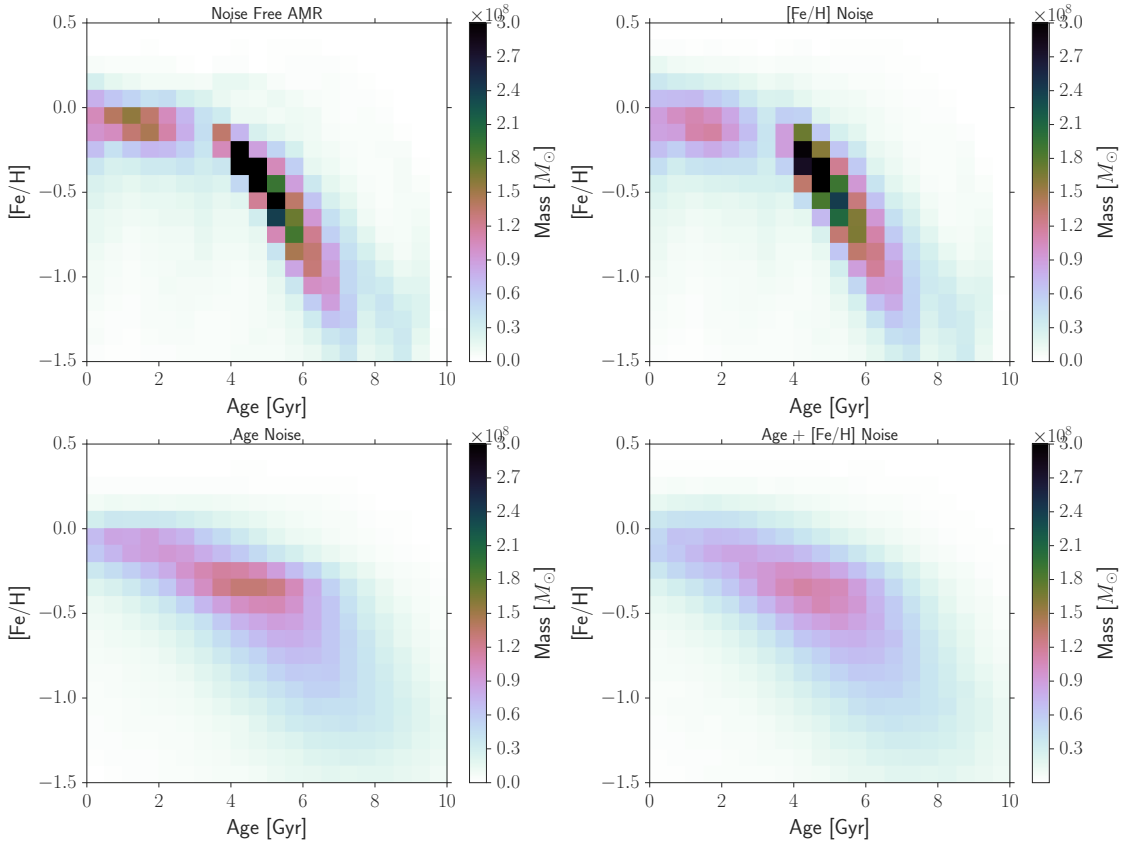

Figure 4.14: *Top Left*: Mass-weighted AMR forming in the warp in the low threshold galaxy. *Top Right*: AMR with ±0.1 dex noise added to [Fe/H]. *Bottom Left*: AMR with ±1.5 Gyr noise added to age. *Bottom Right*: AMR with both age and [Fe/H] noise added.

$R_{\rm final}$ for disc and warp forming populations. In the low threshold run, at a radius greater than $\sim$ 13 kpc, stars forming in the warp dominate when compared with stars formed in the disc at that radius. However at the final output, due to the effect of migration, the radius at which the warp forming stars dominate moves outward to $\sim$ 16 kpc. Since the outer disc is dominated by stars forming in the warp, the AMR shown in Figure 4.16 shows a strong relation as expected when migration is not efficient. Thus we can postulate that the outer discs of warped galaxies may contain strong AMRs, even if the rest of the disc does not. Similarly, stars forming in the warp of the high threshold run dominate at a radius of $\sim$ 13 kpc, yet when considering the final radii, the warp does not dominate at any radius.

4.4 Orbits

We compute stellar orbits for star particles in two regions of the low threshold galaxy, a 'Solar neighbourhood' zone at $7 \leq R \leq 9$ kpc and an outer disc 'post-break' zone at $22 \leq R \leq 25$ kpc. The potential is fixed and the orbits are computed over a 2 Gyr time-period. We compute the orbital eccentricity and maximum height above the plane (hereafter $z_{\rm max}$) to investigate what effect these have on the magnitude of migration and the substructures in the AMR.

In Figure 4.17 we show the distribution of eccentricity and $z_{\rm max}$ for particles born in the warp (black-solid) and in the disc (red-dashed) that end in the Solar neighbourhood. The median eccentricity and $z_{\rm max}$ for stars born in the disc are $0.27^{+0.55}_{-0.15}$ and $1.10^{+2.25}_{-0.69}$ kpc respectively, whilst for stars born in the warp they are $0.27^{+0.46}_{-0.15}$ and $2.19^{+3.49}_{-1.09}$ kpc, where the errors are given by the 15th and 85th percentiles which better describe asymmetric distributions. We postulate that the extended tail to high eccentricities in the disc sample is related to heating being more efficient when particles stay close to the midplane. Alternatively, our cuts separating the warp and disc forming stars is designed to be conservative so the warp remains cleanly

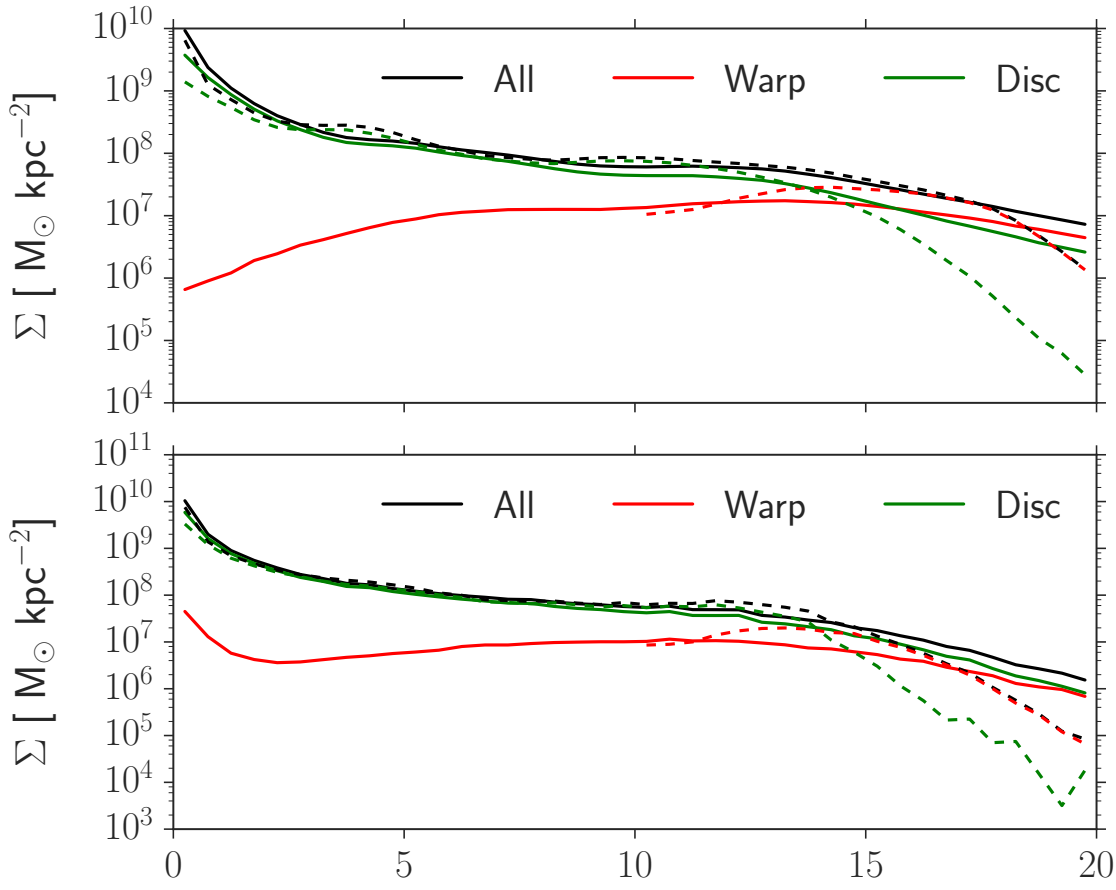

Figure 4.15: Surface density as a function of final radius (solid lines) and formation radius (dashed lines) for warp, disc and total populations as detailed by the insets for the low threshold run (top) and the high threshold run (bottom).

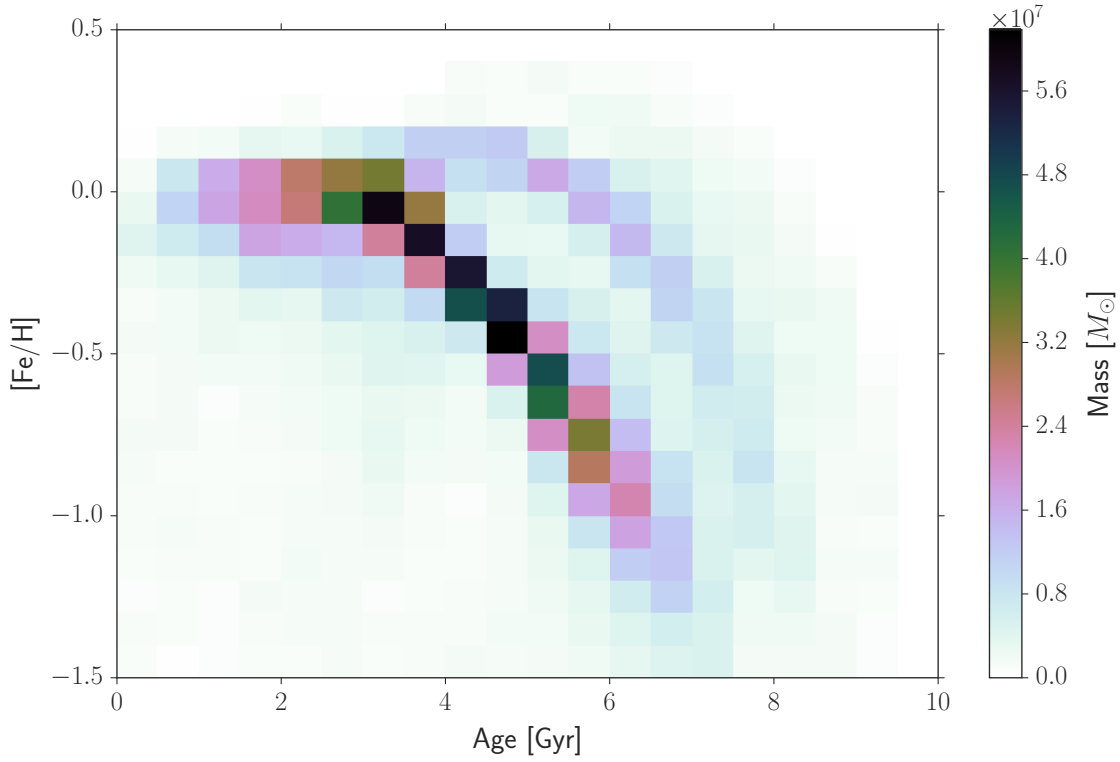

Figure 4.16: Age-metallicity relation for the outer disc region (18 kpc $\leq R \leq$ 20 kpc) of the low threshold run.

cut from the disc, which may leave some contamination of warp stars in the disc population. The stars in this extended tail do not form at any particular radius and are not formed in the bulge. Particles born in the warp show much larger $z_{\rm max}$ then those born in the disc, indicating that even once they settle, the orbits are still vertically hot, meaning the inclusion of a warp will thicken discs at all radii.

We show the distributions of eccentricity and $z_{\rm max}$ for the outer disc sample in Figure 4.18. The mean eccentricity and $z_{\rm max}$ for disc stars are $0.26^{+0.35}_{-0.18}$ and $2.81^{+4.40}_{-1.71}$ kpc respectively, whilst for warp stars these are $0.27^{+0.36}_{-0.18}$ and $4.31^{+6.84}_{-2.42}$ kpc. The eccentricity does not have the same tail as in the Solar neighbourhood and disc and warp stars have very similar eccentricities. Since very few stars form in the post-break region, the outer disc sample will be built up almost entirely from stars that have migrated from the inner regions. For stars to migrate efficiently over large distances, they have to remain in corotation resonance with the spiral perturbations and as such, stars on elliptical orbits will migrate less than those on more circular ones. Since the outer disc is made up almost entirely from migrated particles, then we would expect that the orbital eccentricity of this population would be low. The outer disc shows a thicker component, similar to the Solar neighbourhood, however particles in general reach higher $z_{\rm max}$.

4.5 Chemistry

The $[\alpha/{\rm Fe}] - [{\rm Fe/H}]$ plane is a useful tool for understanding the history of a galaxy. Alpha elements such as C, O, Ne, Mg, Si (i.e. those made by the triple-alpha process) are predominantly produced by type II supernovae from short lived stars, whilst Fe tends to be produced by type Ia supernovae. The progenitors of type Ia systems have longer life-times and so are offset in time compared with the type IIs (Tinsley 1979), which leads to a "knee" in the $[\alpha/{\rm Fe}] - [{\rm Fe/H}]$ plane. At the turning point, the number ratio of Ia/II supernovae is constant, and for the MW this value is

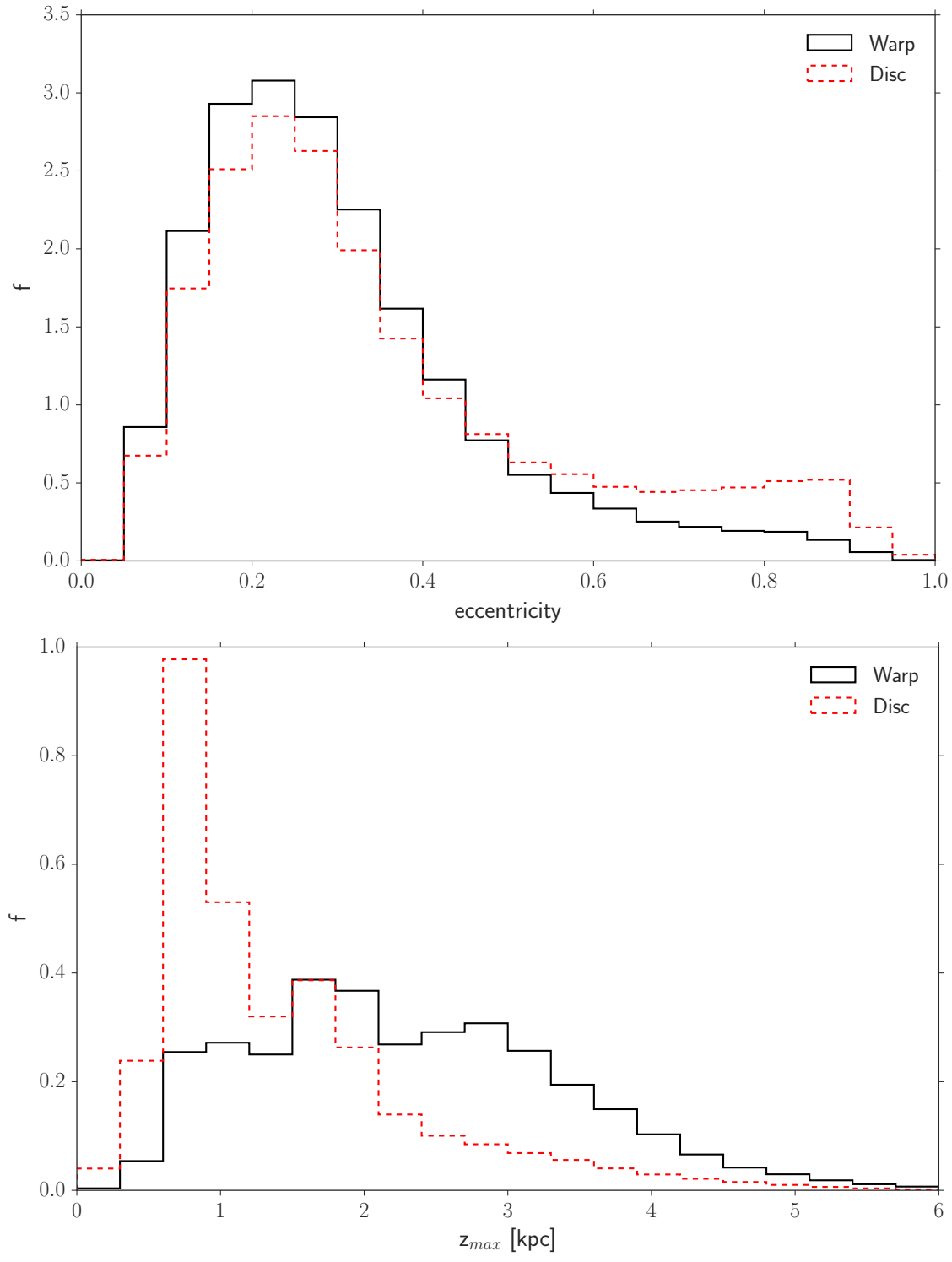

Figure 4.17: *Top*: Normalised distribution of orbital eccentricity in the low threshold run for the warp (black-solid) and disc (red-dashed) in the Solar neighbourhood ($7 \leq R \leq 9$ kpc). *Bottom*: Normalised distribution of maximum orbital height above the plane.

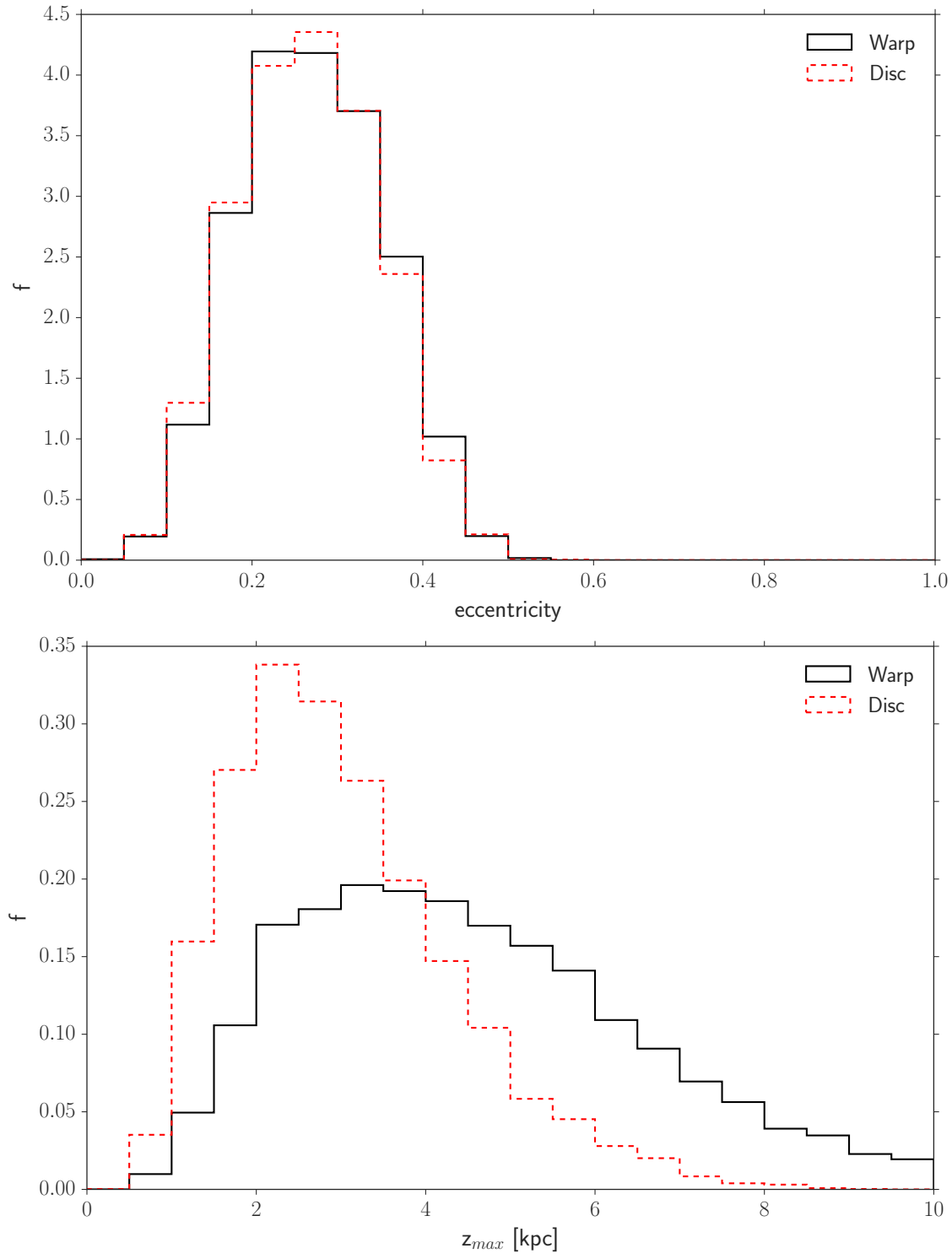

Figure 4.18: Same as Figure 4.17 but for the outer disc ($22 \leq R \leq 25$ kpc).

estimated at [Fe/H] ~ -0.3 dex (Edvardsson et al. 1993).

In the top left panel of Figure 4.19 we show the $[\alpha/\mathrm{Fe}] - [\mathrm{Fe/H}]$ plot for the Solar neighbourhood of the low threshold model. There are three distinct peaks in this distribution. In the subsequent panels we show (clockwise) mean age, formation radius, eccentricity and θ_{form}. We highlight the peaks with the boxes shown to guide the eye across panels. It is evident from the θ_{form} panel that all three of these distinct peaks have $\theta_{\mathrm{form}} < 10^{\circ}$ and therefore do not satisfy our warp selection criteria. However we note that there is some interesting overall trends to be noted. [O/Fe] tends to increase as a function of age, with the younger stars having low [O/Fe], whilst [Fe/H] spans across all ages, which is to be expected in a system with large radial migration. Stars with low α and metallicity tend to be born in the outer disc, whilst those with high α and metallicity tend to be born interior to their final radius. The two higher metallicity peaks at [Fe/H] > 0.15 dex (i.e. the rightmost two boxes) seem to form a single linear feature and have very similar average eccentricities, whilst the lower metallicity peak has a much lower eccentricity. Taken with the age data these imply that younger stars form this secondary peak, but do not give an indication as to why this may be. Since this has a lower metallicity it implies that there has been some sort of injection of pristine material into the disc, yet as we showed in Figure 4.7 the average metallicity of gas in the Solar neighbourhood does not change much between 6–10 Gyr. We also note the lack of the "knee" in these figures which may relate to either some inconsistencies in the relative supernova timescales or a problem with the oxygen feedback processes in GASOLINE. We leave this to be addressed in future work, since it does not directly affect the conclusions contained in this work.

Loebman et al. (2011) found that, although often used as a proxy for age, the age-α plane for thin disc stars is degenerate. They follow the arguments of Lee et al. (2011), who used SDSS SEGUE data to chemically divide the disc into α-enriched

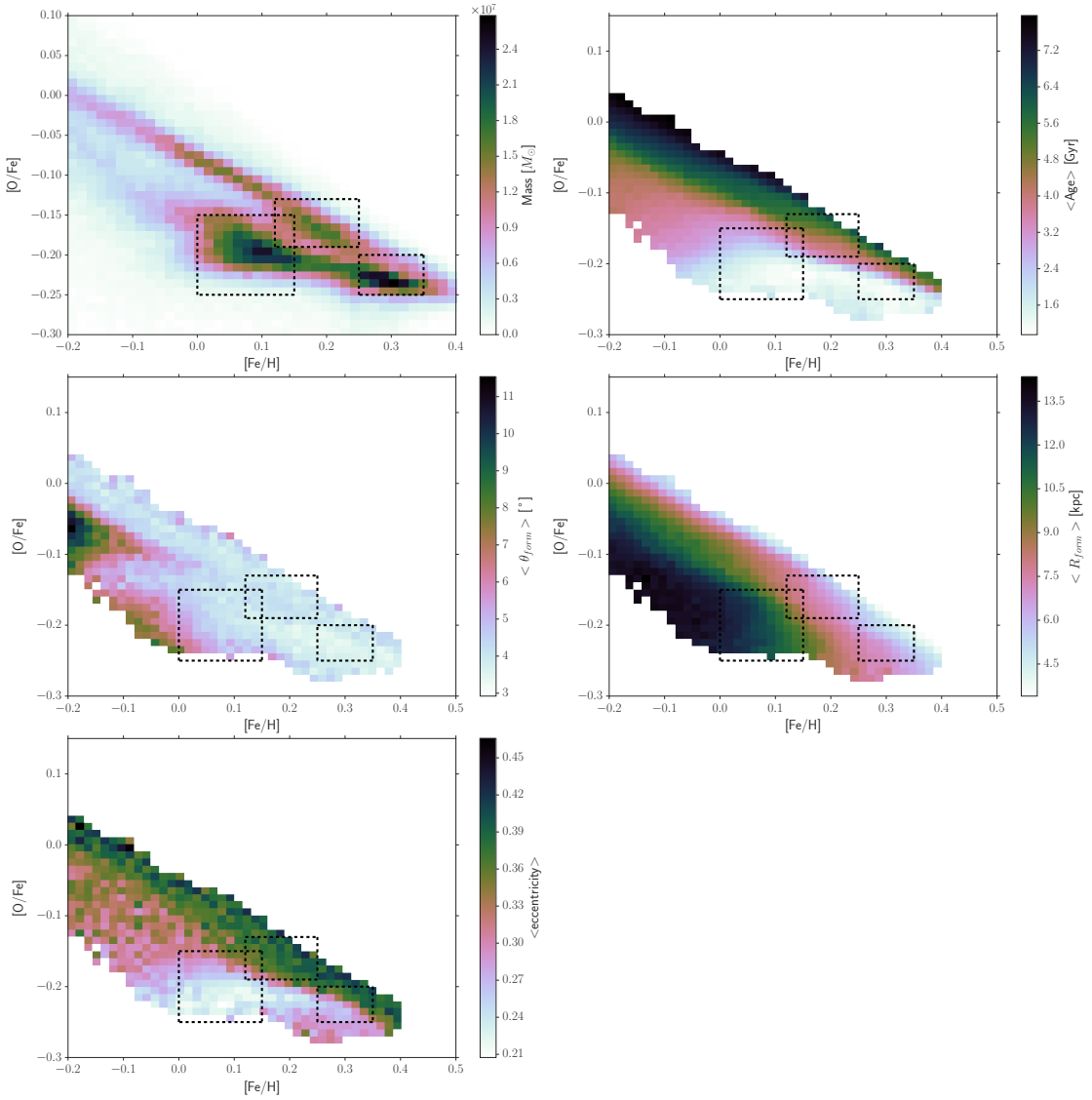

Figure 4.19: ([O/Fe]) versus metallicity [Fe/H] for the Solar neighborhood of the low threshold model. Clockwise from top left: mass-weighted, mean age, mean formation radius, mean eccentricity and mean $\theta_{\rm form}$. We have excluded bins with less than 50 particles to reduce the noise.

and α-poor populations, assigning stars with ([O/Fe] $\geq$ -0.1) as thick disc. This separation indicates that the thick disc is a predominantly old component and shows strong correlation between α and age. Conversely stars with ([O/Fe] $\leq$ -0.1) are assigned as thin disc and show a much weaker correlation. We produce a similar plot in Figure 4.20 for our low threshold run, which shows similar characteristics. However we note that our thick disc region shows a larger spread and shows distinct tracks and substructures, similar to those found in the AMR. We isolate this feature using the bounds represented by the blue box and then plot these particles ($R_{\rm form} - \theta_{\rm form}$) in the bottom panel. This shows that this substructure also results from the warp. We approach this in the opposite manner, and find that using our predefined cuts on $R_{\rm form}$ and $\theta_{\rm form}$, isolates this substructure well and that removing this population and considering only the main disc stars shows good agreement with the results of Loebman et al. (2011). Similarly to the AMR, blurring the age with typical observational uncertainties masks this substructure. As such we conclude that these would typically not be detectable with typical age/α uncertainties. For comparison we show in the bottom panel of Figure 4.20 an observational age-[α/Fe] plot taken from Haywood et al. (2013). As expected due to the large errors in age determination, the correlation is broad and there are no substructures present.

4.6 Conclusions

We have used N-body+SPH simulations to consider the effect that warps have on the AMR of a galaxy. We find that the warp can lead to an AMR which manifests as a substructure imprinted over the flattened and broad AMR of the efficiently migrating main disc. These substructures become weaker when we run the system with a higher star formation threshold, leading to less star formation in the warp, indicating that the chemical properties of the warp behave as one would expect in a galaxy where migration is not efficient. Furthermore, the presence of these

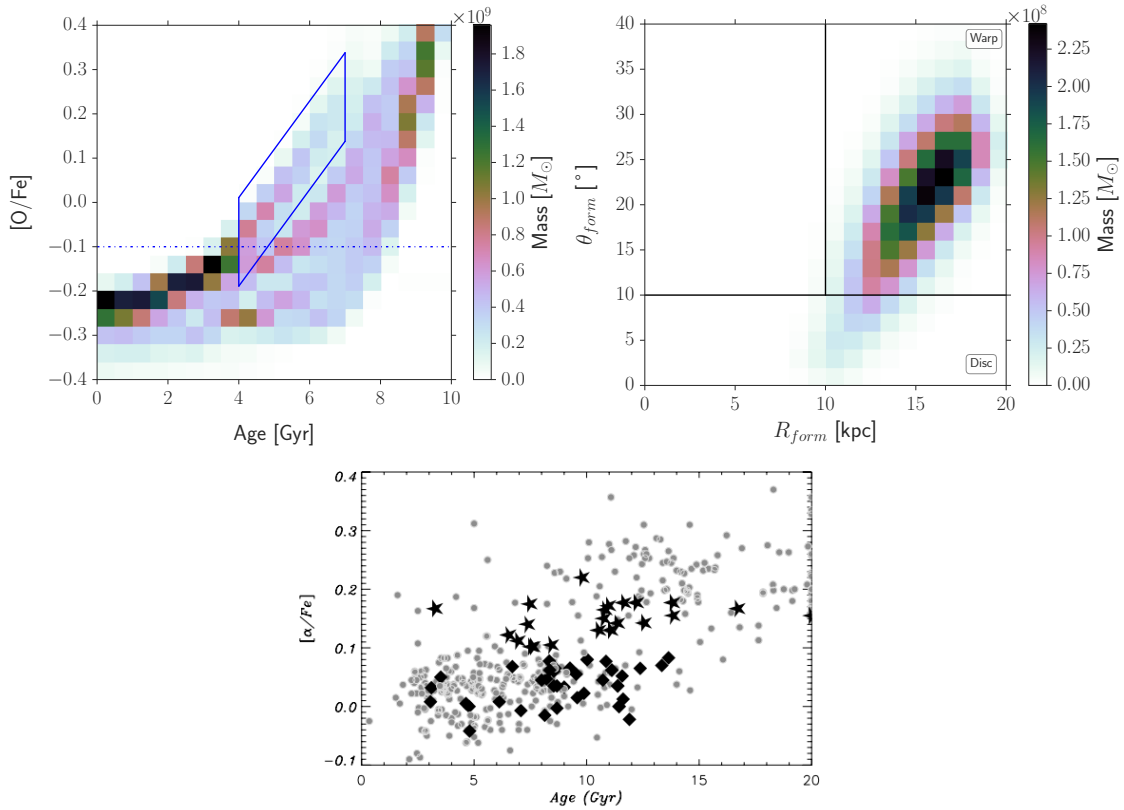

Figure 4.20: *Top Left*: age-[O/Fe] plot for our high threshold run showing the cut at [O/Fe] > -0.1 as thick disc. The blue box shows our cut on the secondary feature. *Top Right*: $R_{\rm form}$ versus $\theta_{\rm form}$ for the cut in the top panel. *Bottom*: Observational age-[α/Fe] plot taken from Haywood (2008). Diamonds show objects that are kinematically considered part of the thick disc yet have [α/Fe] < 0.1 dex, whilst the star symbols are considered transition region stars.

substructures across a large range of radii is suggestive that the stars forming in the warp still migrate efficiently, and we have demonstrated that the particles born in the warp settle into the disc, allowing them to migrate. Furthermore, we have demonstrated that stars born in the disc do not migrate into the warp, allowing this region to remain chemically isolated from the chemical mixing effect of migration. These findings explain why observations of warped regions in M31 show good correlation between age and metallicity (Bernard et al. 2012, 2015). As a by-product of the increased star formation rate in the disc compared with the warp, the average metallicity of the warp is lower than that of the disc. We postulate that it may be possible to infer the presence of a warp in the MW if we find imprinted substructures within the local AMR. However, convolving our data with typical observational uncertainties ($\pm$2 Gyr in age and $\pm$0.1 dex in [Fe/H]) shows that these substructures would not likely be detectable. Even the current best age determinations from Kepler asteroseismology ($\sim$ 20%) does not provide adequate precision. We also find evidence that the warp can be seen in substructures in other parameter space, such as the α-age plane, however these are similarly masked when convolved with typical uncertainties.

We have also investigated the orbital properties of two regions of the galaxy, a Solar neighbourhood region and one in the outer disc. We find that for both these samples, stars born in the warp have larger orbital heights, even once they settle into the disc. Consequently the disc is thicker at all radii because of the warp. We find no difference in the eccentricities between particles born in the warp or in the disc, but note that an extended highly eccentric tail is present in the Solar neighbourhood disc stars, which we postulate results from heating being more efficient near the midplane. Finally we note that particles in the outer disc show lower eccentricities than those in the Solar neighbourhood, a direct consequence of the radial migration mechanism. Since very few stars form in the post-break region, the vast majority

of stars outside of this radius have migrated there, which requires them to be in corotation resonance with transient spirals. This in turn requires that the orbits are not highly eccentric.

Chapter 5

Conclusions and future prospects

This thesis has considered the effect of radial migration on the outskirts of disc galaxies and considered how these effects may influence the Solar neighbourhood. Until the seminal paper by Sellwood & Binney (2002), stars were considered to remain at approximately the same radius, with small deviations due to orbital eccentricities. This paradigm allowed each radial annulus to be treated as an isolated region, allowing the inference of the galactic history at that region. If a region of a galaxy is isolated from its surroundings, then the gradual enrichment of the interstellar medium via feedback mechanisms such as stellar winds and supernovae will cause younger stars to be more metal rich, whilst older stars will be metal poor, leading to an age metallicity relation (AMR). However, when including the effects of migration, one has to relax the assumption that each annulus remains isolated. This vastly complicates uncovering the galactic history, especially since migration does not leave imprints on the stellar kinematics. Including migration has provided an explanation for some inconsistencies between earlier models and observations. The Solar neighbourhood age-metallicity relation has been seen to be flatter and broader than first observed (Edvardsson et al. 1993; Haywood 2008), which becomes the natural state when radial mixing is prevalent (Sellwood & Binney 2002; Roškar et al. 2008a). Migration has also been able to account for an upturn in mean

age, seen past the break-radius in both simulations (Roškar et al. 2008b) and in observations (Yoachim et al. 2010; Radburn-Smith et al. 2012), and as a possible mechanism for the formation of thick discs (Loebman et al. 2011). As such, having a clear understanding of the implications of migration is necessary to uncover the history of our own galaxy and a detailed framework of these implications will be needed to understand observations from upcoming large surveys such as GAIA and LSST. Currently little work has been done on understanding the implications of warps on the chemical properties of discs and the role of migration in these regions. Given the ubiquity of warps in the local universe (Sanchez-Saavedra et al. 1990; Reshetnikov et al. 2002) and the fact that our own galaxy is warped (Burke 1957) this is an important factor to include in Galactic archaeology models. We also aimed to explain the relative excess of type I profiles observed in cluster lenticulars, compared to disc galaxies found in the field (Gutiérrez et al. 2011; Erwin et al. 2012; Roediger et al. 2012; Maltby et al. 2015). Since migration has been shown to greatly effect the outer disc (Roškar et al. 2008a,b), it may be an important factor to include when considering profile changes in these regions.

5.1 Profile and colour changes

In Chapter 2 we demonstrated that a spiral galaxy falling into a gas rich cluster environment develops a type I profile, whilst in isolation, the same galaxy exhibits a type II profile. The cluster galaxy initially forms a type II profile, which transforms into a type I profile at the same time that the galaxy reaches a region of gas dense enough to begin ram pressure stripping of the cold gas. With very little difference in the radial velocity dispersion, we instead find an increase in induced spiral activity which drives large outward migration, explaining the profile changes. To test the importance of the environment on the profile changes, we also hand quenched the isolated model at a time coinciding with the onset of ram pressure stripping and

find that whilst the galaxy continues to exhibit a type II profile, the break appears weaker. We therefore conclude that the termination of star formation is an important factor for break weakening, but is not responsible for the transformation between profile types.

The stripping occurs outside-in, with the last bout of star formation occurring in the bulge, similar to the findings of Johnston et al. (2014). However the central regions of the lenticular galaxy appear redder than the surroundings due to the flux being dominated by the older population and the young stars being more metal rich. Thus care must be taken when using colours to determine the locations of potentially young stars in recently stripped lenticulars. We have also shown that after the transformation, the galaxy exhibits a flat age and metallicity profile, in agreement with the observational results of Roediger et al. (2012) who found flat metallicity and age profiles amongst type I Virgo cluster lenticulars. A flat age gradient can be explained by the termination of star formation along with efficient redistribution of the stellar content via radial migration.

By using a 3D radiative transfer analysis code, DART-RAY, we have also demonstrated that after ram-pressure stripping the galaxy transitions from a blue, star-forming spiral galaxy to a redder lenticular disc. Until ram pressure stripping begins, the cluster and isolated galaxies evolve in unison, and the transformation itself occurs rapidly. Furthermore, we find that the blue spirals in the isolated case show a distinct termination at the break radius, visually agreeing with the findings of Roškar et al. (2008b), that break radii are seeded by a decrease in cold gas surface density (Kennicutt 1989; Schaye 2004) and the outer disc is built up from an outwardly migrating, older population. Observations from SDSS (Schawinski et al. 2014) discovered a distinct bimodality in galaxy distribution in the colour-mass plane, where late type galaxies fall in a blue cloud and early type galaxies form a red sequence. In between these two regions is a sparsely populated green valley. Using DART-RAY,

we have calculated colours and magnitudes for the isolated and cluster galaxies. We find that the isolated galaxy slowly increases its $u-r$ colour and mass, as it converts gas to stars, but remains blue due to the ongoing star formation. In comparison, the cluster galaxy shows a redder $u-r$ and lower mass, in agreement with star formation termination due to ram pressure stripping. Whilst the cluster galaxy ends in the green valley, we have demonstrated that the result is sensitive to our assumptions, both in GASOLINE and DART-RAY. By removing the lowest 25% of metal poor stars in the calculation we have significantly increased the $u-r$ colour. Given that our system begins with pristine initial conditions, a significant population of stars have extremely sub-solar metallicity, an unlikely scenario in nature, given the cosmological context galaxies form in. To fully understand the extent of the colour changes and a galaxies position and evolution through the colour-mass diagram, we need to address these complications.

5.2 Migration and warps

In Chapter 4 we considered the efficiency of migration in warped galaxies. We found that at all radii, the AMR was flat and broadened, as expected if migration is efficiently mixing the populations. Imprinted over this AMR is a substructure not seen previously. By selecting stars that form in the warp, we find a strong AMR, suggesting that this region remains chemically isolated from the effects of migration. To test this, we looked at the evolution of the angle between the angular momentum vector of the disc and the stars. This demonstrated that stars born in the warp, with large angles, settle in to the disc over time and demonstrated that disc stars do not migrate into the warp. This results in the warp being chemically distinct from the disc, however due to the settling of the warp stars over time, the disc does not remain chemically distinct from the warp. Because of the interplay between this settling and the isolated nature of the warp, the stars migrate once they settle, which serves

to imprint the warp AMR across the disc. As such, we considered if it would be possible to infer the presence of a warp, in observed AMRs. Unfortunately, convolving the Solar neighbourhood AMR with typical observational uncertainties masks these substructures. Even using the current most precise asteroseismic age measurements does not provide low enough uncertainties to resolve these substructures. We have also found imprints of the warp in the α-age space.

By fixing the potential and computing orbits of the stars in the Solar neighbourhood and a post-break outer disc region we have found that stars born in the warp tend to show larger orbital heights above the plane. This indicates that some warp stars have vertically hotter orbits compared to the main disc forming population. Together with the finding that warp stars settle into the disc demonstrates that the inclusion of a warp should serve to thicken the disc at all radii. Particles in the outer disc show smaller eccentricities than those in the Solar neighbourhood. We relate this back to the migration mechanism. Since few particles are born past the break radius, the stars that populate this region must have migrated there. Whilst the migration mechanism does not require low eccentricity, a star will only remain in corotation with a spiral and migrate efficiently if it has low eccentricity. As such, highly eccentric orbits will not migrate across large radial changes, explaining the tendency towards lower eccentricities in the outer disc, which is almost completely built from a migrating population.

5.3 Going forward

Our work has provided an explanation for why there is an excess of type I profiles in cluster lenticulars, yet observational evidence indicates that these profiles can also occur in the field or in galaxies in groups. We have demonstrated that there are more spirals induced in the cluster galaxy because of the environment and that these spirals drive an increased level of radial migration. The quenched model has

shown that simply terminating star formation is not sufficient to cause the profile types to change, yet currently it is unclear if the gas stripping is required or simply an increase in spirals can cause these profile changes. For example, small groups or mergers may cause similar increases in spirals. By either converting all the cluster gas to dark matter, or replacing the cluster gas and dark matter with a potential we can determine the importance of the stripping. If the stripping is not needed for the profile changes, it provides an explanation for type I profiles in groups, where the interaction between galaxies may drive stronger spirals, in the same manner that the cluster does in this work. It will not address however how type I profiles occur in field galaxies. Furthermore, in this thesis we have only considered two specific sets of impact parameters. Our full simulation suite will allow us to test the importance of galaxy orientation and infall angle, which will be necessary for making further predictions. A recent paper by Cantale et al. (2016) has found that galaxies in clusters may take a long period (up to 5 Gyr) to fully terminate star formation after being accreted into clusters. We have found qualitatively similar results in this work, however we only have a few examples. Our full simulation suite will allow us to confirm these findings theoretically, and assess the importance of the infall parameters on the star formation rate decline.

That warps remain chemically and kinematically isolated from stars in the disc is a key finding of this work. Since the stars in the warp settle and then migrate across the disc, the local neighbourhood will be populated by stars forming in very different conditions. This will need to be considered when making inferences about the Galactic history.

Finally we have looked at orbital parameters of a few regions, but it would be helpful to have these for the whole disc. Being able to compare and contrast the kinematic properties of stars born in different regions may provide further insight into how the warp stars contaminate the main disc, and may explain features such as

the extended tail to high eccentricity in the Solar neighbourhood. We are currently developing software for highly parallelised distributed processing of orbits on the Worldwide LHC Computing Grid (WLCG) (Bird 2011). This will allow us to obtain orbits for the whole stellar disc and should vastly improve our understanding of these features.

Bibliography

Aarseth, S. J. 1963, *Mon. Not. Roy. Astron. Soc.*

Abadi, M., Navarro, J., Steinmetz, M., & Eke, V. 2003, *Astrophys. J.*, 597, 21

Abraham, R. 1998, ArXiv e-prints

Anders, E. & Grevesse, N. 1989, *Geochimica et Cosmochimica Acta*, 53, 197

Aragon-Salamanca, A., Bedregal, A. G., & Merrifield, M. R. 2006, *Astron. Astrophys.*, 458, 101

Ashman, K. & Zepf, S. 1992, *Astrophys. J.*, 384, 50

Azzollini, R., Trujillo, I., & Beckman, J. 2008, *Astrophys. J. Letters*, 679, L69

Babcock, H. 1939, Lick Obs. Bull., 19, 41

Bakos, J., Trujillo, I., & Pohlen, M. 2008, *Astrophys. J. Letters*, 683, L103

Barbanis, B. & Woltjer, L. 1967, *Astrophys. J.*, 150, 461

Barnes, J. & Hut, P. 1986, *Nature*, 324, 446

Bedregal, A., Aragón-Salamanca, A., & Merrifield, M. 2006, *Mon. Not. Roy. Astron. Soc.*, 373, 1125

Bedregal, A., Cardiel, N., Aragón-Salamanca, A., & Merrifield, M. 2011, *Mon. Not. Roy. Astron. Soc.*, 415, 2063

Bekki, K. 1998, *Astrophys. J. Letters*, 502, L133

Bekki, K., Couch, W. J., & Shioya, Y. 2002, Astrophys. J., 577, 651

Bensby, T., Feltzing, S., Lundström, I., & Ilyin, I. 2005, *Astron. Astrophys.*, 433, 185

Bernard, E., Ferguson, A., Richardson, J., et al. 2015, *Mon. Not. Roy. Astron. Soc.*, 446, 2789

Bernard, E. J., Ferguson, A. M. N., Barker, M. K., et al. 2012, *Mon. Not. Roy. Astron. Soc.*, 420, 2625

Binney, J. 2004, *Mon. Not. Roy. Astron. Soc.*, 347, 1093

Binney, J. & Tremaine, S. 2008, Galactic Dynamics: Second Edition (Princeton, NJ USA: Princeton University Press)

Bird, I. 2011, Annu. Rev. Nucl. Part. Sci., 61, 99

Bird, J., Kazantzidis, S., Weinberg, D., et al. 2013, *Astrophys. J.*, 773, 43

Bird, J. C., Kazantzidis, S., & Weinberg, D. H. 2012, *Mon. Not. Roy. Astron. Soc.*, 420, 913

Bland-Hawthorn, J., Vlajić, M., Freeman, K., & Draine, B. 2005, *Astrophys. J.*, 629, 239

Block, D. & Wainscoat, R. 1991, *Nature*, 353, 48

Borlaff, A., Eliche-Moral, M., Rodríguez-Pérez, C., et al. 2014, *Astron. Astrophys.*, 570, A103

Bosma, A. 1978, PhD thesis, PhD Thesis, Groningen Univ., (1978)

Bovy, J., Allende Prieto, C., Beers, T., et al. 2012a, *Astrophys. J.*, 759, 131

Bovy, J., Rix, H.-W., & Hogg, D. W. 2012b, *Astrophys. J.*, 751, 131

Briggs, F. H. 1990, *Astrophys. J.*, 352, 15

Brook, C., Stinson, G., Gibson, B., Wadsley, J., & Quinn, T. 2012, *Mon. Not. Roy. Astron. Soc.*, 424, 1275

Brook, C. B., Kawata, D., Gibson, B. K., & Freeman, K. C. 2004, *Astrophys. J.*, 612, 894

Bullock, J. S., Dekel, A., Kolatt, T. S., et al. 2001, *Astrophys. J.*, 555, 240

Burbidge, E., Burbidge, G., Fowler, W., & Hoyle, F. 1957, Rev. Mod. Phys., 29, 547

Burke, B. 1957, *Astron. J.*, 62, 90

Burstein, D. 1979, *Astrophys. J.*, 234, 829

Bush, S. J., Kennicutt, R. C., Ashby, M. L. N., et al. 2014, *Astrophys. J.*, 793, 65

Buta, R., Byrd, G., & Freeman, T. 2003, *Astron. J.*, 125, 634

Byrd, G., Freeman, T., Howard, S., & Buta, R. 2008, *Astron. J.*, 135, 408

Byrd, G., Thomasson, M., Donner, K., et al. 1989, Celest. Mech., 45, 31

Cantale, N., Jablonka, P., Courbin, F., et al. 2016, *Astron. Astrophys.*, 589, A82

Cappellari, M., Emsellem, E., Krajnović, D., et al. 2011, *Mon. Not. Roy. Astron. Soc.*, 416, 1680

Carignan, C., Chemin, L., Huchtmeier, W., & Lockman, F. 2006, *Astrophys. J. Letters*, 641, L109

Carlberg, R., Dawson, P., Hsu, T., & Vandenberg, D. 1985, *Astrophys. J.*, 294, 674

Casagrande, L., Silva Aguirre, V., Schlesinger, K. J., et al. 2015, *Mon. Not. Roy. Astron. Soc.*, 455, 987

Casuso, E. & Beckman, J. 2004, *Astron. Astrophys.*, 419, 181

Chamaraux, P., Balkowski, C., & Fontanelli, P. 1986, *Astron. Astrophys.*, 165, 15

Chen, B., Stoughton, C., Smith, J., et al. 2001, *Astrophys. J.*, 553, 184

Chevalier, R. 1974, *Astrophys. J.*, 188, 501

Chiba, M. & Beers, T. 2000, *Astron. J.*, 119, 2843

Comerón, S., Elmegreen, B., Knapen, J., et al. 2011, *Astrophys. J.*, 741, 28

Couch, W., Barger, A., Smail, I., Ellis, R., & Sharples, R. 1998, *Astrophys. J.*, 497, 188

Crocker, A., Bureau, M., Young, L., & Combes, F. 2011, *Mon. Not. Roy. Astron. Soc.*, 410, 1197

Crowl, H., Kenney, J., van Gorkom, J., & Vollmer, B. 2005, *Astron. J.*, 130, 65

Davis, M., Efstathiou, G., Frenk, C., & White, S. 1985, *Astrophys. J.*, 292, 371

De Rijcke, S., Van Hese, E., & Buyle, P. 2010, *Astrophys. J. Letters*, 724, L171

de Vaucouleurs, G. 1959, Handb. der Phys., 53, 311

de Vaucouleurs, G., de Vaucouleurs, A., Corwin Jr., H., et al. 1991, Third Reference Catalogue of Bright Galaxies. Volume I: Explanations and references. Volume II: Data for galaxies between 0ˆ{h} and 12ˆ{h}. Volume III: Data for galaxies between 12ˆ{h} and 24ˆ{h}. (New York: Springer-Verlag)

de Zeeuw, T. & Franx, M. 1991, *Ann. Rev. Astron. Astrophys.* , 29, 239

Debattista, V., Roškar, R., Valluri, M., et al. 2013, *Mon. Not. Roy. Astron. Soc.*, 434, 2971

Debattista, V., van den Bosch, F., Roškar, R., et al. 2015, *Mon. Not. Roy. Astron. Soc.*, 452, 4094

Debattista, V. P., Mayer, L., Carollo, C. M., et al. 2006, *Astrophys. J.*, 645, 209

Debattista, V. P. & Sellwood, J. A. 1999, *Astrophys. J.*, 513, L107

Dekel, A. & Silk, J. 1986, *Astrophys. J.*, 303, 39

Draine, B. & Li, A. 2007, *Astrophys. J.*, 657, 810

Dressler, A. 1980, *Astrophys. J.*, 236, 351

Dressler, A., Oemler Jr., A., Couch, W., et al. 1997, *Astrophys. J.*, 490, 577

Drinkwater, M. J., Gregg, M. D., & Colless, M. 2001, *Astrophys. J.*, 548, L139

Dunne, L., Gomez, H., da Cunha, E., et al. 2011, *Mon. Not. Roy. Astron. Soc.*, 417, 1510

Edvardsson, B., Andersen, J., Gustafsson, B., et al. 1993, *Astron. Astrophys.*, 500, 391

Elmegreen, B. 1990, *Astrophys. J. Letters*, 361, L77

Elmegreen, D. & Elmegreen, B. 1982, *Mon. Not. Roy. Astron. Soc.*, 201, 1021

Erwin, P., Beckman, J., & Pohlen, M. 2005, *Astrophys. J. Letters*, 626, L81

Erwin, P., Gutiérrez, L., & Beckman, J. 2012, *Astrophys. J. Letters*, 744, L11

Erwin, P., Pohlen, M., & Beckman, J. 2008, *Astron. J.*, 135, 20

Faber, S. M. & Gallagher, J. S. 1976, *Astrophys. J.*, 204, 365

Freeman, K. 1970, *Astrophys. J.*, 160, 811

Fuhrmann, K. 1998, *Astron. Astrophys.*, 338, 161

Gallagher III, J. & Hunter, D. 1984, *Ann. Rev. Astron. Astrophys.* , 22, 37

Garcia Gomez, C. & Athanassoula, E. 1993, *Astron. Astrophys. Suppl.*, 100, 431

García-Ruiz, I., Sancisi, R., & Kuijken, K. 2002, *Astron. Astrophys.*, 394, 769

Garnavich, P., Kirshner, R., Challis, P., et al. 1998, *Astrophys. J. Letters*, 493, L53

Gilmore, G., Randich, S., Asplund, M., et al. 2012, The Messenger, 147, 25

Gilmore, G. & Reid, N. 1983, *Mon. Not. Roy. Astron. Soc.*, 202, 1025

Gingold, R. & Monaghan, J. 1977, *Mon. Not. Roy. Astron. Soc.*, 181, 375

Goldreich, P. & Lynden-Bell, D. 1965, *Mon. Not. Roy. Astron. Soc.*, 130, 125

Grevesse, N. & Noels, A. 1993, in Orig. Evol. Elem., ed. N. Prantzos, E. Vangioni-Flam, & M. Casse, 15–25

Grosbøl, P., Patsis, P., & Pompei, E. 2004, *Astron. Astrophys.*, 423, 849

Gunn, J. E. & Gott, J. Richard, I. 1972, *Astrophys. J.*, 176, 1

Gutiérrez, L., Erwin, P., Aladro, R., & Beckman, J. 2011, *Astron. J.*, 142, 145

Haywood, M. 2008, *Mon. Not. Roy. Astron. Soc.*, 388, 1175

Haywood, M., Di Matteo, P., Lehnert, M. D., Katz, D., & Gómez, A. 2013, *Astron. Astrophys.*, 560, A109

Herpich, J., Stinson, G., Dutton, A., et al. 2015a, *Mon. Not. Roy. Astron. Soc.*, 448, L99

Herpich, J., Stinson, G. S., Rix, H.-W., Martig, M., & Dutton, A. A. 2015b, ArXiv e-prints

Hockney, R. & Brownrigg, D. 1974, *Mon. Not. Roy. Astron. Soc.*, 167, 351

Holmberg, E. 1941, *Astrophys. J.*

Holmberg, J., Nordström, B., & Andersen, J. 2009, *Astron. Astrophys.*, 501, 941

Holwerda, B. W., Pirzkal, N., & Heiner, J. S. 2013, *Mon. Not. Roy. Astron. Soc.*, 427, 3159

Huang, S. & Gu, Q.-S. 2009, *Mon. Not. Roy. Astron. Soc.*, 398, 1651

Hubble, E. 1926, *Astrophys. J.*, 64, 321

Hultman, J. & Pharasyn, A. 1999, *Astron. Astrophys.*, 347, 769

Ikebe, Y., Ohashi, T., Makishima, K., et al. 1992, *Astrophys. J.*, 384, L5

Ivezic, Z., Axelrod, T., Becker, A. C., et al. 2008, in AIP Conf. Proc., Vol. 1082 (AIP), 359–365

Jenkins, A. & Binney, J. 1990, *Mon. Not. Roy. Astron. Soc.*, 245, 305

Jiang, I.-G. & Binney, J. 1999, *Mon. Not. Roy. Astron. Soc.*, 303, L7

Johnston, E., Aragón-Salamanca, A., & Merrifield, M. 2014, *Mon. Not. Roy. Astron. Soc.*, 441, 333

Johnston, E., Aragón-Salamanca, A., Merrifield, M., & Bedregal, A. 2012, *Mon. Not. Roy. Astron. Soc.*, 422, 2590

Julian, W. & Toomre, A. 1966, *Astrophys. J.*, 146, 810

Katz, N., Hernquist, L., & Weinberg, D. 1992, *Astrophys. J. Letters*, 399, L109

Katz, N., Weinberg, D. H., & Hernquist, L. 1996, *Astrophys. J. Supple.*, 105, 19

Kazantzidis, S., Bullock, J., Zentner, A., Kravtsov, A., & Moustakas, L. 2008, *Astrophys. J.*, 688, 254

Kennicutt, R. 1989, *Astrophys. J.*, 344, 685

Kereš, D., Katz, N., Weinberg, D., & Davé, R. 2005, *Mon. Not. Roy. Astron. Soc.*, 363, 2

Kerr, F. 1957, *Astron. J.*, 62, 93

Koopmann, R. & Kenney, J. 2004, *Astrophys. J.*, 613, 866

Kormendy, J. & Kennicutt Jr., R. 2004, *Ann. Rev. Astron. Astrophys.* , 42, 603

Kovac, J., Leitch, E., Pryke, C., et al. 2002, *Nature*, 420, 772

Kronberger, T., Kapferer, W., Ferrari, C., Unterguggenberger, S., & Schindler, S. 2008a, *Astron. Astrophys.*, 481, 337

Kronberger, T., Kapferer, W., Unterguggenberger, S., Schindler, S., & Ziegler, B. 2008b, *Astron. Astrophys.*, 483, 783

Kroupa, P. 2001, *Mon. Not. Roy. Astron. Soc.*, 322, 231

Kuijken, K. & Garcia-Ruiz, I. 2001, in Astronomical Society of the Pacific Conference Series, Vol. 230, Galaxy Disk. Disk Galaxies, ed. J. Funes & E. Corsini, 401–408

Larsen, J. & Humphreys, R. 2003, *Astron. J.*, 125, 1958

Larson, R. B., Tinsley, B. M., & Caldwell, C. N. 1980, Astrophys. J., 237, 692

Lee, Y. S., Beers, T. C., An, D., et al. 2011, *Astrophys. J.*, 738, 187

Leitherer, C., Schaerer, D., Goldader, J., et al. 1999, *Astrophys. J. Supple.*, 123, 3

Levine, E., Blitz, L., & Heiles, C. 2006, *Astrophys. J.*, 643, 881

Lin, C. & Shu, F. 1966, Proc. Natl. Acad. Sci., 55, 229

Lin, C. C. & Shu, F. H. 1964, *Astrophys. J.*, 140, 646

Lindegren, L., Babusiaux, C., Bailer-Jones, C., et al. 2008, in IAU Symposium, Vol. 248, IAU Symp., ed. W. Jin, I. Platais, & M. Perryman, 217–223

Lintott, C., Schawinski, K., Bamford, S., et al. 2011, *Mon. Not. Roy. Astron. Soc.*, 410, 166

Loebman, S. R., Debattista, V. P., Nidever, D. L., et al. 2016, Astrophys. J., 818, L6

Loebman, S. R., Roškar, R., Debattista, V. P., et al. 2011, *Astrophys. J.*, 737, 8

Lucy, L. 1977, *Astron. J.*, 82, 1013

Maltby, D., Aragón-Salamanca, A., Gray, M., et al. 2015, *Mon. Not. Roy. Astron. Soc.*, 447, 1506

Markevitch, M., Gonzalez, A., Clowe, D., et al. 2004, *Astrophys. J.*, 606, 819

Martel, H., Urban, A., & Evans II, N. 2012, *Astrophys. J.*, 757, 59

McKee, C. & Ostriker, J. 1977, *Astrophys. J.*, 218, 148

Mihos, J. C. & Hernquist, L. 1994, *Astrophys. J.*, 425, L13

Miller, G. & Scalo, J. 1979, *Astrophys. J. Supple.*, 41, 513

Minchev, I. & Famaey, B. 2010, *Astrophys. J.*, 722, 112

Minchev, I., Famaey, B., Combes, F., et al. 2011, *Astron. Astrophys.*, 527, A147

Minchev, I., Famaey, B., Quillen, A., et al. 2012, *Astron. Astrophys.*, 548, A126

Mo, H., van den Bosch, F. C., & White, S. 2010, Galaxy Form. Evol.

Momany, Y., Zaggia, S., Bonifacio, P., et al. 2004, *Astron. Astrophys.*, 421, L29

Momany, Y., Zaggia, S., Gilmore, G., et al. 2006, *Astron. Astrophys.*, 451, 515

Monaghan, J. 1992, *Ann. Rev. Astron. Astrophys.* , 30, 543

Moore, B., Ghigna, S., Governato, F., et al. 1999, *Astrophys. J. Letters*, 524, L19

Moore, B., Katz, N., Lake, G., Dressler, A., & Oemler, A. 1996, *Nature*, 379, 613

Moore, G. E. 1965, Electronics, 38

Nasonova, O. G., de Freitas Pacheco, J. A., & Karachentsev, I. D. 2011, *Astron. Astrophys.*, 532, A104

Natale, G., Popescu, C. C., Tuffs, R. J., et al. 2015, *Mon. Not. Roy. Astron. Soc.*, 449, 243

Natale, G., Popescu, C. C., Tuffs, R. J., & Semionov, D. 2014, *Mon. Not. Roy. Astron. Soc.*, 438, 3137

Navarro, J. & White, S. 1993, *Mon. Not. Roy. Astron. Soc.*, 265, 271

Navarro, J. F., Frenk, C. S., & White, S. D. M. 1995, *Astrophys. J.*, 462, 22

Nelson, E., van Dokkum, P., Brammer, G., et al. 2012, *Astrophys. J. Letters*, 747, L28

Newton, K. & Emerson, D. 1977, *Mon. Not. Roy. Astron. Soc.*, 181, 573

Nordström, B., Mayor, M., Andersen, J., et al. 2004, *Astron. Astrophys.*, 418, 989

Oort, J., Kerr, F., & Westerhout, G. 1958, *Mon. Not. Roy. Astron. Soc.*, 118, 379

Ostriker, E. & Binney, J. 1989, *Mon. Not. Roy. Astron. Soc.*, 237, 785

Padmanabhan, T. 2001, Theoretical Astrophysics - Volume 2, Stars and Stellar Systems (Cambridge University Press), 594

Patel, S., van Dokkum, P., Franx, M., et al. 2013, *Astrophys. J.*, 766, 15

Perlmutter, S., Aldering, G., Goldhaber, G., et al. 1999, *Astrophys. J.*, 517, 565

Perryman, M., de Boer, K., Gilmore, G., et al. 2001, *Astron. Astrophys.*, 369, 339

Pilkington, K., Gibson, B. K., Brook, C. B., et al. 2012, *Mon. Not. Roy. Astron. Soc.*, 425, 969

Planck Collaboration, Ade, P. A. R., Aghanim, N., et al. 2015, ArXiv e-prints

Pohlen, M., Balcells, M., Lütticke, R., & Dettmar, R.-J. 2004, *Astron. Astrophys.*, 422, 465

Postman, M., Franx, M., Cross, N., et al. 2005, *Astrophys. J.*, 623, 721

Prochaska, J., Naumov, S., Carney, B., McWilliam, A., & Wolfe, A. 2000, *Astron. J.*, 120, 2513

Prochaska Chamberlain, L., Courteau, S., McDonald, M., & Rose, J. 2011, *Mon. Not. Roy. Astron. Soc.*, 412, 423

Querejeta, M., Eliche-Moral, M., Tapia, T., et al. 2015, *Astron. Astrophys.*, 573, A78

Quilis, V. 2000, Science (80-.)., 288, 1617

Quillen, A. C., Minchev, I., Bland-Hawthorn, J., & Haywood, M. 2009, *Mon. Not. Roy. Astron. Soc.*, 397, 1599

Quinn, P., Hernquist, L., & Fullagar, D. 1993, *Astrophys. J.*, 403, 74

Quinn, T. & Binney, J. 1992, *Mon. Not. Roy. Astron. Soc.*, 255, 729

Radburn-Smith, D., Roškar, R., Debattista, V., et al. 2012, *Astrophys. J.*, 753, 138

Rémy-Ruyer, A., Madden, S., Galliano, F., et al. 2014, *Astron. Astrophys.*, 563, A31

Renzini, A. 1999, in Form. Galact. Bulges, ed. C. Carollo, H. Ferguson, & R. Wyse, 9

Reshetnikov, V., Battaner, E., Combes, F., & Jiménez-Vicente, J. 2002, *Astron. Astrophys.*, 382, 513

Roediger, E. & Brüggen, M. 2007, *Mon. Not. Roy. Astron. Soc.*, 380, 1399

Roediger, J., Courteau, S., Sánchez-Blázquez, P., & McDonald, M. 2012, *Astrophys. J.*, 758, 41

Roškar, R., Debattista, V. P., Brooks, A. M., et al. 2010, *Mon. Not. Roy. Astron. Soc.*, 408, 783

Roškar, R., Debattista, V. P., & Loebman, S. R. 2013, *Mon. Not. Roy. Astron. Soc.*, 433, 976

Roškar, R., Debattista, V. P., Quinn, T. R., Stinson, G. S., & Wadsley, J. 2008a, Astrophys. J., 684, L79

Roškar, R., Debattista, V. P., Quinn, T. R., & Wadsley, J. 2012, *Mon. Not. Roy. Astron. Soc.*, 426, 2089

Roškar, R., Debattista, V. P., Stinson, G. S., et al. 2008b, *Astrophys. J.*, 675, L65

Rubin, V. & Ford Jr., W. 1970, *Astrophys. J.*, 159, 379

Ruiz-Lara, T., Pérez, I., Florido, E., et al. 2016, *Mon. Not. Roy. Astron. Soc.*, 456, L35

Sales, L., Helmi, A., Abadi, M., et al. 2009, *Mon. Not. Roy. Astron. Soc.*, 400, L61

Sanchez-Saavedra, M., Battaner, E., & Florido, E. 1990, *Mon. Not. Roy. Astron. Soc.*, 246, 458

Sánchez-Saavedra, M., Battaner, E., Guijarro, A., López-Corredoira, M., & Castro-Rodríguez, N. 2003, *Astron. Astrophys.*, 399, 457

Sancisi, R. 1976, *Astron. Astrophys.*, 53, 159

Sancisi, R., Fraternali, F., Oosterloo, T., & van der Hulst, T. 2008, *Astron. Astrophys. Rev.*, 15, 189

Scannapieco, C., Wadepuhl, M., Parry, O., et al. 2012, *Mon. Not. Roy. Astron. Soc.*, 423, 1726

Schawinski, K., Urry, C., Simmons, B., et al. 2014, *Mon. Not. Roy. Astron. Soc.*, 440, 889

Schaye, J. 2004, *Astrophys. J.*, 609, 667

Schönrich, R. & Binney, J. 2009a, *Mon. Not. Roy. Astron. Soc.*, 396, 203

Schönrich, R. & Binney, J. 2009b, *Mon. Not. Roy. Astron. Soc.*, 399, 1145

Schweizer, F. 1976, *Astrophys. J. Supple.*, 31, 313

Sellwood, J. 2000, *Astrophys. Space Sci.*, 272, 31

Sellwood, J. & Carlberg, R. 1984, *Astrophys. J.*, 282, 61

Sellwood, J. & Sparke, L. 1988, *Mon. Not. Roy. Astron. Soc.*, 231, 25P

Sellwood, J. A. & Binney, J. J. 2002, *Mon. Not. Roy. Astron. Soc.*, 336, 785

Shen, J. & Sellwood, J. A. 2006, *Mon. Not. Roy. Astron. Soc.*, 370, 2

Shen, S., Wadsley, J., & Stinson, G. 2010, *Mon. Not. Roy. Astron. Soc.*, 407, 1581

Silk, J. 2003, *Mon. Not. Roy. Astron. Soc.*, 343, 249

Solway, M., Sellwood, J. A., & Schönrich, R. 2012, *Mon. Not. Roy. Astron. Soc.*, 422, 1363

Spitzer Jr., L. & Schwarzschild, M. 1951, *Astrophys. J.*, 114, 385

Spitzer Jr., L. & Schwarzschild, M. 1953, *Astrophys. J.*, 118, 106

Springel, V. & Hernquist, L. 2003, *Mon. Not. Roy. Astron. Soc.*, 339, 289

Stadel, J. G. 2001, PhD thesis, University of Washington

Stinson, G., Bailin, J., Couchman, H., et al. 2010, *Mon. Not. Roy. Astron. Soc.*, 408, 812

Stinson, G., Bovy, J., Rix, H.-W., et al. 2013, *Mon. Not. Roy. Astron. Soc.*, 436, 625

Stinson, G., Seth, A., Katz, N., et al. 2006, *Mon. Not. Roy. Astron. Soc.*, 373, 1074

Thacker, R. & Couchman, H. 2000, *Astrophys. J.*, 545, 728

Thilker, D., Bianchi, L., Meurer, G., et al. 2007, *Astrophys. J. Supple.*, 173, 538

Thilker, D. A., Bianchi, L., Boissier, S., et al. 2005, *Astrophys. J.*, 619, L79

Thornley, M. 1996, *Astrophys. J. Letters*, 469, L45

Thornley, M. & Mundy, L. 1997, *Astrophys. J.*, 484, 202

Tinsley, B. 1977, *Astrophys. J.*, 216, 548

Tinsley, B. 1979, *Astrophys. J.*, 229, 1046

Tinsley, B. M. 1975, *Astrophys. J.*, 197, 159

Toomre, A. 1964, *Astrophys. J.*, 139, 1217

Toomre, A. 1981, in Struct. Evol. Norm. Galaxies, ed. S. Fall & D. Lynden-Bell, 111–136

Toomre, A. & Toomre, J. 1972, *Astrophys. J.*, 178, 623

Tremonti, C. A., Heckman, T. M., Kauffmann, G., et al. 2004, *Astrophys. J.*

Tully, R. & Fisher, J. 1977, *Astron. Astrophys.*, 54, 661

Vallée, J. 2015, *Mon. Not. Roy. Astron. Soc.*, 450, 4277

van den Bosch, F. & Swaters, R. 2001, *Mon. Not. Roy. Astron. Soc.*, 325, 1017

van Gorkom, J. 2004, Clust. Galaxies Probes Cosmol. Struct. Galaxy Evol., 305

van Woerden, H. 1977, in Astrophysics and Space Science Library, Vol. 70, Top. Interstellar Matter, ed. H. van Woerden, 261–283

Verdes-Montenegro, L., Bosma, A., & Athanassoula, E. 2002, *Astron. Astrophys.*, 389, 825

Villalobos, Á. & Helmi, A. 2008, *Mon. Not. Roy. Astron. Soc.*, 391, 1806

Vlajić, M., Bland-Hawthorn, J., & Freeman, K. 2011, *Astrophys. J.*, 732, 7

von Hoerner, S. 1960, Z. Astrophys. 50

Wadsley, J., Stadel, J., & Quinn, T. 2004, New Astron., 9, 137

Weinberg, M. D. & Blitz, L. 2006, *Astrophys. J.*, 641, L33

White, S. 1979, *Mon. Not. Roy. Astron. Soc.*, 189, 831

Wilczynski, E. 1896, *Astrophys. J.*, 4, 97

Willett, K., Lintott, C., Bamford, S., et al. 2013, *Mon. Not. Roy. Astron. Soc.*, 435, 2835

Williams, B., Dalcanton, J., Dolphin, A., Holtzman, J., & Sarajedini, A. 2009, *Astrophys. J. Letters*, 695, L15

Wilson, M., Helmi, A., Morrison, H., et al. 2011, *Mon. Not. Roy. Astron. Soc.*, 413, 2235

Woolf, V. & West, A. 2012, *Mon. Not. Roy. Astron. Soc.*, 422, 1489

Wyse, R., Gilmore, G., & Franx, M. 1997, *Ann. Rev. Astron. Astrophys.* , 35, 637

Yepes, G., Kates, R., Khokhlov, A., & Klypin, A. 1997, *Mon. Not. Roy. Astron. Soc.*, 284, 235

Yoachim, P., Roškar, R., & Debattista, V. 2010, *Astrophys. J. Letters*, 716, L4

Younger, J., Cox, T., Seth, A., & Hernquist, L. 2007, *Astrophys. J.*, 670, 269

Zhukovska, S., Gail, H.-P., & Trieloff, M. 2008, *Astron. Astrophys.*, 479, 453

Zwicky, F. 1955, *Pub. Astron. Soc. Pac.*, 67, 232